Verification of the Theoretical Discharge Coefficient of a Sub-Critical Flow Meter

by

D.J. Lahti

September, 1990

GE Aircraft Engines

Technical Information Series

Title Page

Author	Subject	Number
D.J. Lahti LAHTI, D.J.	SUB-CRITICAL AIRFLOW METERING	R90AEB406 Date 10/11/90

Title
GE Class II Government Class U
VERIFICATION OF THE THEORETICAL DISCHARGE COEFFICIENT OF A SUB-CRITICAL FLOW METER

GE Class II
Government Class Unclassified

Copies available from
Aircraft Engines Technical Information Center
☐ Lynn 24001 ☒ Evendale N-32

Number pages 131

Summary
GE Class II Government Class Unclassified

The objectives of this program were to study the factors leading to increased errors in sub-critical flow metering, utilize existing theoretical methods to design a new sub-critical flow meter for very high accuracy, predict its discharge coefficient, and then experimentally verify it by calibration with an industry standard critical flow meter. The meter design was typical of that used for modern, lightweight, engine mounted bellmouths, but its size was small enough to allow its calibration in a high accuracy laboratory environment. Thus this program provides a "calibration" of the theoretical method and establishes the link between a traceable metering standard and large engine bellmouths whose air flow rates exceed the capacity of any of the worlds calibration facilities.

Key Words
Theoretical discharge coefficient, sub-critical airflow metering, Venturi calibration

Contract Number N/A

Sponsoring Organization AEROTHERMO SYSTEMS INTEGRATION

Approved by N/A
(Author's Manager) (Organization)

Department/Operation ADVANCED TECHNOLOGY OPERATION Location Governor's Hill

GT217 (6-87) Formerly DV217

TECHNICAL INFORMATION SERIES

DISTRIBUTION

EVENDALE TECHNICAL INFORMATION CENTER, N-32 - 6 COPIES EVENDALE REPORTS. ALL CLASSES: 1 COPY LYNN REPORTS. CLASSES 1,2, & 3 only

LYNN TECHNICAL INFORMATION CENTER, 24001 - 3 COPIES LYNN REPORTS. ALL CLASSES. 1 COPY EVENDALE REPORTS. CLASSES 1,2, & 3 ONLY.

TECHNICAL INFORMATION CENTER, SCHENECTADY, BLDG. 5 RM 321 - 3 COPIES UNCLASSIFIED CLASS 1 THRU 3 ONLY.

RECORDS RETENTION CENTER, LYNN 3109A - MASTER PLUS 5 COPIES. UNCLASSIFIED LYNN CLASS 1 THRU 3 REPORTS ONLY

THE DISTRIBUTION OF THIS TECHNICAL INFORMATION SERIES REPORT IS LIMITED TO THE DISTRIBUTION LISTED BELOW EXCEPT AS APPROVED IN ACCORDANCE WITH THE REQUIREMENTS OF AEBG 630.10, APPENDIX A.

DISTRIBUTION - LYNN

Brian Acampa	34022
Dennis Evans	164X9
Tom Scott	34043

DISTRIBUTION - EVENDALE

W.A. Bailey	A-317
C. Balan	A-330
D.A. Dietrich	A-317
D.K. Dunbar	A-330
R.G. Keller	K-96
A.P. Kuchar	A-330
A. Lingen	G-14
B.W. Lord	J-40
L.J. McVey	A-317
D.W. Rogers	H-308
R.E. Russell	H-308
E.J. Stringas	G-14
M.W. Thomas	K-96
I.W. Victor	J-40

ABSTRACT

Historically, when high accuracy compressible gas flow measurements are required, flow meters designed for critical (choked) conditions have been used. Two standard critical flow meter designs whose discharge coefficients have been well established are now widely used throughout the world for such measurements. However in many situations either critical flow conditions cannot be achieved or these standard meters cannot be adapted to the physical set up of the installation where the flow measurements are to be made. An example of such a situation is the flow metering bellmouth placed in front of a typical large turbofan engine on an outdoor test stand. When sub-critical flow conditions exist measurement errors increase, and when non-standard meter designs must be used, such as is the case for most engine bellmouths, their discharge coefficients must be determined first. When high flow rates exist the only known way for obtaining the discharge coefficients of non-standard flow meters is to determine them theoretically.

The objectives of this program were to study the factors leading to increased errors in sub-critical flow metering, utilize existing theoretical methods to design a new sub-critical flow meter for very high accuracy, predict its discharge coefficient, and then experimentally verify it by

calibration with an industry standard critical flow meter. The meter design was typical of that used for modern, lightweight, engine mounted bellmouths, but its size was small enough to allow its calibration in a high accuracy laboratory environment. Thus this program provides a "calibration" of the theoretical method and establishes the link between a traceable metering standard and large engine bellmouths whose air flow rates exceed the capacity of any of the worlds calibration facilities. Detailed comparisons of the theoretical and experimental results are shown and the effects of uncertainties in the experimental results are assessed for their impact on discharge coefficient. Finally recommendations are made for future experimental work that will further improve our ability to design high accuracy low pressure loss sub-critical flow meters.

TABLE OF CONTENTS

LIST OF FIGURES

NOMENCLATURE

SYMBOL	DEFINITION
A.	Area, $in.^2$
C.	Curvature, 1/in.
D.	Diameter, in.
C_D	Discharge Coefficient
C_f	Friction Coefficient
C_P	Pressure Coefficient
g.	Gravitational Constant, ft/sec^2
H.	Enthalpy, BTU/lbm
M.	Mach Number
P.	Pressure, lb/in^2
r,R.	Radius, in.
R.	Gas Constant, $(ft\text{-}lbf)/(lbm\text{-}^\circ R)$
Re	Reynolds Number, $\frac{\rho VD}{\mu}$
S.	Entropy, BTU/lbm
T.	Temperature, $^\circ R$
u.	Axial Velocity
v,V.	Normal, Total Velocity, ft/sec
W.	Weight Flow, lb/sec
X.	Axial Distance
y.	Vertical Distance

SYMBOL	DEFINITION
γ.	Ratio of Specific Heats
δ.	Boundary Layer Thickness, in.
δ^*	Displacement Thickness, in.
θ.	Momentum Thickness, in.
μ.	Viscosity, lb-sec/ft^2
ρ.	Density, lbm/ft^3
ϕ.	Velocity Potential
ψ.	Stream Function

SUBSCRIPTS	DEFINITION
amb.	Ambient
id	Ideal
j	Jet
l	Local
O,T.	Stagnation, Total Conditions
S	Static
SW	Wall Static
1-D.	One-dimensional

Chapter I

INTRODUCTION AND BACKGROUND

For most engineering purposes the measurement of physical phenomena is based on an accepted standard. Unfortunately the measurement of fluid flow has no exact standard of extremely high accuracy such as is possible with length, time, mass, pressure, temperature and many others. This is particularly true when the flow rates are very large. Although it is possible to measure time accurately and also density, which is the correlation between volume flow and weight flow, the accurate measurement of large weight or volume is difficult (Reference 1). It is difficult and expensive to attempt to operate large weigh tanks or volume tanks in other than a laboratory specifically designed for the measurement of fluid flow. Although there are several facilities in existence for the direct, or primary measurement of relatively small quantities of fluid flow, there are only a handful in existence capable of measuring large quantities of fluid flow. In addition, this is only true for cases where the fluid is a liquid. Because of the low density of gases compared to liquids, the direct measurement of large quantities of gas flow is not possible, and to this author's knowledge there are only four facilities in the free world (Reference 2) where the direct, primary measurement of small quantities of gas flow is

performed. The largest flowrate any of these facilities is capable of measuring is about 10 pounds per second.

Primary methods of flow measurement, by definition, are accomplished without calibrations by other flow measurement devices. So called secondary methods require calibrations which serve as corrections that are applied as discharge coefficients in calculating the flow rate. Since some accuracy is lost each time a calibration is transferred from one flowmeter to another, it is desirable to minimize the number of calibration steps between the primary method and the flow measurement that is required. As Arnberg, et al, (Reference 3) point out it would be desirable to obtain the required measurement directly by means of a primary method, so that no calibration transfers would be needed. However, as they note there are two limitations to this ideal in practice. First, all primary methods do not have the same accuracy. Since there is nothing that requires high accuracy in a primary method, it is possible that a secondary measurement based on a primary calibration of high accuracy could be more accurate than a measurement obtained directly by a primary method of poor accuracy. Second, since most primary methods of gas flow measurement lack flexibility when designed for the highest possible accuracy, they are often incompatible with the installation circumstances of the particular flow measurement needed.

Therefore in the case of compressible gas flow measurement there has evolved over the past thirty years two accepted standard flow meter designs that represent an "optimum" compromise between the high accuracy obtainable by the best primary calibration methods and the flexibility of secondary methods with a minimum loss of accuracy due to calibration transfer. These standard flow meters are the Smith and Matz critical flow circular-arc throat venturi and the ASME critical flow nozzle.

Both Smith and Matz (References 4, 5) and Stratford (Reference 6) discussed many of the advantages of metering airflow using critical flow circular arc venturis. In their pioneering work to demonstrate the advantages of choked flow metering Smith and Matz (Reference 5) argued that metering at conditions where the Mach numbers across the meter throat were at or near unity provided a situation where errors in calculated flow rate due to pressure measurement errors would be minimized. They stated that "at critical flow conditions an error in total pressure of ± 0.25 percent results in an airflow rate error of only $\pm$ 0.25 percent, and no additional error contribution results from the static pressure measurement. At critical flow conditions the throat static pressure is constant and, what is much more important, need not be measured at all because it can be calculated from consideration of the properties of the

flowing gas." They go on to state "For a given accuracy of pressure measurement then, the error in flow rate at Mach number 0.3 is, for the case where errors are additive, 15 times as great as the error at the critical flow rate." They go on to discuss the factors which lead to the selection of a suitable venturi contour for metering flow at critical conditions. It is interesting to note that one of them relates to the contour being of a simple enough geometric shape that its flow field could be calculated on a theoretical basis. At the time that their work was done (Circa 1958-1963) the most relied upon method for the calculation of the transonic flow field in a nozzle throat was that due to Oswatitsch and Rothstein (Reference 7). It was an approximate method for the solution to the velocity potential equation utilizing series expansions for the axial and radial velocity components and simple analytical expressions for the wall geometry. The method was only valid in the immediate vicinity of the nozzle throat where the wall slopes were small. The turbulent boundary layers were calculated utilizing Tucker's (Reference 8) approximate method. They argued that in spite of the limitations of these theoretical methods, when operating at critical flow conditions predictions of the discharge coefficient were accurate to within ± 0.25 percent for their recommended circular arc throat contour which was blended into a conical exhaust diffuser. They then built and tested their

recommended venturi design. In order to experimentally determine the discharge coefficient of the meter it was built large enough (5.64 inch throat diameter) to allow fundamental measurements of the throat static pressure profile and wall boundary layer thickness. Thus, in principle, they "calibrated" the flow meter using a theoretical prediction and verified that the predictions were valid to within a certain accuracy. Their results showed that their predictions of discharge coefficient were within approximately 0.05 percent of the experimental values over the range of Reynold's numbers of the tests. On the basis of this work their recommended circular arc venturi has become an industry standard design and is now used in test facilities throughout the world.

Stratford (Reference 6) argued along similar grounds that the most accurate gas flow meter is a circular arc throat contour operating at critical conditions. His recommended throat contour was only slightly larger than that of Smith and Matz on the grounds that the larger throat wall radius of curvature reduces the radial pressure profile in the throat and thus minimizes the error in predicted discharge coefficient due to inadequacies in the then available transonic flow field predictions.

The origin of the critical flow ASME nozzle is not as clear as that of the Smith and Matz circular arc venturi. Its use as a critical flow meter appears to have evolved over time from its use as a liquid only flow meter. It was originally promoted by the Instruments and Apparatus for the Measurement of Fluid Flow Subcommittee of the ASME Power Test Codes Committee circa 1934. Its discharge coefficient has been well established for incompressible fluids (Reference 9) in primary (direct-weigh) calibration facilities. The normal practice has been to apply the results from such calibrations with incompressible fluids directly to the compressible measurement problems by appeal to the laws governing dynamic similarity of the flows. This appeal to similarity is made at constant values of Reynolds number based on the throat diameter with some Mach number constraints. The one recommendation by the ASME (Reference 9) is that this method can be used as long as the throat Mach number is less than 0.95. Smith and Matz (Reference 10) conducted an exhaustive and systematic search of U.S. and foreign technical journals and other archive documents and found no evidence of reports of systematic experiments to determine quantitatively the tolerances involved in this appeal by the ASME to dynamic similarity between compressible and incompressible flows, at least in the size range of throat diameters greater than several inches.

To this author's knowledge the only known experimental work to establish the discharge coefficient of critical flow ASME nozzles was performed by Holdhusen and Peruse (Reference 11). In these tests the meter exit boundary layer profiles were measured and the resulting mass and momentum deficits were used to compute the discharge and thrust coefficients respectively. Since the meter was always choked and its throat section is cylindrical, Holdhusen and Peruse argued that the influence of a non-uniform radial pressure profile is negligible. In the test meter they placed static pressure taps along the throat wall to verify this argument. Although the flow was not surveyed across the throat, the wall taps would indicate the maximum influence of a non-uniform radial profile since the highest velocity occurs there. Their static pressure measurements confirmed their belief. They showed that the maximum effect of a non-uniform radial velocity profile to have less than a 0.1% impact on discharge coefficient. Although this work was not widely published it was significant because it proved for critical flow conditions only the effect of the throat boundary layer blockage need be accounted for in determining ASME nozzle discharge coefficients. Over the past twenty five years this work gradually received wide scale acceptance and thus critical flow ASME nozzles are also widely used in test facilities throughout the world.

Although it is desirable to utilize critical flow meters whenever possible because of their inherent accuracy "advantage" it is often not possible. In many industrial applications it is necessary to accurately measure the air flow in devices not capable of generating the pressure differential necessary to produce critical conditions in the meter throat. There are also situations where choked flow could be produced in the meter throat, but other factors prevent the use of a critical flow meter. Situations where the available space prevents the use of a standard circular-arc venturi with its relatively long supersonic diffuser can dictate the use of a much shorter non-standard meter design. If there is a requirement that the discharge pressure loss and/or distortion be kept to a minimum, critical flow meters could not be used because of their inherently high pressure loss and distortion associated with the shock system and boundary layer separation in the supersonic diffuser. Coupled with the fact that there are no facilities (either primary or secondary) capable of calibrating compressible gas meters where the flowrates exceed approximately 300 pounds per second it is clear that there is a need for a procedure to "calibrate" non-standard subcritical flow meters having high flow rates.

In the absence of facilities for calibrating such non-standard sub-critical flow meters the industry has

resorted to a variety of methods for filling this void. The most worthy attempts have been based in some way on the use of theoretical methods; however, to this day no systematic procedure has emerged as being the accepted best. In addition, most such attempts go undocumented and are not reported in the open literature. Although there have been several successful attempts at the theoretical prediction of the discharge coefficient of critical flow meters since the work of Smith and Matz as discussed previously, only one such case has been found in the open literature for sub-critical flow meters. This work was also performed by Smith and Matz (Reference 10) approximately ten years after their work on circular-arc critical flow venturis.

This work was motivated by the question of whether the discharge coefficient established for a nozzle from an incompressible calibration using water would be the same as that obtained for the nozzle using a compressible gas at the same Reynolds number but at sub-critical throat Mach numbers.

They conducted an elaborate program consisting of calibrations of an 8 inch throat diameter ASME nozzle using both water and air. The water calibrations were performed using the primary method of direct weighing of the water. The air calibrations were performed using a 5.64 inch

diameter circular-arc critical flow venturi whose discharge coefficient had been determined using the theoretical procedure they had established approximately 10 years earlier as discussed previously.

Both the water and air calibrations were conducted with identical pressure instrumentation in the ASME nozzle to minimize differences in discharge coefficient due to differences in the instrumentation itself. In addition to the instrumentation necessary for discharge coefficient determination, a large amount of diagnostic instrumentation was included to ascertain the details of the flow fields upstream of the nozzle entrance as well as throughout the nozzle itself.

As mentioned previously theoretical predictions of the ASME nozzle compressible flow field were also made in support of this extensive test program. These calculations were made in order to compare with the diagnostic flow field measurements to aid in understanding and interpreting the discharge coefficient results. Although details of the computer code were not discussed in their paper, the following general description about it was given. "The Wehofer-Moger transonic flow computer program employs a direct numerical integration of the differential equations for continuity, radial momentum, axial momentum, and energy

posed in the unsteady or time-dependent form. The gas involved is assumed to be inviscid, adiabatic, and thermally perfect."

The application of this computer code to the ASME low beta ratio nozzle is the first (and only) known such work on an unchoked compressible gas metering standard that has been published in the open literature.

Their compressible flow calibrations of the ASME nozzle were conducted over a range of throat Mach numbers from 0.4 to 1.0. The incompressible flow (water) calibrations were conducted over the same range of throat Reynolds numbers as for the compressible calibrations. Theoretical flow field solutions were conducted for the same conditions as for the compressible flow calibrations.

Figures 1a and 1b show the results of the compressible flow calibrations obtained by Smith and Matz. These two figures are taken directly from their paper (Reference 10). The upper figure (1a) shows the discharge coefficients obtained for three values of throat Mach number based on the ASME recommended static pressure tap size and placement. Smith and Matz noted that some of the coefficients were greater than unity and there was large scatter in the data, particularly for throat Mach numbers less than 1.0.

In comparing their theoretical solutions with their static pressure survey data at the meter throat they noted good agreement in both pressure level and profile except at the wall (where the measured pressures were obtained from the ASME recommended 0.125 inch diameter taps as opposed to their survey probe). As a result of this observation they corrected the measured wall pressure data based on the results of an experimental study by Rayle (Reference 12) which showed the effect of tap size on indicated pressure. This corrected data is shown in the lower plot Figure 1b. Clearly the correction reduced the scatter in the discharge coefficient for the unchoked Mach numbers, but it is still nearly twice as large (± 0.5 percent) as the critical flow data shown.

Smith and Matz draw several important conclusions from this work. First they determined that the ASME recommended discharge coefficients based on incompressible water tests could not be used for compressible gases. At the lowest throat Mach number of 0.4 the water results differed from the compressible results by more than one percent.

Their final conclusion was stated as follows: "A precise theoretical model of the complex flow field for both subsonic and critical-flow conditions in the ASME long radius low beta ratio nozzle has been developed and has been

verified by comparison with experimental data. Use of this powerful analytical tool should provide a means for an improved correlation of experimental measurements of nozzle discharge coefficient." Unfortunately they did not show comparisons of predicted discharge coefficients versus their measurements, and they did not make detailed boundary layer measurements which might have provided a better understanding of the source of the large data scatter. It is also unfortunate that although their work was conducted nearly thirty years ago there have been virtually no published works since then which attempt to build upon their experience and the suggested insight that the improved theoretical methods could provide. The partial success of Smith and Matz and other successes in the use of CFD since then, along with the continued push for increased flow metering accuracy in sub-critical flow environments, led to the idea that a comprehensive experimental program was still needed to provide a highly accurate sub-critical flow meter design that did not have many of the limitations of unchoked ASME metering nozzles.

Therefore the main objective of this program was to experimentally verify the accuracy of a theoretical method for determining the discharge coefficient of a sub-critical flowmeter of non-standard design to an accuracy comparable

to that of standard critical flow venturis, which is ±0.25 percent. The rationale for this was that once the method had been verified it could be utilized on any sub-critical flow meter independent of its size, and in particular very large flow meters where there are no other means available for establishing their discharge coefficients.

A second objective was to establish a new sub-critical compressible flow metering standard to replace the ASME low beta ratio nozzle which has many inherent problems when used for unchoked flows. To this author's knowledge a program such as this has never been conducted. It was intended that the data obtained could also be used by others to serve as a benchmark for establishing the accuracy of other theoretical methods that presently exist or will be developed in the future. The program formulated to accomplish this is described below. It represented a blending of existing theoretical methods with established critical flow metering standards and procedures.

Chapter II

STATIC PRESSURE MEASUREMENT ISSUES FOR SUB-CRITICAL FLOW METERS

2.1 INTRODUCTION:

A head type flow meter produces a constriction in the gas stream that causes a pressure differential which is a function of the flow rate through it. The higher the flow rate the higher the pressure differential.

The discharge coefficient of a head type flow meter is defined as the ratio of the actual flow rate to the ideal one-dimensional inviscid flow rate that would exist if all the flow were at the velocity corresponding to the static pressure at the meter throat wall. The more uniform the velocity profile across the throat of the meter the higher its discharge coefficient. A discharge coefficient of unity would imply a perfectly uniform velocity profile and no wall boundary layer. Thus the accurate determination of the discharge coefficient of a flow meter is dependent on three primary factors. The first is the velocity level that exists at the throat of the meter, the second is the profile of velocity (pressure) across the meter throat and the third is the thickness of the throat wall boundary layer.

There are four methods for determining the discharge coefficient of a head type flow meter. The first is to survey the velocity, pressure and temperature fields across the meter throat to determine the ρV profile which can then be integrated to determine the actual mass flow rate. The second is to compute these same quantities using a theoretical method and then performing the same integration of the ρV profile. The third is to physically weigh the quantity of fluid that is passed through the meter in a given amount of time. This is called a primary calibration because the actual mass is measured directly. The fourth is to calibrate the flow meter using another flow meter whose discharge coefficient is already known. This type of calibration is called a secondary method because the actual mass flow through the meter is not measured directly, but rather it is calculated using the known discharge coefficient of another flow meter.

As discussed in Chapter I the determination of discharge coefficients of compressible gas meters using primary calibration methods is limited to flow rates of approximately 10 pounds per second. Secondary methods have been used to determine compressible gas meter discharge coefficients for flow rates up to approximately 300 pounds per second. Thus the only methods available for determining meter discharge coefficients at flow rates exceeding about

300 pounds per second involve either measuring the throat pressure profile or calculating it using a theoretical method.

Since the purpose of this program was to verify the accuracy of the theoretical method for determining discharge coefficient it involved both the calculation of the throat pressure profiles and then comparing them to the measured profiles of a specific flow meter design. Before proceeding to a discussion of the flow meter design itself it is important to discuss the issues relating to static pressure measurement that will influence the design of any sub-critical flow meter.

2.2 STATIC PRESSURE MEASUREMENT ACCURACY REQUIREMENTS

As discussed in Chapter I, when mass flow is to be measured when sub-critical flow conditions exist, it becomes necessary to accurately determine the static pressure field across the meter throat. Although in principle this is simple, in practice it is an extremely difficult task and in fact, it is because of this difficulty there are no known standard subcritical flow meters in existence today with accuracies that match those of critical flow meters.

The importance of accurate static pressure measurement in the throat of an unchoked flow meter is illustrated with the aid of Figures 2 and 3. The isentropic flow function $\frac{w\sqrt{T_o}}{P_o A}$, also called Fliegner's Formula, (Reference 13), is given by

$$\frac{w\sqrt{T_o}}{P_o A} = \left(\frac{P_S}{P_o}\right)^{\frac{1}{\gamma}} \sqrt{\frac{2\gamma g}{R(\gamma - 1)} \left[1 - \left(\frac{P_S}{P_o}\right)^{\frac{\gamma - 1}{\gamma}}\right]}$$

where w/A is the weight flow per unit area, T_O and P_O are the stagnation temperature and pressure respectively and P_S is the static pressure. In Figure 2 the isentropic flow function is plotted as a function of the static-to-total pressure ratio P_S/P_O.

As one moves away from unity Mach number in either the subsonic or supersonic direction, the slope of the isentropic flow function curve becomes increasingly steep. Thus errors in the measurement of static pressure will have an increasingly larger effect on the weight flow error the further away from unity Mach number. If the flow function equation is differentiated with respect to pressure ratio, P_S/P_O, one obtains

$$\frac{d\left(\frac{w\sqrt{T_o}}{P_o A}\right)}{d\left(\frac{P_S}{P_o}\right)} = K(T_1 + T_2)$$

where $K = \sqrt{\frac{2\gamma g}{R(\gamma - 1)}}$

$$T_1 = \frac{1}{\gamma} \left(\frac{P_S}{P_o}\right)^{\frac{1-\gamma}{\gamma}} \sqrt{1 - \left(\frac{P_S}{P_o}\right)^{\frac{\gamma-1}{\gamma}}}$$

and

$$T_2 = \frac{(\gamma - 1)}{2\gamma \sqrt{\left[1 - \left(\frac{P_S}{P_o}\right)^{\frac{\gamma-1}{\gamma}}\right]}}$$

This equation can now be used to compute the error in weight flow W as a function of the pressure ratio. This is shown in Figure 3 where the error in weight flow rate due to an error in static pressure (Ps) of 1% is plotted as a function of Mach number. This curve illustrates why critical (sonic) flow meters are used whenever possible. It also shows that if one is to achieve flow measurement accuracy within 1% at a meter throat Mach number less than approximately 0.65, the static pressure must be measured with an error of less than 1%. The pressure measurement accuracy requirement increases rapidly as throat Mach number decreases. For example, at a throat Mach number of 0.1 a static pressure measurement error of 1% would produce a flow measurement error of approximately 60%.

2.3 INFLUENCE OF STATIC PRESSURE PROFILE

In order to determine the discharge coefficient of any flow metering device, an accounting of the throat static pressure profile must be taken. In a critical flow meter the profile is only dependent on the meter geometry (excluding the minor secondary influence of the meter wall boundary layer) whereas the profile in an unchoked meter is not only dependent on the meter geometry, but also ironically on the flow rate itself. As the flow rate through the meter is decreased, the radial variation of the static pressure decreases and the absolute level of pressure increases. Thus, although the variation in pressure across the meter throat is reduced, because the Mach number is also decreasing, the sensitivity to measurement error is increasing and the need to measure the profile more accurately increases. This is illustrated in Figure 4, where the radial profiles of static-to-total pressure ratio were calculated using the method of Reference 14 for a typical large jet engine bellmouth for a range of specific flows represented by the indicated average Mach numbers. The dashed lines on either side of each profile show the range of pressure ratio variation representative of a $\pm$ 0.5% flow rate variation. At the lowest average Mach number shown, the $\pm$ 0.5% variation band is very small even though

the difference between the wall value and centerline value is less than half of the difference at the highest average Mach number.

2.4 INFLUENCE OF STATIC PRESSURE MEASUREMENT DEVICES

The difficulties associated with measurement of the throat radial static pressure profile is the major factor which prevents subcritical flow meters from being used more widely for high accuracy meters. The main reason for this difficulty is that the devices used to measure static pressure disturb the flow field being measured, thus altering the local pressure at the point of measurement. Figure 5 shows the error in airflow that would result from the disturbance to the local pressure (as indicated by pressure coefficient, Cp)

$$\text{where } Cp = \frac{P_S - P_1}{\frac{\gamma}{2} P_1 M_1^2}$$

and P_1 and M_1 are the true local undisturbed pressure and Mach number respectively, and Ps is the sensed pressure caused by the placement of the measurement device in the local flow field. As indicated in this figure the pressure coefficients for a minimum error of 0.25% are very small. At a true undisturbed Mach number of 0.7 the pressure coefficient on the static probe must be less than 0.01. At an ambient pressure of 14.7 psia this means a true pressure

disturbance of less than 0.05 psia. At a true Mach number of 0.2 the pressure coefficient would have to be less than .005, which means an absolute pressure disturbance of less than 0.0021 psia.

This problem is further illustrated in Figures 6 and 7. Figure 6 shows a typical static pressure probe design which consists of a cylindrical tube with a hemispherical head. The four static pressure ports are usually located some distance (X) aft of the nose leading edge. Shown beneath the probe are its characteristic pressure distributions (Reference 15) for a range of free stream Mach numbers. It is seen that for all subsonic flow along the probe the effect of this nose geometry is to depress the pressure below the local ambient pressure for about 4 probe diameters. As the freestream Mach number is increased (but still remains subsonic), such that local supersonic flow exists at the cylindrical portion, the shock wave formed causes the pressure at the sensing ports to be higher than the local ambient. Although many other static probe head designs have been utilized over the years (Reference 16), they all require the placement of the sensing ports a significant distance downstream of the leading edge in order to be out of the influence of the nose pressure field. Often for very large sub-critical flow meters these static probes are mounted in a radial array on a fixed structure

that either spans the throat of the meter or is centilevered from one wall. Depending upon the anticipated circumferential non-uniformity of the static pressure field to be measured, there can be as many as eight of these "rakes" or as few as one. Typically each of these rakes would have up to 8 static probes, thus providing for as many as 64 individual static pressure measurement locations within the throat.

Since the radial structural struts that support the individual probes must be rigid enough to accurately maintain the probe positions under their aerodynamic loading, they are significantly larger than the probes themselves. Depending upon the aerodynamic environment (pressure level, temperature, and Mach number) in which they will be located, they may have a wide variety of cross-sectional shapes ranging from circular to airfoil-like. A typical cross section for relatively low Mach numbers would have a hemispherical leading edge with parallel side walls and a hemispherical trailing edge as shown in Section A-A of Figure 7 along with a typical static probe array. Since the static pressure sensing ports of the probe are in front of the relatively blunt support strut, they must be placed far enough forward of the strut to be out of the influence of its leading edge stagnation region. Krause (Reference 17) conducted an experimental study to map

the stagnation region in front of support struts having a cylindrical cross section. A summary of those results are shown in Figure 8. It is seen that the pressure ports must be placed at least 12 to 15 diameters forward of the support strut to be sensibly removed from its influence. These results, along with those of Reference 15 show that the placement of the pressure ports far enough aft of the probe leading edge influence and far enough forward of the support strut leading edge influence is a critical factor in achieving a high level of accuracy in static pressure measurement. Usually aerodynamic interference and measurement accuracy are not the only factors considered in determining the placement of the static pressure ports. Structural design considerations as well as the physical blockage of the rake are also important. As mentioned previously, it is desirable to place the pressure ports at least 12 to 15 support strut thicknesses forward of the strut leading edge. However, the structural stiffness of the cantilevered probe on the cantilevered strut is often not sufficient to allow the pressure port placement that far forward without significant vibration or divergence problems. Under these circumstances the pressure ports are located within either the influence of the probe tip or the strut leading edge, or both. When this is the case the influence of the probe/strut combination is usually unknown

and the rake must be calibrated. That is the rake with its unique placement of the static pressure sensing ports and its unique aerodynamic geometry must be placed in an aerodynamic flow field whose local static pressure and Mach number are known a-priori and the sensed pressure and Mach number can be calibrated to these known values.

CHAPTER III

TEST FACILITY SELECTION CRITERIA

3.1 CALIBRATION USING A STANDARD CRITICAL FLOW METER

In order to verify a procedure to theoretically determine sub-critical flow meter discharge coefficients to the level of accuracy that matches that of critical flow meters, it was felt that the program must include the use of one of the two accepted critical flow metering standard nozzles. Either the Smith and Matz circular-arc venturi (Reference 4) or the ASME low beta ratio nozzle (Reference 9) was considered acceptable. Thus the chosen critical flow meter whose discharge coefficient is already known would be used as the transfer standard to perform a secondary calibration of the non-standard sub-critical flow meter designed for this program.

Figure 9 shows a typical test set up that would be used for such a calibration. In this arrangement the non-standard flow meter is connected in series with the standard critical flow meter whose discharge coefficient is known. As discussed in Section 2.1 the discharge coefficient of the non-standard nozzle is defined as the ratio of the actual mass flow to the ideal one-dimensional inviscid flow that

would be passed by the nozzle if all the flow were at the velocity corresponding to the wall static pressure and the upstream total pressure and temperature. Therefore for each flow rate through the system the actual flow is determined from the calibrated upstream critical flow metering nozzle and the ideal one-dimensional flow is calculated from the measured total pressure (P_T), total temperature (T_T), throat wall static pressure (P_{SW}), and throat area A in the non-standard nozzle.

The issue of greatest importance with respect to the test facility selection for this purpose is that it had to have the capability and demonstrated experience to conduct such tests to the levels of accuracy and precision required. The final assessment of the success or failure of the theoretical procedure to predict the discharge coefficient of the non-standard sub-critical flow meter design would be based on how well the theoretical predictions compared with the discharge coefficients established from these secondary calibrations.

3.2 CALIBRATION USING THROAT FLOW FIELD SURVEYS

As discussed in Section 2.1 another method for determining the discharge coefficient of a non-standard flow meter is to survey the throat pressure and temperature profiles from

which the ρV profile can be calculated and then integrated to establish the actual flow rate. Although this method is the least accurate of the three known methods for determining sub-critical flow meter discharge coefficients as discussed in Section 2.3 and 2.4, it was considered to be an important secondary, or back-up requirement in selecting the test facility. Such back-up measurements provide a means for reconciling the observed discharge coefficients obtained from the critical flow meter with the observed throat flow field measurements and thus serve as an important diagnostic tool. Therefore the facility selected had to have a large enough airflow delivery capacity to allow a meter physical size large enough to permit throat static pressure surveys and wall boundary layer surveys over the full range of throat Mach numbers planned.

3.3 FREE-JET CALIBRATION OF THROAT PITOT-STATIC SURVEY PROBE

As a consequence of the intention to determine the meter discharge coefficient from throat static pressure profile surveys a third factor considered in selecting the test facility was the requirement for conducting free-jet calibrations of the pitot-static probe to be used in the surveys. As discussed in Section 2.4 it is imperative that whenever a particular static pressure measuring device is to

be used for high accuracy testing, it must be calibrated in a known flow field. Therefore the test facility had to have the capability to conduct a high accuracy free-jet calibration where the jet size was commensurate with that of the meter throat where the pressure profile surveys were to be taken.

3.4 CAPACITY FOR MEASUREMENT OF LARGE NUMBERS OF STATIC PRESSURES

Finally the last significant factor in the test facility selection was the capability for making a large number of accurate wall static pressure measurements throughout the meter. The rationale for this requirement was to provide enough detailed flow field measurements throughout the meter for detailed and extensive comparisons with the theoretical predictions which were to be performed. These static pressure measurements were also intended to provide a data base for others wanting to validate their own theoretical methods.

The facility selected for conducting the tests was FluiDyne Engineering Corporation in Minneapolis, Minnesota. The test facilities at their Medicine Lake Aerodynamic Laboratory were ideally suited for the planned tests. This facility

has a number of test channels which are normally used for scale model exhaust nozzle testing. The model size finally selected was chosen such that existing facility adapter hardware could be used. A detailed description of the test set up and procedure is provided in Chapter V.

CHAPTER IV

METER DESIGN AND PRE-TEST PREDICTIONS

4.1 FLOW METER DESIGN

The meter design was developed in conjunction with the facility selection, the intended future use of the sub-critical flow metering procedure specifically for large engine flow rate determination, and the verification of the metering procedure using an existing critical flow metering standard.

The flow meter aerodynamic contour definition is shown in Figure 10. Figure 11 shows the aerodynamic contour along with the theoretically predicted wall pressure distribution using the STC inviscid computer code. The meter design will be discussed with reference to these two figures. In Figure 10 it is seen that the meter consists of four main segments. The upstream contracting section has an elliptical contour from the so called "hilite" station (X = 0, R = 4.8785). The upstream 6.125 inch radius pipe is part of the facility adapter hardware. A radial line connects the two at station 0. The throat region of the meter consists of a 1.827 inch cylindrical section from the end of the elliptical section to the start of the diffuser.

The throat radius is chosen based on a compromise between two conflicting requirements. Since it is desirable to operate the meter over a wide range of flow rates, the throat should be kept as small as possible in order that the Mach number be as high as possible to minimize the effect of pressure measurement error at the lowest anticipated flow. However since the meter is intended to be used in front of a jet engine, the throat must be large enough so as not to cause choking at the highest anticipated flow. In addition, the diffuser area ratio must be small enough, and its contour gradual enough to prevent boundary layer separation which would generate undesirable pressure distortion at the engine face.

The cylindrical section which connects the upstream contraction with the downstream diffuser is intended to provide a region of constant physical flow area for ease of area measurement. Since the absolute flow rate through any meter depends on its actual throat area, and one's ability to measure it, a cylindrical section is chosen to minimize the area measurement uncertainties. Although this may not be a critical problem for small meters whose contour can be inspected with great accuracy on modern contour measuring machines, it is a problem on very large meters whose size prohibits this possibility. The length of the cylindrical section is determined in an iterative procedure which

involves theoretical solutions such as shown in Figure 11. This figure shows that there are two localized overaccelerations at the curvature discontinuities that occur at each end of the cylinder between the end of the contracting section and the start of the diffusing section. Between these two locations it is seen that there is a relatively flat region in the pressure distribution. This pressure "flat" is highly desirable from an experimental error point of view. When seeking to determine the axial location of the throat wall static pressure taps, small errors in their placement in the meter are minimized since the pressure in this region is changing slowly. Thus to determine the length of the cylindrical section for a given flow meter, the theoretical solution for each assumed length is examined to find one having a pressure flat that is long enough to accommodate the expected static pressure tap location uncertainty. Figure 12 shows an expanded view of the calculated pressure distribution in this region for the selected meter design at the nominal throat Mach number of 0.767. The variation in pressure distribution is such that an error in pressure tap placement of approximately a half inch would cause no more than about a 0.25% flow error.

In order to ascertain that the diffuser would remain separation free over the complete flow range of the meter, a boundary layer solution was conducted using the pressure

distribution from an STC solution at the highest anticipated flow rate. Since the steepest adverse pressure gradient in a diffuser occurs at the highest throat Mach number (flow rate), if it does not separate at this condition it will remain separation free at all lower Mach numbers. Figure 13 shows the computed skin friction coefficient for the case of the maximum nominal throat Mach number of 0.767. The skin friction coefficient remains well above a value of 0.001 throughout the diffuser.

4.2 STATIC PRESSURE TAP PLACEMENT

The pressure distribution in Figure 11 was used to determine where the static taps should be placed throughout the model. Since one of the purposes of this program was to prcvide a data base for establishing how well current theoretical methods could predict such subsonic flowfields the model was very heavily instrumented. A total of eighty static pressure taps were installed along the wall of the meter. In addition to providing a detailed description of the axial pressure distribution for comparison with the theoretical predictions, at some axial stations taps were placed at several circumferential locations for use in assessing the uniformity of the flow in the model. There were 8 taps placed every 45 degrees around the circumference of the throat metering plane at X = 4.031. These 8 taps were to be

used to provide the basic wall static pressure reading as the means for measuring the actual airflow through the meter in conjunction with the theoretically determined discharge coefficient.

In addition to providing detailed static pressure data along the meter wall, it was planned that throat static pressure surveys also would be obtained. Therefore a pitot static probe was designed using the static port placement criteria of Reference 17 and shown in Figures 6 and 8. Since the profiles were to be obtained at the throat metering plane (station 4.031) the probe tip extends upstream of this location by 4 probe diameters in order that its influence not be felt at the static ports which are located at X = 4.031. Similarly the aft support rod is downstream of X = 4.031 by 12 diameters to remove its upstream influence. Details of the model hardware and instrumentation are discussed in Chapter V.

4.3 PRE-TEST PREDICTIONS

During this program the meter design was accomplished in conjunction with the aerodynamic performance and flow field predictions because of the iterative nature of the process. The previous section discussed meter design issues. This section will discuss the meter aerodynamic flowfield and

discharge coefficient prediction issues which ultimately led to the determination of the data points that were selected for the test matrix.

As discussed previously the Streamtube Curvature (STC) Computer Program (Reference 14) was selected for use in predicting the meter discharge coefficients. The STC program was chosen for several reasons. Although it was developed for predicting transonic flowfields about nacelles, this author's experience with it in predicting internal flowfields having all subsonic Mach numbers throughout has been very good. Because the program utilizes a streamline-orthogonal line coordinate system and global mass conservation is an integral part of its solution procedure (see Appendix A), its use in cases such as this program (airflow determination) was natural. The boundary layer program chosen for use in this effort was that of J.E. Harris, Reference 18.

In order to determine the theoretical discharge coefficient based on the throat wall static pressure, STC and boundary layer solutions were obtained over the complete range of anticipated airflows. Since the STC program requires overall airflow as an input, the procedure is simple. It is as follows:

1. Specify the desired total airflow, W_{STC}. The program output is the wall static inviscid pressure distribution.

2. Based on the computed pressure at the location of the static taps (X = 4.031) calculate an ideal one dimensional airflow, W_{id}, using the same values of stagnation pressure and temperature as specified in the STC solution, and the physical area at the static tap location.

3. Compute the potential flow discharge coefficient, $C_{D_{POT}}$.

$$C_{D_{POT}} = \frac{W_{STC}}{W_{id}}$$

4. From the boundary layer solution obtained from the pressure distribution in step 1, find the value of the displacement thickness at the static tap location.

5. Compute the displacement thickness blockage coefficient, $C_{D_{\delta^*}}$

$$C_{D_{\delta^*}} = 1 - 4\delta^*/D$$

where D is the diameter at the static tap location.

6. Compute the overall discharge coefficient, $C_{D_{SW}}$.

$$C_{D_{SW}} = C_{D_{POT}} * C_{D_{\delta^*}}$$

7. Utilizing the calculated boundary layer displacement thickness, adjust the value of wall static pressure at the throat metering plane location to account for the viscous blockage. This yields the final value of wall static pressure P_{SW} that corresponds to the discharge coefficient, $C_{D_{SW}}$, determined in Step 6.

This process is repeated for each input flow rate and a curve of $C_{D_{SW}}$ versus P_T/P_{SW} is obtained. Figures 14, 15, and 16 show the predicted wall static pressure distributions, throat displacement thickness, and predicted discharge coefficient versus wall static pressure ratio respectively. The equation given in Figure 16 is simply derived from a curvefit of the calculated points. The meter

discharge coefficient depends on only two components, an inviscid part that accounts for the radial pressure variation in the throat, and a viscous part that accounts for the effective boundary layer blockage.

The inviscid part of the discharge coefficient, $C_{D_{POT}}$, depends only on the meter geometry and is independent of scale. The viscous part is Reynolds number dependent and thus depends on the model size, pressure and temperature. The potential flow and viscous flow parts of the overall discharge coefficient are also shown in Figure 16. For other scale size meters only the viscous component, $C_{D\delta^*}$ would change. The boundary layers were calculated assuming a stagnation point at the intersection of the 12.25 inch diameter adapter pipe and the radial extension of the "hilite" point at the start of the meter contracting section (See Figure 10). Since the meter was to be tested with atmospheric discharge, the stagnation pressure was varied to produce the flow rate changes. At the highest flow rate of the test the meter Reynolds number based on throat diameter was approximately 2.98×10^6 and at the lowest flow it was approximately 4×10^5. This rather low range of Reynolds numbers coupled with the overacceleration and then diffusion at the entrance to the meter throat (see Figure 11) resulted in a computed laminar separation there. In order to overcome this, it was assumed that the laminar separation was followed by a

was followed by a turbulent re-attachment and transition was initiated at this location for all the boundary layer computations. It was felt that the extent to which this was a valid assumption would be determined from the test results.

For very large meters of this same design, boundary layer transition can occur upstream of the entrance to the throat cylindrical section, the distance upstream depending on the physical size of the meter as well as the Reynolds number. In order to determine the expected sensitivity of the overall discharge coefficient to the transition location for the test, transition was initiated just downstream of the stagnation point so an all turbulent $C_{D\delta}^*$ could be calculated for the range of test Reynolds numbers. These results are shown in Figure 17 and are indicated by the dashed line.

Chapter V

TEST FACILITY, APPARATUS, AND PROCEDURE

5.1 TEST FACILITY

All tests were performed in Channel 12 at FluiDyne's Medicine Lake Aerodynamics Laboratory. Channel 12 is a cold-flow static thrust stand normally used for exhaust nozzle testing. The basic arrangement of this facility is shown in Figure 18. High pressure dried air from the facility storage system was throttled, metered through an ASME long-radius critical flow metering nozzle and discharged to atmosphere through either the 6.9915-inch diameter ASME nozzle used for the probe calibration tests or the flow meter designed for this program.

5.2 TEST APPARATUS

5.2.1 ASME Nozzle

The 6.9915-inch diameter ASME long-radius flow metering nozzle was used for two purposes: (1) for facility checkout tests to demonstrate flow rate measurement accuracy prior to performing the non-standard flowmeter tests and (2) to provide the free-jet flow field to calibrate the pitot-static probe.

This ASME nozzle is shown in Figure 19. The test arrangement for both checkout tests and probe calibration tests is shown in Figure 20. The upstream adapter pipe contains three perforated plates and three screens for flow conditioning. Charging station instrumentation consists of three 8-probe area-weighted total pressure rakes and four wall static pressure taps.

5.2.2 Pitot Static Survey Probe

The pitot-static probe is shown in Figure 21. The probe consists of a coned-out forward facing total pressure orifice and four manifolded static taps. The probe extension is removable so that the stem may be installed in a small access hole from the inside of the flow meter. The probe support assembly and traverse mechanism bolts to the flow meter and is actuated by a screw drive capable of positioning the probe within approximately 0.010 inch of a specified radial location.

5.2.3 Flow Meter

The flow meter model of Figure 10 was fabricated from a single piece of aluminum. Figure 22 shows additional details of the model assembly. The meter was instrumented with 76 surface static pressure taps. Eight taps (every 45^{o}) were installed at the throat plane, X = 4.031, to accurately define the average wall static pressure, P_{sw}.

Four taps were installed in the model adapter between the charging station and the elliptical contraction. Both the pitot static probe and boundary layer survey probe access holes are located such that the surveys are all made at the throat plane, X = 4.031.

5.2.4 Boundary Layer Survey Probe

The flow meter throat boundary layer probe consisted of a .020-inch diameter stainless steel tube with a flattened, sharpened leading edge. The overall inspected height of the finished leading edge is .006-inch with wall thickness less than .001-inch. The center of pressure was assumed to be the geometric centroid of the probe face for all measurements, i.e., probe displacement corrections were judged to be negligible for such a small probe. Positive wall contact was determined with an electrical grounding light. A plastic sleeve insulated the probe stem from the model. The probe was clamped in a micrometer-drive traverse mechanism which had a radial positioning accuracy of $\pm$.0005-inch. Figure 23 shows the complete assembly of the flow meter with the upstream charging station instrumentation, pitot-static survey probe, and boundary layer survey probe installed. Also tabulated in Figure 23 are all static pressure tap locations.

5.3 TEST PROCEDURE

5.3.1 Pitot-Static Probe Calibration

The pitot-static probe calibration process requires extreme care since the magnitude of the pressure adjustments is small on an absolute basis. In order to produce an aerodynamic flow field of known Mach number and Reynolds number that duplicates the aerodynamic environment of the flow meter the free jet produced by the ASME nozzle discussed in Section 5.2.1 was used.

Figure 24 illustrates the relevant factors in the probe calibration. A free jet is used because after the flow has discharged from the jet producing nozzle, the streamlines will achieve an axial direction, and within a short distance of the nozzle exit (approximately one nozzle radius, R_j) the static pressure across the jet will be uniform and equal to the ambient pressure. Thus the reference pressure for the calibration is the ambient static pressure which can be measured with great accuracy. However, the nozzle diameter must be large enough such that the shear layer between the jet and the ambient air at the probe location, X, is small enough to allow a large inviscid core relative to a characteristic dimension on the probe, Dp.

If this is not the case the sensed pressure will not be representative of what the probe would "feel" if it were operating in an airstream of infinite extent relative to its diameter Dp. Figure 25 shows the results of a study that was performed using the STC computer program (Reference 14) to determine the minimum jet width required for the pressure at two points near an airfoil to be the same as that for the airfoil when it is in a jet of infinite width. It is seen that for jet widths larger than approximately 6 airfoil thicknesses the sensed pressure is the same as that for a jet of infinite width. This study suggests that when calibrating pressure probes and rakes in a free jet, care must be taken to assure the jet is large enough to be representative of the true aerodynamic environment they will be exposed to in the actual test.

Since the static pressure field associated with each static probe and support strut combination is unique to that particular design, every such design must be calibrated. For this test the probe was set on the centerline of the ASME nozzle, and aligned perpendicular to the nozzle exit plane. For tests with the probe inclined, the probe was in the vertical plane containing the nozzle centerline, and was set at the specified inclination angle with respect to horizontal. The specified distance between the nozzle exit and the probe tip (X_p, Figure 20) was then set. Tests were

performed at 0^{o} and $\pm 1^{o}$ pitch angle, and X_p=3.5 inches and 7 inches. The free-jet Mach number was set between 0.25 and 0.85.

The manifolded static pressure taps were connected to 10 ports of a Pressure Systems Inc. (PSI) multi-port pressure transducer. The total pressure orifice was connected to 4 ports of the PSI unit. The ASME adapter charging station instrumentation was also hooked up to the PSI unit. All instrumentation lines were leak-checked prior to testing.

5.3.2 Throat Static Pressure Profile Surveys

The calibrated pitot-static probe was installed in the flowmeter model and secured to the screw drive traverse mechanism. The probe instrumentation hookup was the same as for the probe calibration. The 8 throat static taps at X = 4.031 and the 28 charging station taps were also hooked up. The probe was centered on the flow meter centerline; probe axial alignment was facilitated by slipping the probe tip into the centering hole of a plug (sized to fit in the throat). The plug was removed and the airflow started. The probe was moved to the ten specified radial positions where the probe pressures, charging station pressures, and throat static pressures were all acquired.

5.3.3 Flow Meter Airflow Calibration

All charging station and meter static presure instrumention was hooked up to the PSI unit. The meter total pressure (P_{T_1}) was measured with a Statham differential pressure transducer referenced to atmosphere. Atmospheric pressure was determined by averaging the readings from 14 atmospheric reference ports in the PSI unit. The calibration of the PSI unit was referenced to a Haas mercury barometer. The meter total temperature (T_{T_1}) was measured using a shielded iron-constantan thermocouple.

Outputs from the Statham transducer and the thermocouple were measured and recorded with a VIDAR data acquisition system. Beginning zeros were taken before the start of a run, and up to 5 data points were obtained before shutting down and taking end zeros.

5.3.4 Throat Boundary Layer Surveys

The boundary layer probe was installed in the meter, secured to the micrometer drive mechanism, and connected to 4 ports of the PSI unit. The 8 bellmouth throat static and 28 charging station taps were also hooked up.

The probe was zeroed (just touching the wall as indicated by the electrical contact light) and the airflow started. The probe was moved to the 10 specified radial locations; probe pressures, charging station pressures and throat static pressure data were acquired at each location.

Chapter VI

TEST RESULTS AND DISCUSSION

The scale model test program consisted of four phases. The first phase consisted of calibrating the traversing pitot-static probe that was to be used for surveying the meter throat static pressure profiles.

The second phase involved obtaining the throat static pressure survey data. The third phase involved obtaining the overall discharge coefficient data using the in-series critical flow ASME standard nozzle, and in the final phase the meter throat boundary layer surveys were made.

6.1 PITOT-STATIC PRESSURE PROBE CALIBRATION

Figure 26 shows the calibration results for two axial placements of the probe. It was expected that both placements would yield the same results. In addition it was expected that for low Mach numbers the calibration would yield a pressure coefficient near zero since the probe was designed to keep the static ports out of the influence of both the nose and the aft support rod.

The fact that this didn't happen illustrates the importance of calibrating static pressure survey devices whatever their intended use may be.

6.2 METER THROAT STATIC PRESSURE SURVEYS

Throat static pressure profile surveys were obtained at three flow rates which spanned the operating range of the meter. The procedure used to obtain the data was as follows:

1. Set the probe position at the meter centerline.

2. Establish the desired throat pressure ratio using the charging station total pressure rakes and the 8 throat wall static pressure taps.

3. Read the probe static pressure.

4. Move probe to next radial position.
   For each survey readings were obtained at nine radial positions.

Figure 27 shows the survey results adjusted for the effects of the probe calibration shown in Figure 26. Also shown in this figure are the theoretically predicted profiles. All

of the profiles shown are normalized by the centerline value of Mach number. This was done because the stagnation pressure in the upstream supply tanks could not be maintained at a constant value during the course of a complete survey. Figure 28 shows the potential discharge coefficient, $C_{D_{POT}}$, obtained by integrating the measured profiles from Figure 27. Although the experimentally derived potential discharge coefficients agree reasonably well with the theoretical predictions, it is felt that this was somewhat fortuitous because of the disagreement between the measured and predicted radial pressure profiles shown in Figure 27. Although it was anticipated at the outset of the program that the presence of the survey probe in the meter would have some effect on the local flow field around the probe, it was not expected to be as large as the measurements subsequently indicated. The probe produced both a blockage effect and a flow field distortion which the following paragraphs describe.

In order to determine the impact of the variable blockage on the throat plane average wall static pressure, the following steps were taken. A plot of the stagnation-to-throat wall static pressure ratio, P_T/P_{SW}, versus overall pressure ratio, P_T/P_{amb}, was made for all the test runs that were conducted without the survey probe installed. This plot is shown in Figure 29. The curvefit of this data is indicated

by the solid line. For each of the probe survey test runs a corresponding plot was made. These results are shown in Figure 30, 31, and 32. In each figure the lower curve is the actual measured data, and the upper curve is computed from the curvefit of Figure 29 at the overall pressure ratio that existed at the time in the survey that the actual measurement was made. Therefore each symbol represents the pressure ratio that existed when the probe was at the indicated radial position, (r/R). In each of these figures the survey was started at the highest overall pressure ratio and completed at the lowest indicated pressure ratio. The convergence of these two curves at the lower pressure ratios, (as the probe is withdrawn from the model) is a direct measure of its blockage effect.

Figures 33, 34, and 35 show the circumferential variation in the throat wall static pressures for three radial positions of the survey probe for the highest nominal overall pressure ratio. From these figures it is seen that the probe produces a major distortion in the throat as well as an altering of the absolute level of pressure such that nearly all of the taps fall outside of the $\pm$0.1% airflow error band. Although not shown, the survey probe produced the same levels of distortion at the lower overall pressure ratios P_T/P_{amb} as well. It is also seen in Figures 33

through 35 that the wall static pressure at the 45° circumferential location (which is nearest the 30° traverse plane) is significantly higher than that implied by the calibrated pitot static probe. This suggests that the free jet calibration of the pitot static probe is inadequate when the probe will be used in a confined flow field such as a sub-critical flow meter or engine bellmouth.

6.3 MEASURED DISCHARGE COEFFICIENTS

Figure 36 shows the measured discharge coefficients based on the ASME critical flow metering nozzle calibrations compared with the pre-test predictions for both natural transition and an all turbulent boundary layer assumption. Table I is a tabulation of all the measured discharge coefficients that are plotted in Figure 36. The agreement between the predicted discharge coefficient for natural transition and the measured data is excellent except at the lowest pressure ratio of 1.01 where larger scatter was expected. At pressure ratios above approximately 1.3 the measured results tend to fall away slightly from the natural transition predictions. In order to understand the reason for this behavior a boundary layer trip was placed in the contracting section of the meter. It was located as shown in Figure 37. Number 100 garnet sandblasting grit, having a mean particle diameter of 0.006 in., was used for the trip. This grit

size was chosen to initiate transition immediately downstream of the trip using the criteria of Reference 19. Its location was chosen such that it was far enough upstream on the meter wall to represent as closely as possible an all turbulent boundary layer, but far enough downstream such that relaminarization would not occur in the strong favorable pressure gradient in the contracting section. After application of the boundary layer trip nine more data points were obtained. These data are shown in Figure 38 along with the natural transition data. The difference between the tripped and untripped data is very close to the difference between the natural transition and all turbulent boundary layer predictions. These results suggest that the slight fall away of the data from the predictions was due to the real boundary layer displacement thickness being larger than predicted at pressure ratios above about 1.3.

6.4 BOUNDARY LAYER SURVEYS

Four boundary layer surveys were made at the meter throat. Three surveys were done without the boundary layer trip installed, and one was made with it installed. In order to obtain maximum accuracy in determining the boundary layer integral thicknesses as well as skin friction coefficient, compressible Law of the Wall-Law of the Wake curvefits of the measured data were obtained using a program specifically

written for this purpose. Once the curve-fits of the measured data were obtained, they were then integrated to obtain the displacement thickness and momentum thickness. Figures 39, 40 and 41 show the measured data points along with the corresponding curvefits for the three natural transition cases. Figure 42 shows the same information for the tripped boundary layer.

Figures 43 through 46 show comparisons of the measured boundary layer profiles with the pre-test predictions and Figure 47 summarizes all of these results. Figure 47 shows that for the natural transition cases the predictions are in excellent agreement with the measurements. It is also seen that the measured boundary layer for the tripped case is not as thick as was predicted. This difference would represent a difference in discharge coefficient of less than 0.1%.

Since the boundary layer surveys indicate excellent agreement with predictions for the natural transition cases, and the measured boundary layer is not as thick as predicted for the tripped case, the difference between the predicted and measured discharge coefficients in Figure 38 cannot be explained on the basis of boundary layer differences alone. Since the measured boundary layers are slightly thinner than predicted the original hypothesis of a thicker than expected

boundary layer being responsible for the lower than predicted discharge coefficients at pressure ratios above 1.3 was incorrect.

6.5 WALL PRESSURE DISTRIBUTIONS

Since differences between the predicted and measured boundary layers did not explain the differences between the predicted and measured discharge coefficients in Figure 38, further examination of the inviscid or potential flow predictions was necessary. In order to make direct comparisons between the predicted and measured pressure distributions one must make use of the predicted discharge coefficient curve itself. This is accomplished by computing the flow rate for the wall static pressure ratio of the data point to be compared, and then using that flow rate as input for the STC solution. This was done for six test data points that spanned the range of meter operation. When using this procedure the predicted pressure at the meter throat station (X = 4.031) should exactly match the average of the eight wall static taps for the given operating pressure ratio.

Figures 48 through 50 show the measured wall static pressures at the throat station for the six meter pressure ratios for which the comparisons with predictions were made.

Except for the lowest pressure ratio (data point 6, Figure 48), the circumferential variation of static pressure was extremely small, indicating very uniform flow within the meter.

Figures 51 through 53 show the axial distributions of measured wall static pressure compared with the predictions using the STC program for the same six data points. The agreement is seen to be excellent over the full length of the meter. The slight disagreement near the exit of the meter is characteristic of an uncoupled inviscid diffusing flow field calculation which is adjusted for the calculated boundary layer displacement thickness.

The excellent agreement between the measurements and predictions of the throat radial static pressure profiles and the wall axial static pressure profiles suggests that the slight disagreement between predicted and measured discharge coefficients at high pressure ratio is not due to the inviscid flow field being different than predicted.

6.6 CHARGING STATION REFERENCE PRESSURE

Since the difference between the predicted and measured discharge coefficients was not explained by differences between predicted and measured throat boundary layers the

charging station pressure measurements were examined more closely. The meter discharge coefficient is defined as the ratio of the measured flow from the reference standard critical flow ASME metering nozzle to the computed ideal flow based on the pressure ratio P_T/P_{SW}, where P_T is the measured charging station total pressure and P_{SW} is the average wall static pressure in the meter throat. As shown in Figures 48 through 50 the average throat wall static pressure as determined from a numerical average of the eight static pressure taps has a very small uncertainty. These figures show that the implied uncertainty in airflow due to an error in P_{SW} is significantly less than 0.1% at pressure ratios above 1.3. These static pressure measurement errors may be ruled out as an explanation for the difference.

Figures 54 through 56 show the charging station total pressure profiles for each of the three rakes over the range of throat wall static pressure ratios. Since the probes were located at centers of equal annular area within the duct, the individual probe readings may be arithmetically averaged to obtain an area averaged total pressure for the flow entering the meter.

It is seen that rake 1 (located 5 degrees from vertical) has a generally decreasing pressure toward the duct wall whereas rakes 2 and 3 have generally flatter profiles. Since only

three rakes were used to measure the charging station pressure it cannot be determined whether distortions large enough to cause a flow error of approximately 0.10% existed at circumferential locations where the pressure was not measured. However it would seem unlikely that such a distortion existed. In order to cause a discharge coefficient error of 0.10% at a throat wall static pressure ratio of 1.5 the average charging station pressure would have to be lowered by 0.2%. This would mean that local pressures at other circumferential locations would have to be considerably less than those for the lowest values shown for rake 1. If distortions that large were to exist in the flow field, there would likely be greater scatter in the wall static pressures elsewhere in the meter. Since such scatter was not seen it was concluded that distortion in the charging station total pressures were not likely any larger than indicated in Figures 54 through 56.

Chapter VII

CONCLUSIONS AND RECOMMENDATIONS

7.1 CONCLUSIONS

A comprehensive subcritical flowmeter design and test program has been conducted which clearly demonstrates that current theoretical methods can predict discharge coefficients to within 0.25% of those obtained from calibration with an industry standard critical flow ASME nozzle. To this author's knowledge this is the only such program that has ever been conducted on a subcritical flow metering device which demonstrates this high level of accuracy.

Airflow measurements made with a boundary layer trip, as well as meter throat boundary layer surveys clearly show the importance of transition location on accurate discharge coefficient predictions. Detailed surveys of the meter throat flow field demonstrate that such surveys are not capable of measuring the radial static pressure profiles with sufficient accuracy to determine discharge coefficient to within 0.25%. The survey probe produces disturbances which alter the flow field being measured. Freejet calibration of the survey probe are incapable of correcting for these effects.

Comparisons of theoretically predicted wall static pressure distribution with measured data suggests that as long as the flow remains subsonic newer time dependent Euler methods, or even Navier-Stokes solvers, probably cannot improve upon the accuracy of the STC method because the agreement is nearly perfect.

7.2 RECOMMENDATIONS

It is recommended that the meter designed for this program, or variations of the basic design, be adopted as a standard for low pressure loss subcritical airflow metering. The upstream contracting section and the cylindrical throat section produce a predictable inviscid flow field with extremely small distortion. The diffusing section area ratio may be altered to suit the circumstances of a particular flow measurement situation.

It is recommended that the flow meter hardware used for this investigation be utilized to establish its discharge coefficient behavior over a wider range of pressure ratios and Reynolds numbers. Pressure ratios should be increased to near critical to determine how the potential part of the overall discharge coefficient approaches its maximum value. This could be done in conjunction with theoretical calculations to study the influence of the overacceleration

and rapid diffusion which occurs at the entrance to the cylindrical throat section. As the meter pressure ratio is increased to near its critical value this will develop into a shock wave. Since the model has a large number of static pressure taps and a throat boundary layer survey probe measurements could be made of the shock boundary layer interaction. The meter was designed with a large flange at its exit location so that it could be connected to a vacuum supply instead of discharging to ambient pressure. This would allow investigations to be made at reduced Reynolds numbers for laminar boundary layers. In addition it could be run over the same range of pressure ratios as was done for the present program but with varying back pressure to keep the Reynolds number constant, thus allowing the isolation of the Reynolds number effects from the potential flow effects.

Finally, as part of these same studies, it is recommended that the grit strip location and size be varied to determine if a more favorable location could be found for purposes of routine airflow measurements. In addition it would be useful to determine if surface roughening could be used instead of the application of grit. This would allow a more rugged boundary layer trip which would not be subject to erosion as is the case with the application of grit that is glued to the surface.

REFERENCES

1 Bond, M.M., "Volume Calibration of the Gas Storage Tank Used in the Primary Gas Flow Measurement Facility at Nunn, Colorado," Periodic Report prepared for National Aeronautics and Space Administration, August 15, 1969, under Contract SC-NSR 06-043-001.

2 Seidl, W. "Private Communication," Colorado Engineering Experiment Station, Nunn, Colorado, February 1989.

3 Arnberg, B.J., Britton, C.L., and Seidl, W.F., "Discharge Coefficient Correlations for Circular-Arc Venturi Flowmeters at Critical (Sonic) Flow," Journal of Fluids Engineering, June 1974, pp. 111-123.

4 Smith, R.E., Matz, R.J., "Verification of a Theoretical Method of Determining Discharge Coefficients For Venturis Operating at Critical Flow Conditions," Arnold Engineering Development Center Report No. AEDC-TR-61-8, September 1961.

5 Smith, R.E., Matz, R.J., "A Theoretical Method of Determining the Discharge Coefficients for Venturis Operating at Critical Flow Conditions,", Transactions of the ASME, Journal of Basic Engineering, pp. 435-446, December, 1962.

6 Stratford, B.S., "The Calculation of the Discharge Coefficient of Profile Choked Nozzles and the Optimum Profile for Absolute Air Flow Measurement," Journal of the Royal Aeronautical Society, Vol. 68, April 1964, pp. 237-245.

7 Oswatitsch, K. and Rothstein, W., "Flow Pattern in a Converging Diverging Nozzle," NACA TM 1215, March, 1949.

8 Tucker, M., "Approximate Calculation of Turbulent Boundary Layer Development in Compressible Flow," NACA TN 2337, April 1951.

9 American Society of Mechanical Engineers, Supplement to POWER TEST CODES. Chapter A: "Flow Measurement Part 5-Measurement of Quantity of Materials," ASME, PTC 19.5, April 1959.

REFERENCES

10 Smith, R.E. and Matz, R.J., "Performance Characteristics of an 8 Inch Diameter ASME Nozzle Operating at Compressible and Incompressible Conditions," Journal of Fluids Engineering, December 1973, pp. 542-550.

11 Holdhusen, J.S., and Peruse, D., "Determination of Discharge and Thrust Coefficients of a Choked ASME Nozzle From Exit Flow Surveys," FluiDyne Engineering Corporation Report 0470, Sept., 1965.

12 Rayle, R.E., "Influence of Orifice Geometry on Static Pressure Measurements," ASME Paper 59-A-234, Presented at ASME Annual Meeting, Atlantic City, N.J., Nov. 29 - Dec. 4, 1959.

13 Shapiro, Ascher H., "The Dynamics and Thermodynamics of Compressible Fluid Flow," Volume I, The Roland Press Company, New York, 1953.

14 Keith, J.S., Ferguson, D.R., Merkle, C.L., Heck, P.H., and Lahti, D.J., "Analytical Method for Predicting the Pressure Distribution About a Nacelle at Transonic Speeds," NASA CR-2217, July 1973.

15 Hsieh, T., "Hemisphere-Cylinder in Transonic Flow, M_O = 0.7 - 1.0," AIAA Journal, Vol. 13, No. 10, October 1975, pp. 1411-1413.

16 Weust, W., "AGARD Flight Test Instrumentation Series on Pressure and Flow Measurement," Agardograph No. 160, Vol. 11, July 1980

17 Krause, L.N., " Effects of Pressure-Rake Design Parameters on Static-Pressure Measurement For Rakes Used in Subsonic Free Jets," NACA TN 2520, October 1951.

18 Harris, J.E., and Blanchard, Doris K., "Computer Program for Solving Laminar, Transitional, or Turbulent Compressible Boundary Layer Equations for Two-Dimensional and Axisymmetric Flow," NASA Technical Memorandum 83207, 1982.

REFERENCES

19 Braslow, A.L., Hicks, R.M. and Harris, R.V., "Use of Grit-Type Boundary Layer Transition Trips on Wind Tunnel Models," NASA TN-D3579, 1968.

20 Smith, L.H., Jr., "The Radial-Equilibrium Equation of Turbo-Machinery," Journal of Engineering for Power, Trans. ASME, Series A, Vol. 88, 1966, pp. 1-12.

21 Novak, R.A., "Streamline Curvature Computing Procedures for Fluid Flow Problems," ASME Paper 66-WA/GE-3, 1966.

22 Katsanis, T., "Use of Arbitrary Quasi-Orthogonals for Calculating Flow Distribution in the Meridinal Plane of a Turbomachine," NASA TN D-2546, 1964.

23 Murman, E.M. and Cole, J.D., "Calculation of Plane Steady Transonic Flows," AIAA Journal, Vol. 9, No. 1, January 1971, pp. 114-121.

TABLE I

DISCHARGE COEFFICIENT TEST RESULTS

DATA POINT No.	P_T/P_{SW}	$R_{e_D} \times 10^{-6}$	$C_{D_{SW}}$
1	1.013	.535	.9826
2	1.014	.562	.9787
3	1.011	.500	.9704
4	1.012	.504	.9700
5	1.010	.473	.9715
6	1.012	.524	.9783
7	1.011	.498	.9737
8	1.107	1.514	.9837
9*	1.108	1.515	.9799
10*	1.109	1.514	.9791
11*	1.108	1.518	.9800
12	1.109	1.532	.9841
13	1.110	1.581	.9825
14	1.105	1.597	.9827
15	1.104	1.513	.9845
16	1.207	2.053	.9856
17	1.208	2.059	.9863
18	1.205	2.046	.9860
19	1.204	2.042	.9858
20	1.201	2.023	.9856
21	1.296	2.389	.9872
22	1.295	2.389	.9872
23*	1.295	2.373	.9842
24*	1.296	2.372	.9840
25*	1.296	2.382	.9831
26	1.299	2.415	.9885
27	1.286	2.384	.9886

* INDICATES GRIT STRIP INSTALLED

TABLE I

DISCHARGE COEFFICIENT TEST RESULTS
(Continued)

DATA POINT No.	P_T/P_{SW}	$R_{e_D} \times 10^{-6}$	$C_{D_{SW}}$
28	1.303	2.663	.9883
29	1.303	2.442	.9887
30	1.305	2.442	.9895
31	1.351	2.562	.9889
32	1.353	2.565	.9888
33	1.352	2.560	.9888
34	1.355	2.564	.9891
35	1.353	2.577	.9893
36	1.399	2.689	.9888
37	1.403	2.698	.9895
38	1.401	2.693	.9892
39	1.404	2.692	.9895
40	1.396	2.671	.9896
41	1.501	2.908	.9902
42*	1.498	2.869	.9876
43*	1.501	2.874	.9873
44*	1.500	2.885	.9871
45	1.500	2.899	.9902
46	1.500	2.901	.9903
47	1.504	2.893	.9913
48	1.499	2.889	.9913
49	1.502	2.916	.9910
50	1.503	2.940	.9912

* INDICATES GRIT STRIP INSTALLED

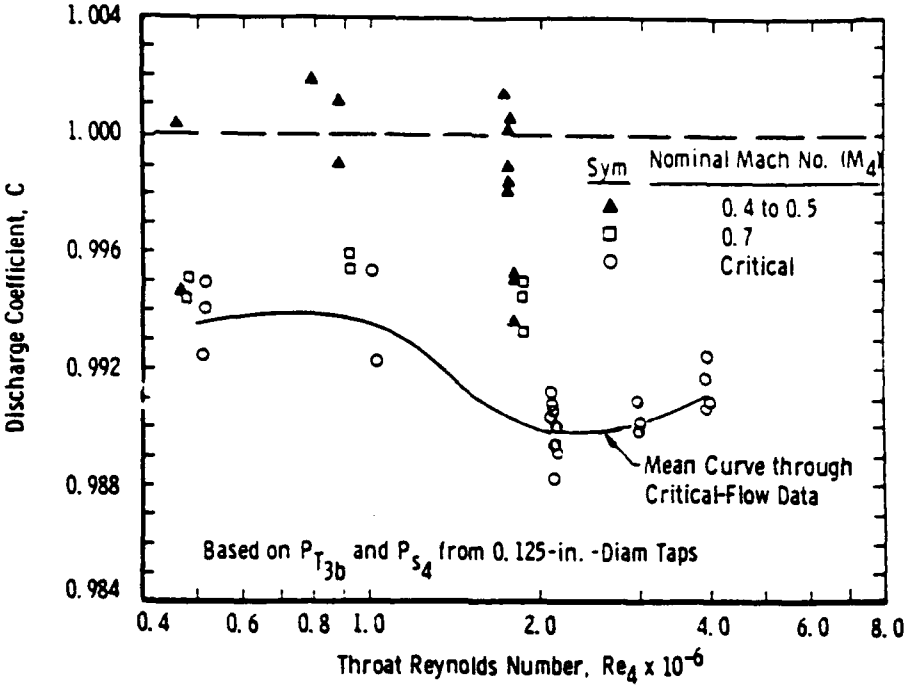

FIGURE 1a. ASME NOZZLE DISCHARGE COEFFICIENT BASED ON 0.125-IN.DIA. THROAT TAP READINGS-COMPRESSIBLE FLOW (AIR) TESTS.

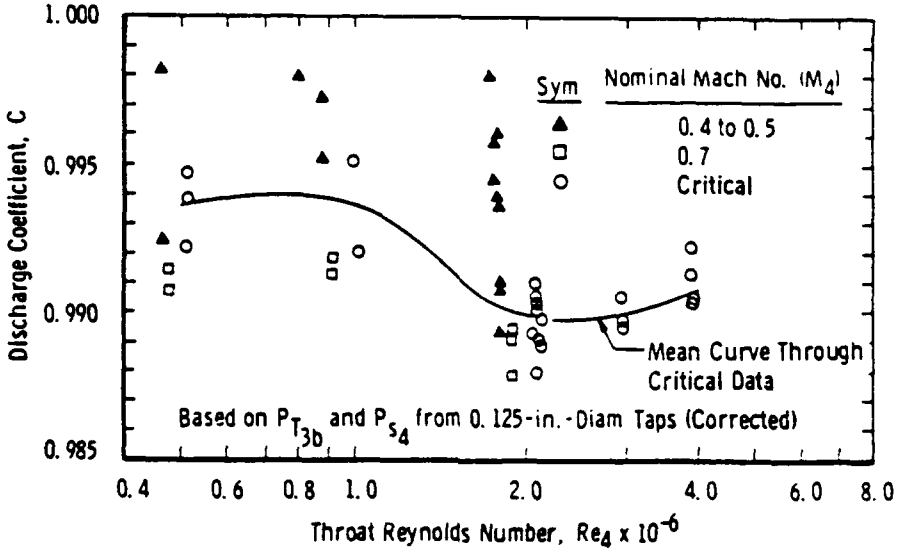

FIGURE 1b. COMPRESSIBLE FLOW ASME DISCHARGE COEFFICIENTS BASED ON CORRECTED THROAT TAP READINGS.

RESULTS FROM SMITH AND MATZ (REFERENCE 10) ASME SUB-CRITICAL FLOW METER CALIBRATION TEST.

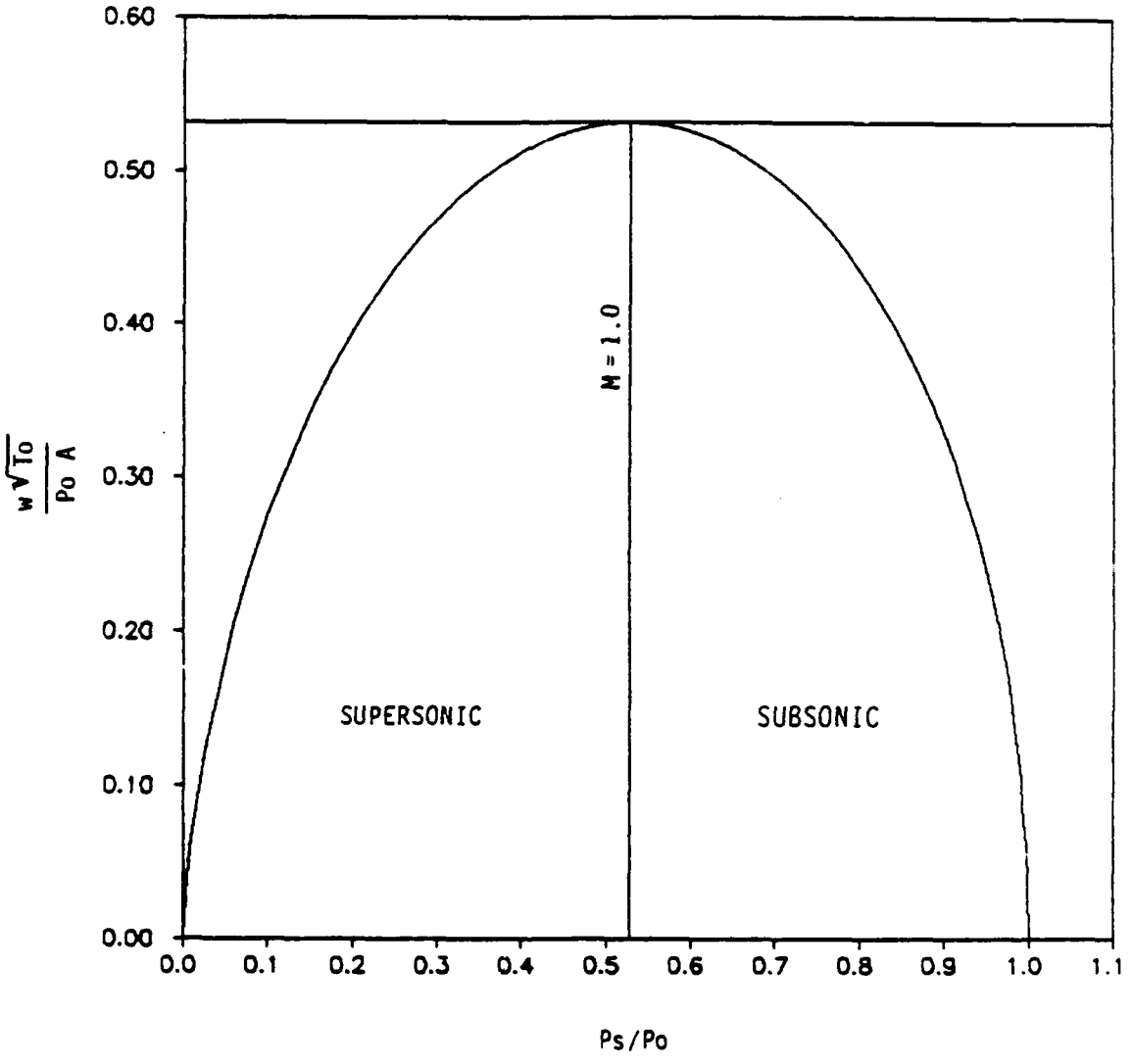

FIGURE 2. ISENTROPIC FLOW FUNCTION, γ = 1.4.

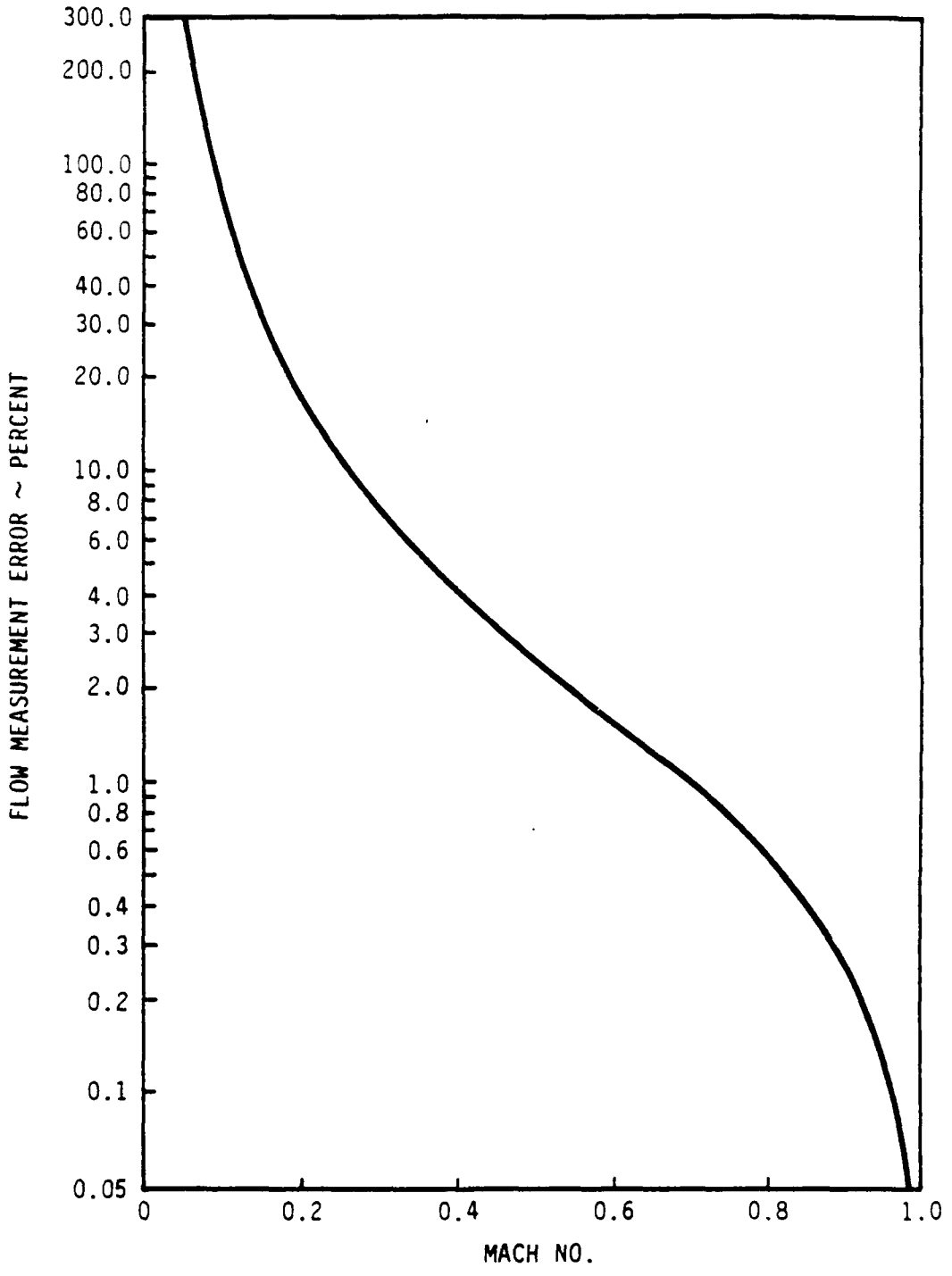

FIGURE 3. FLOW MEASUREMENT ERROR FOR 1% ERROR IN STATIC PRESSURE MEASUREMENT VERSUS MACH NUMBER.

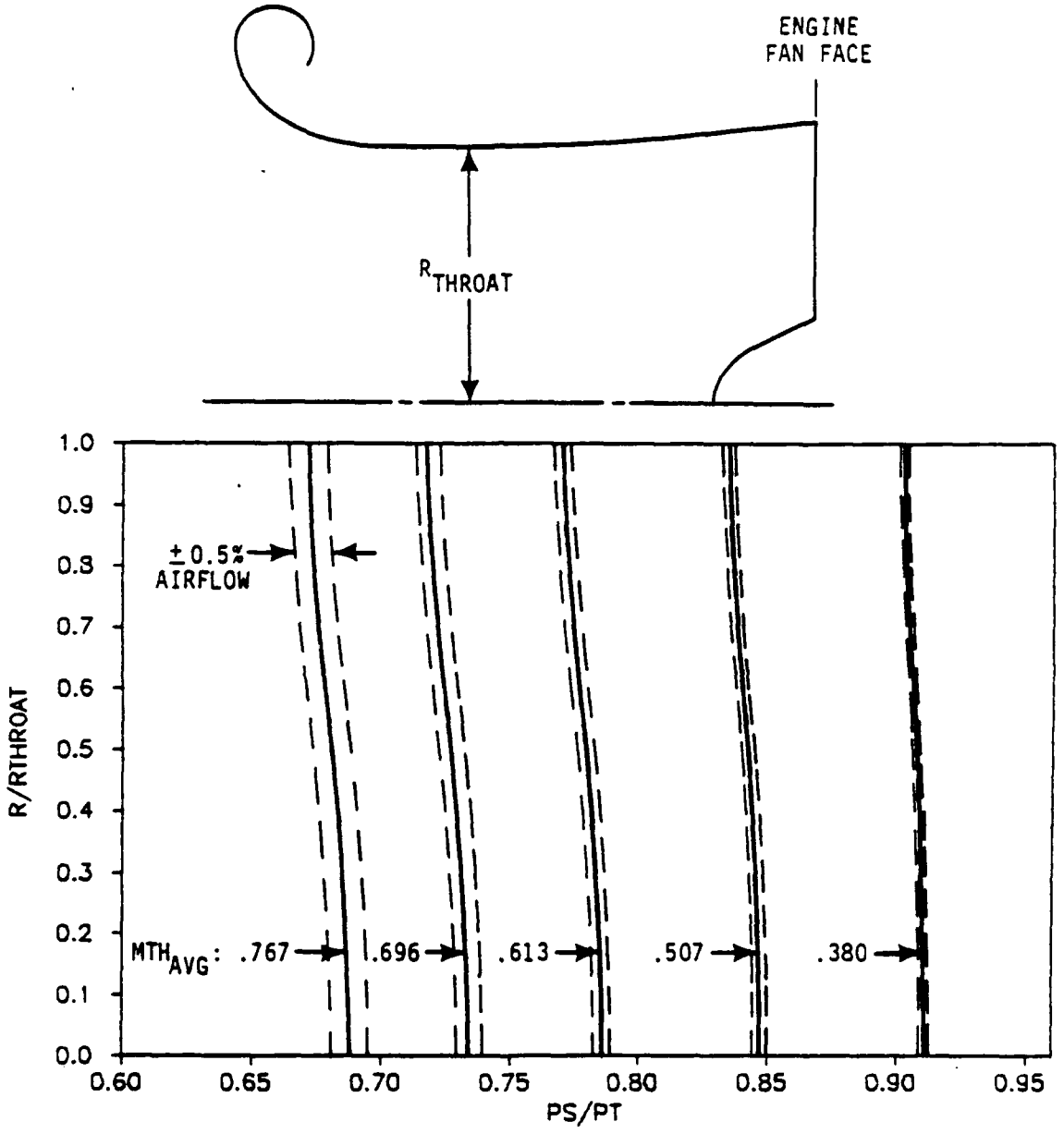

FIGURE 4. THROAT STATIC PRESSURE PROFILES.

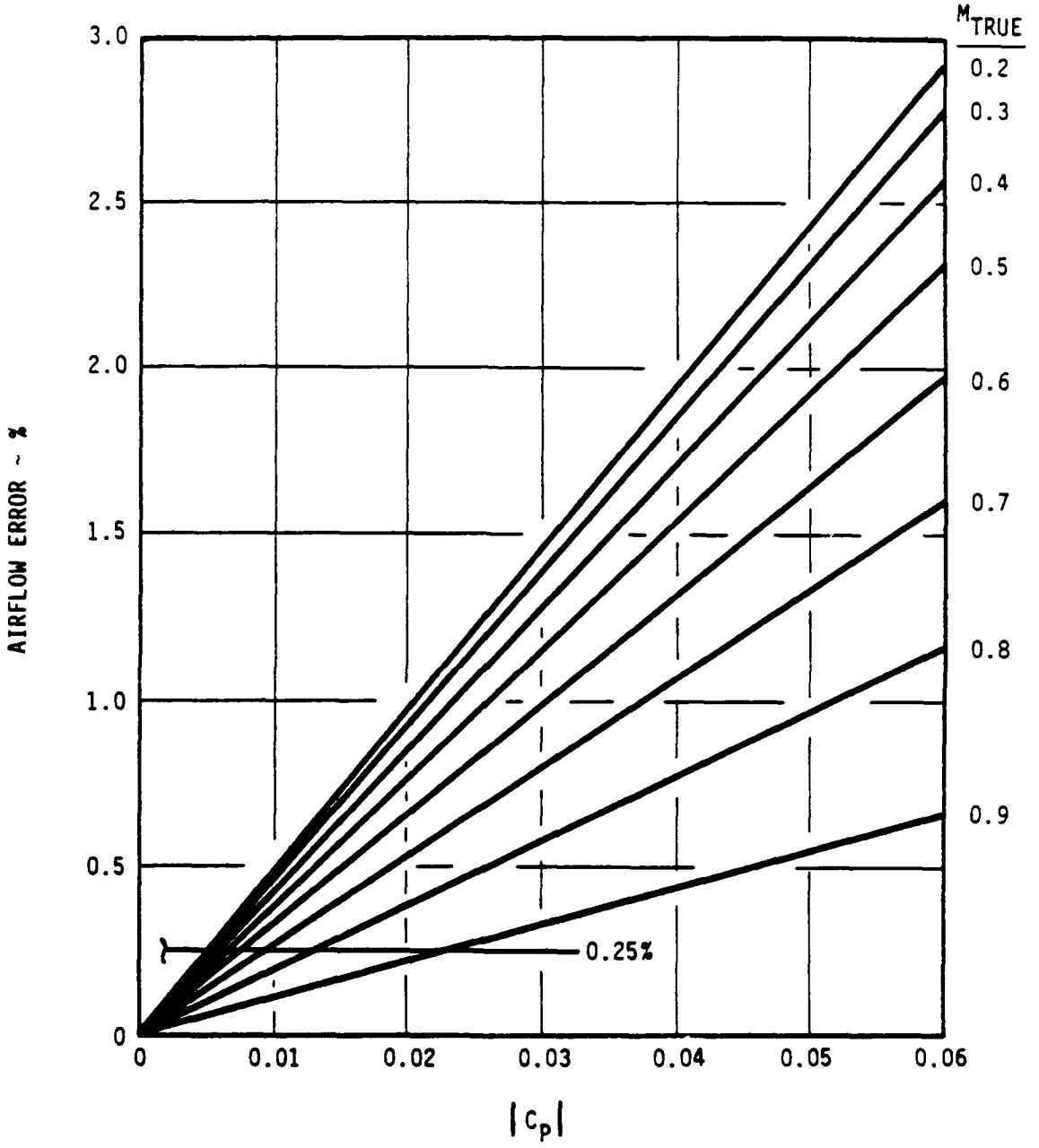

FIGURE 5. AIRFLOW ERROR VERSUS PRESSURE COEFFICIENT.

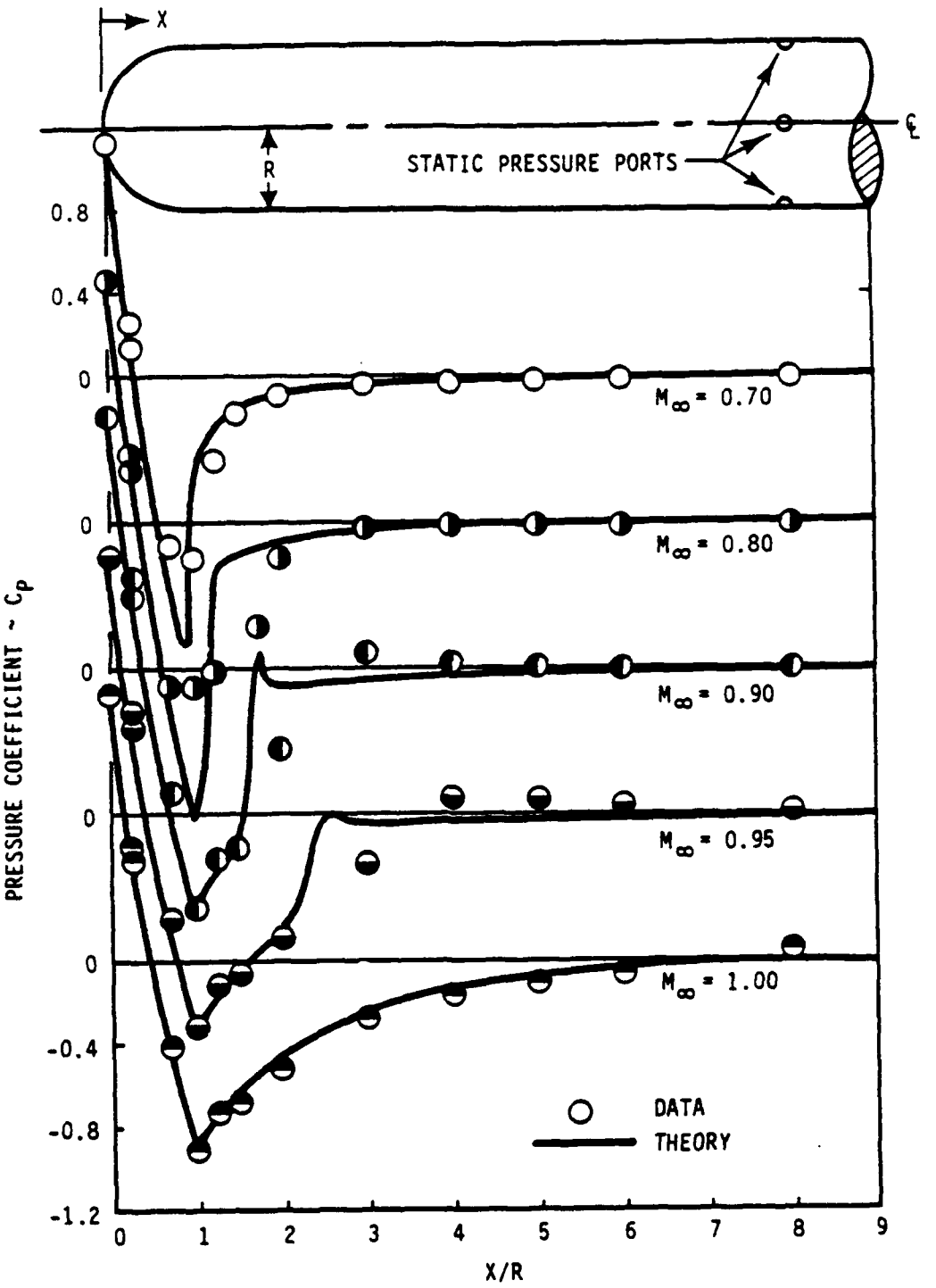

FIGURE 6. HEMISPHERICAL HEAD STATIC PRESSURE PROBE (REFERENCE 15).

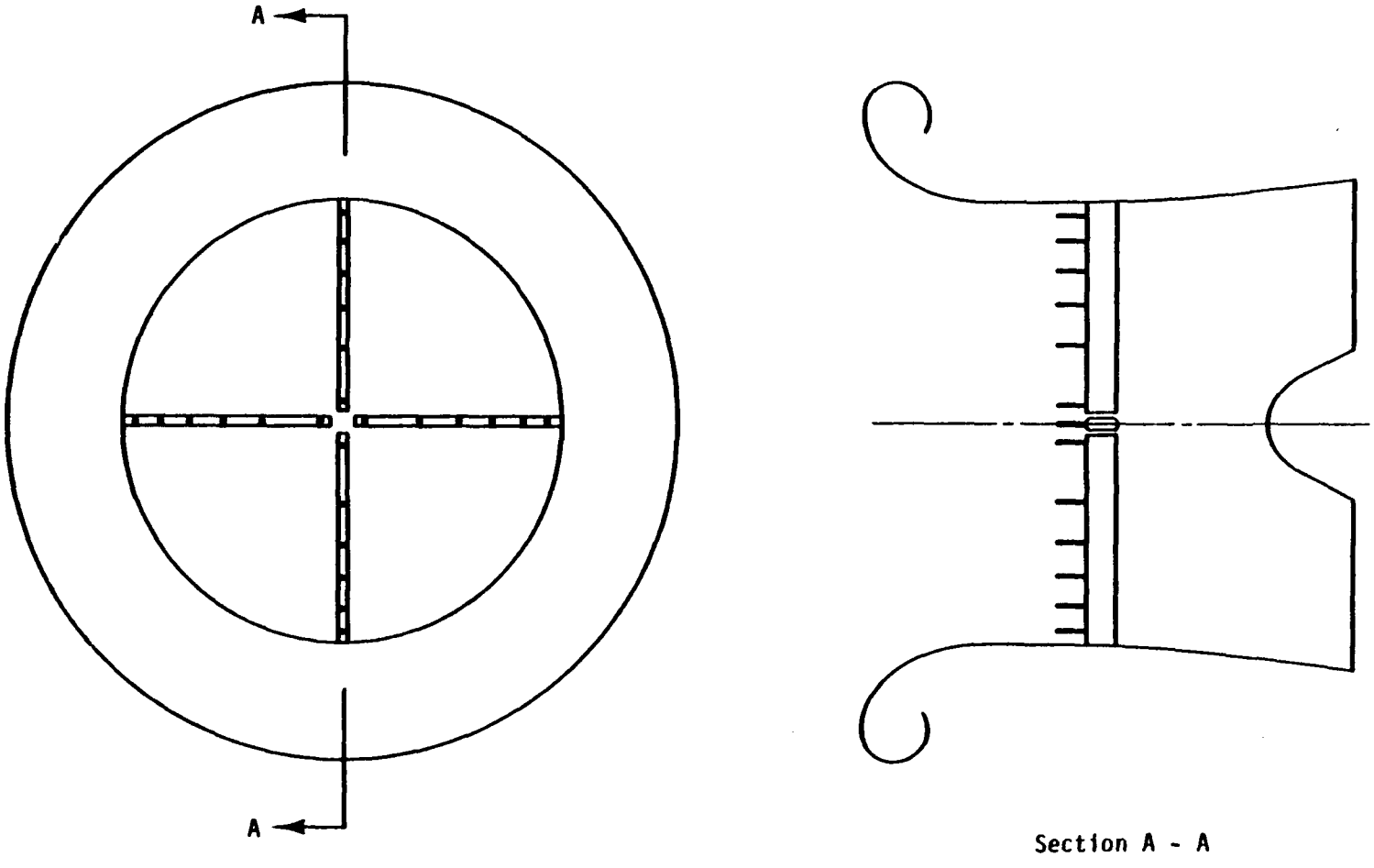

FIGURE 7. TYPICAL METER THROAT STATIC PRESSURE MEASUREMENT RAKE ARRAY.

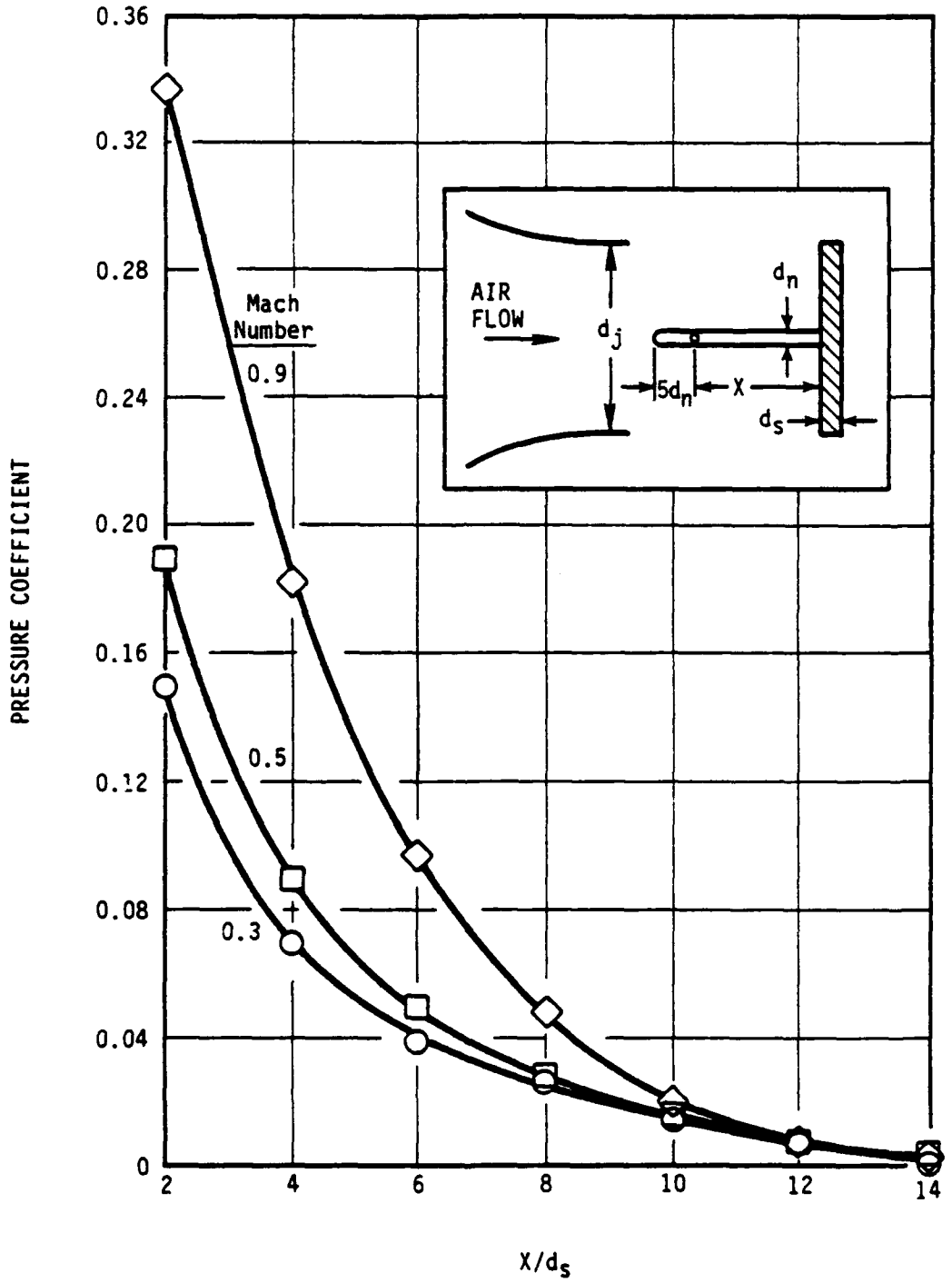

FIGURE 8. PRESSURE COEFFICIENT VARIATION FORWARD OF PROBE SUPPORT CYLINDER (REFERENCE 17).

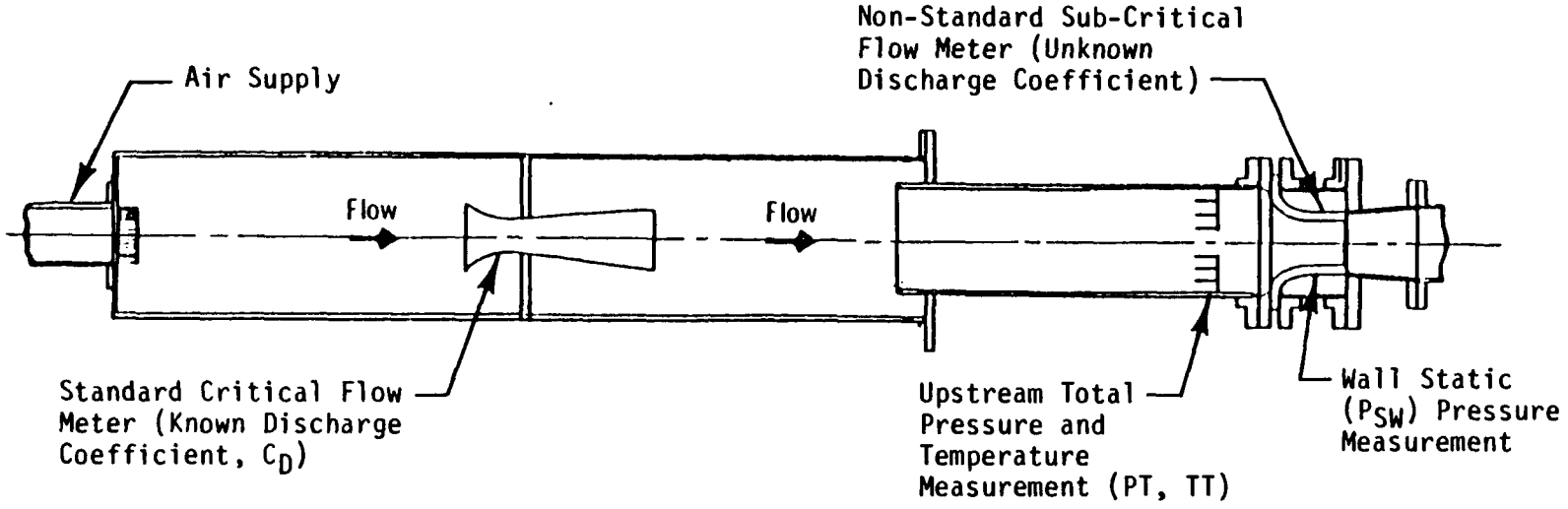

FIGURE 9. TYPICAL NON-STANDARD NOZZLE SECONDARY DISCHARGE COEFFICIENT CALIBRATION TEST SETUP.

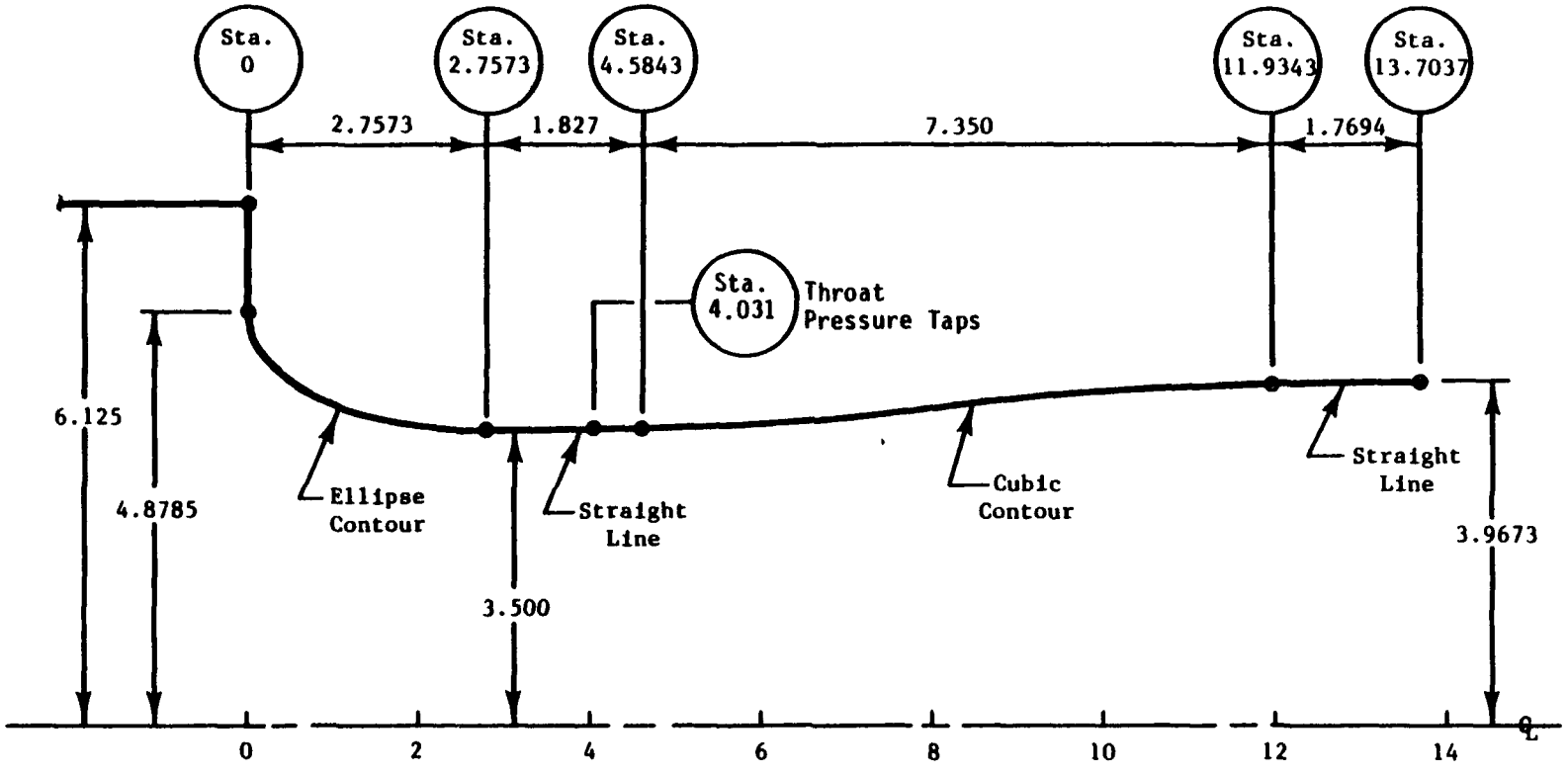

FIGURE 10. FLOW METER AERODYNAMIC CONTOUR DEFINITION.

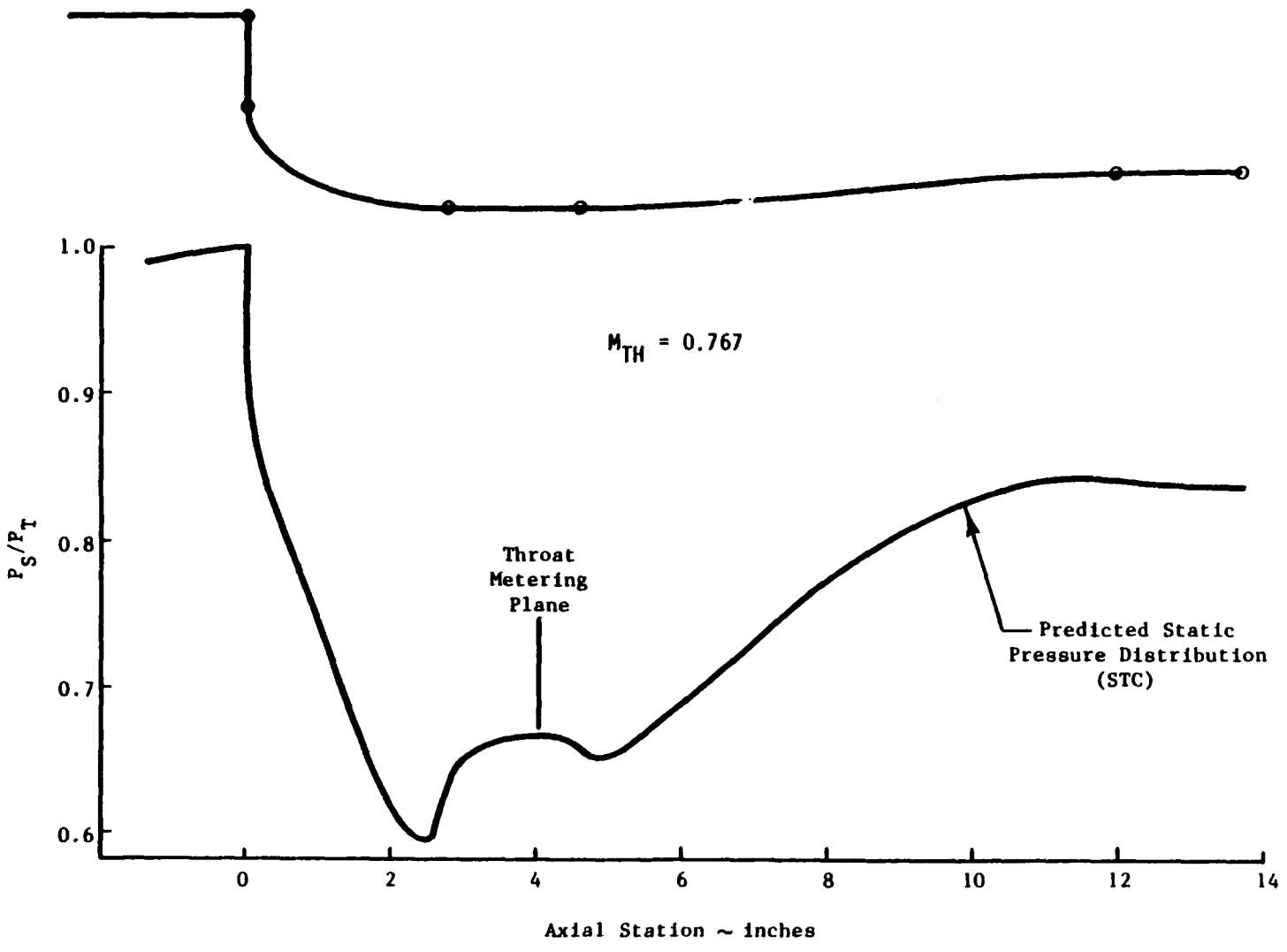

FIGURE 11. FLOW METER THEORETICAL PRESSURE DISTRIBUTION.

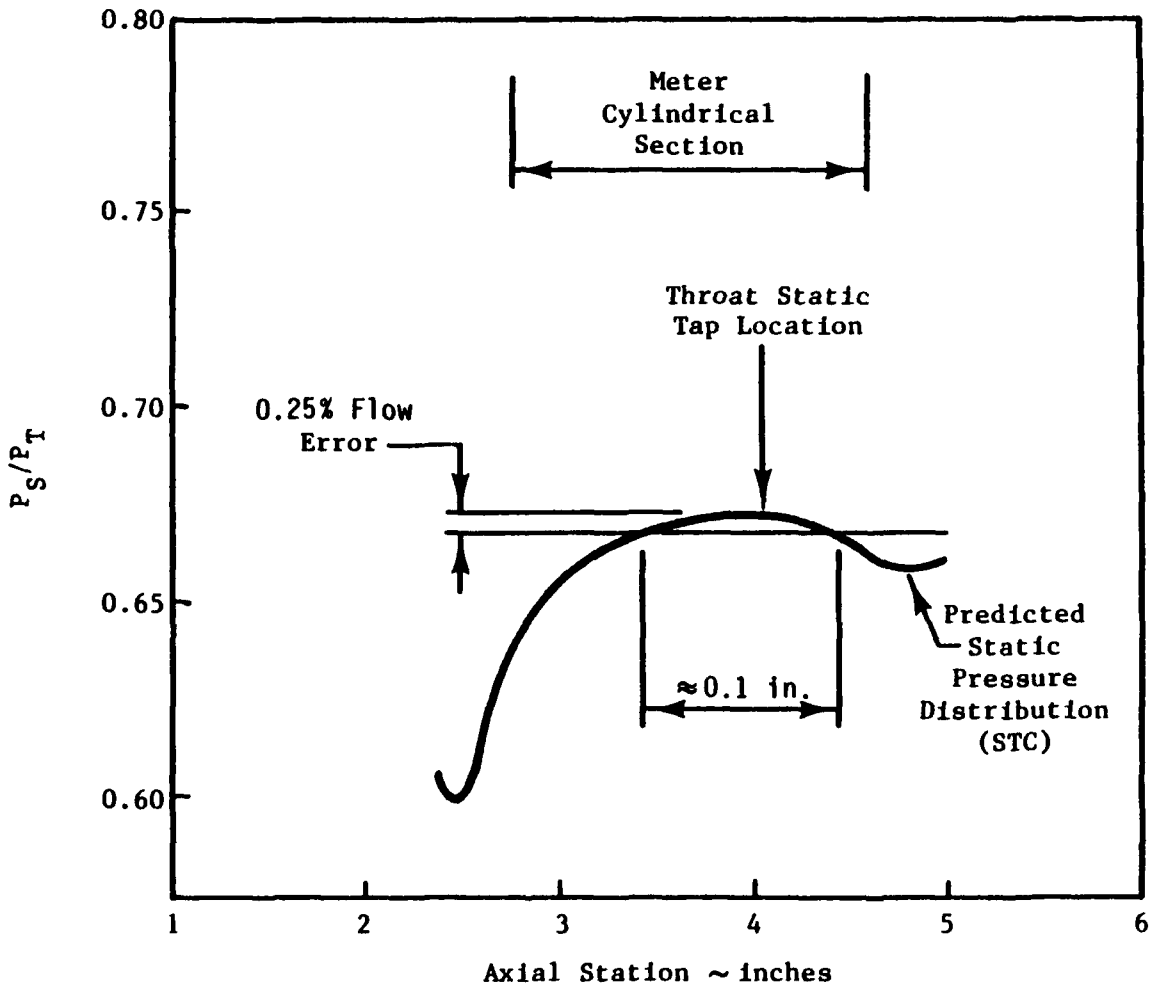

FIGURE 12. FLOW METER THEORETICAL PRESSURE DISTRIBUTION IN THROAT REGION.

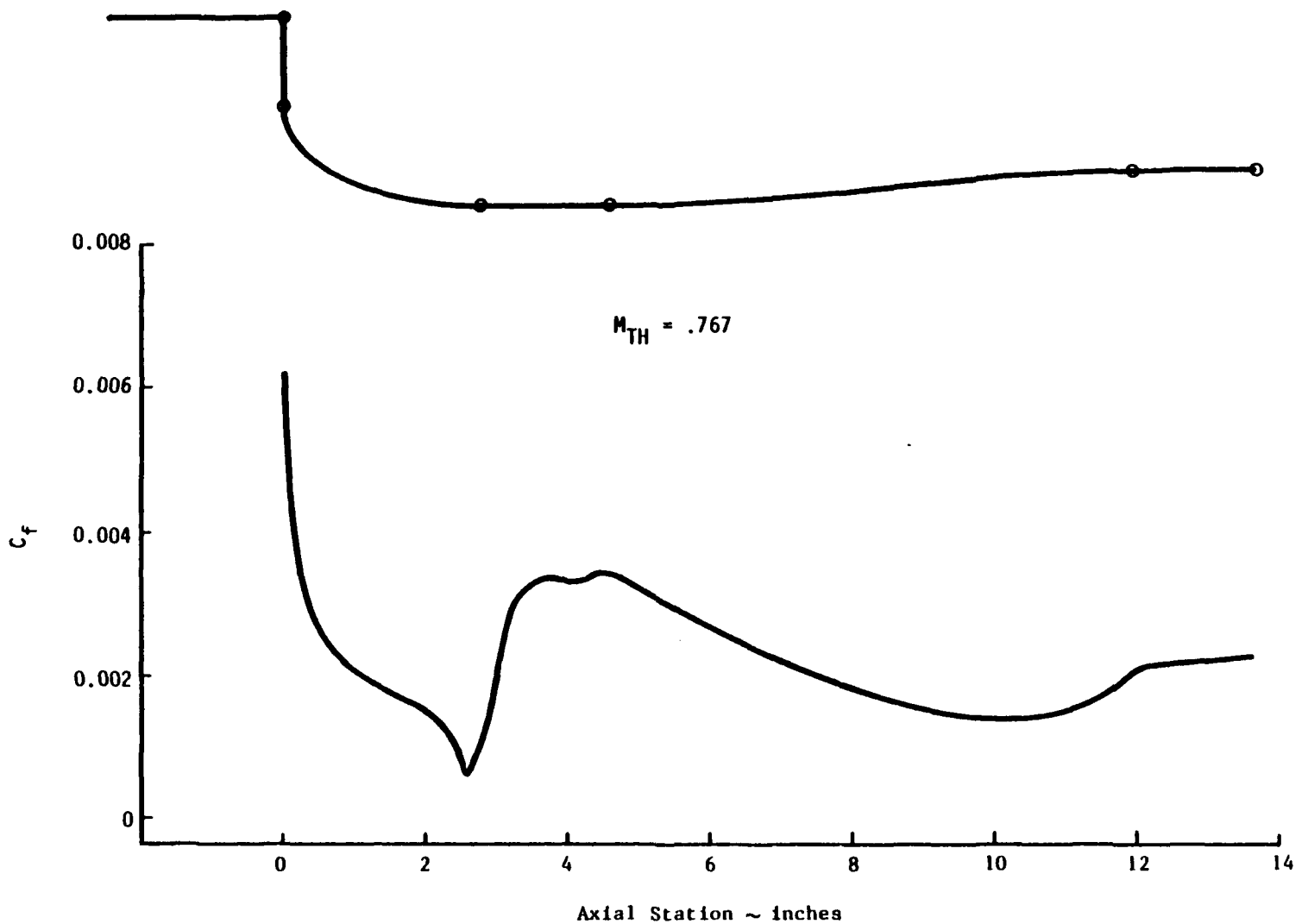

FIGURE 13. CALCULATED SKIN FRICTION COEFFICIENT FOR MAXIMUM THROAT MACH NUMBER.

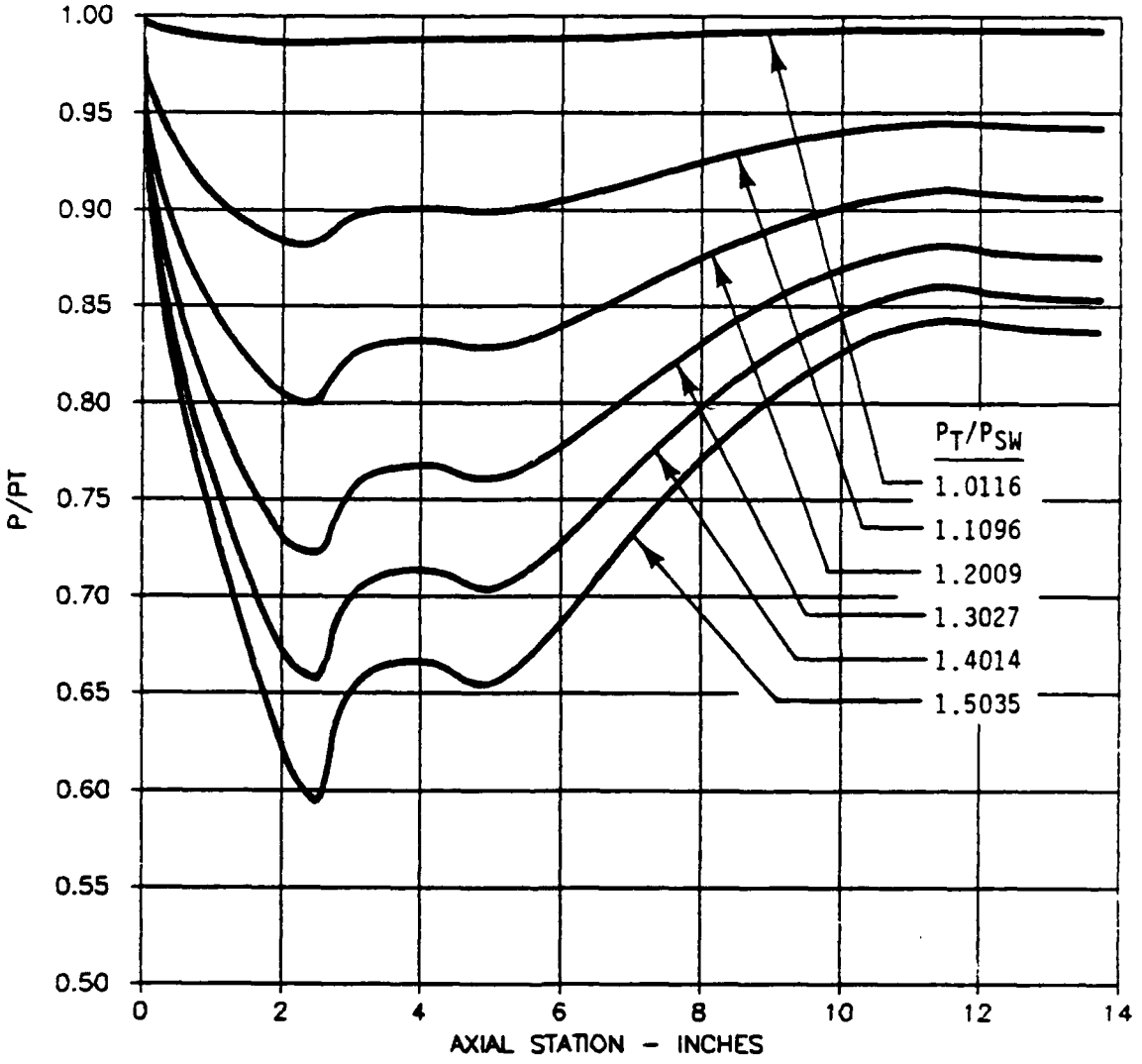

FIGURE 14. PREDICTED PRESSURE DISTRIBUTIONS.

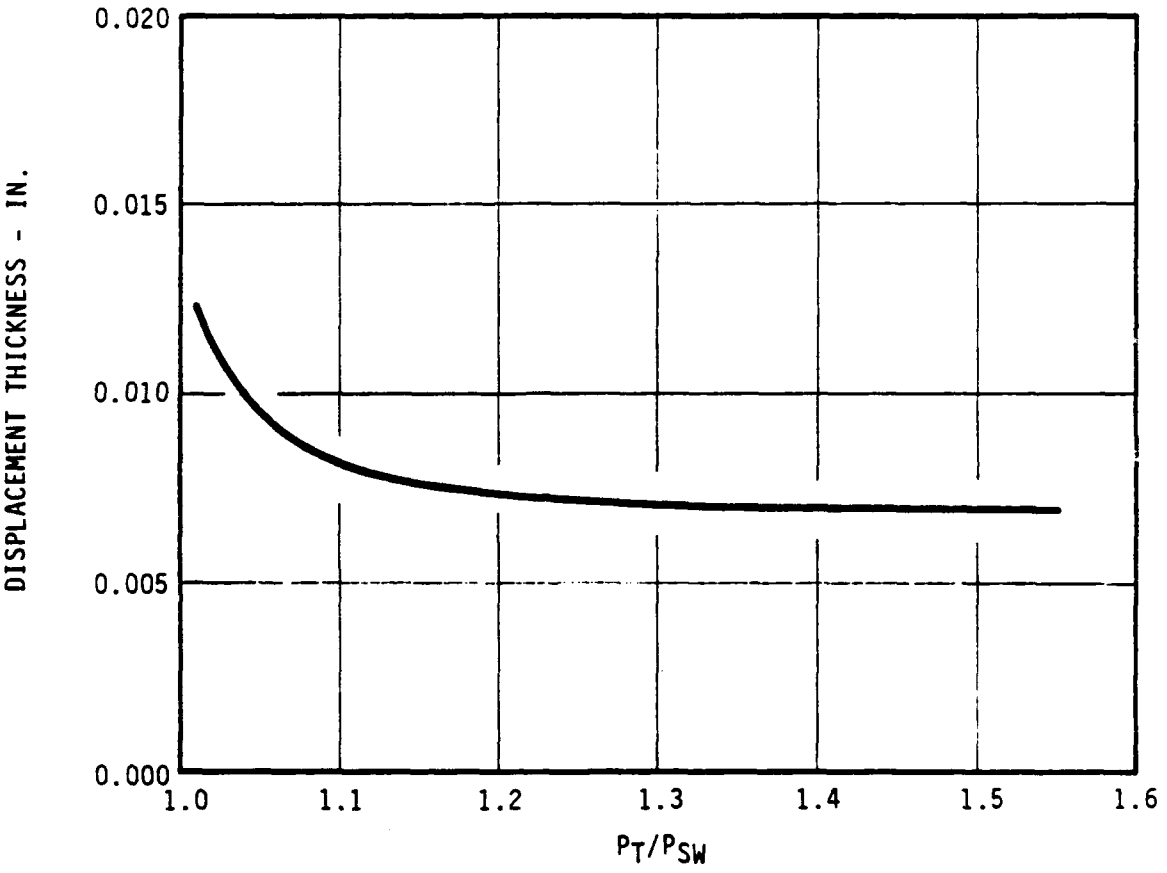

FIGURE 15. PREDICTED THROAT DISPLACEMENT THICKNESS.

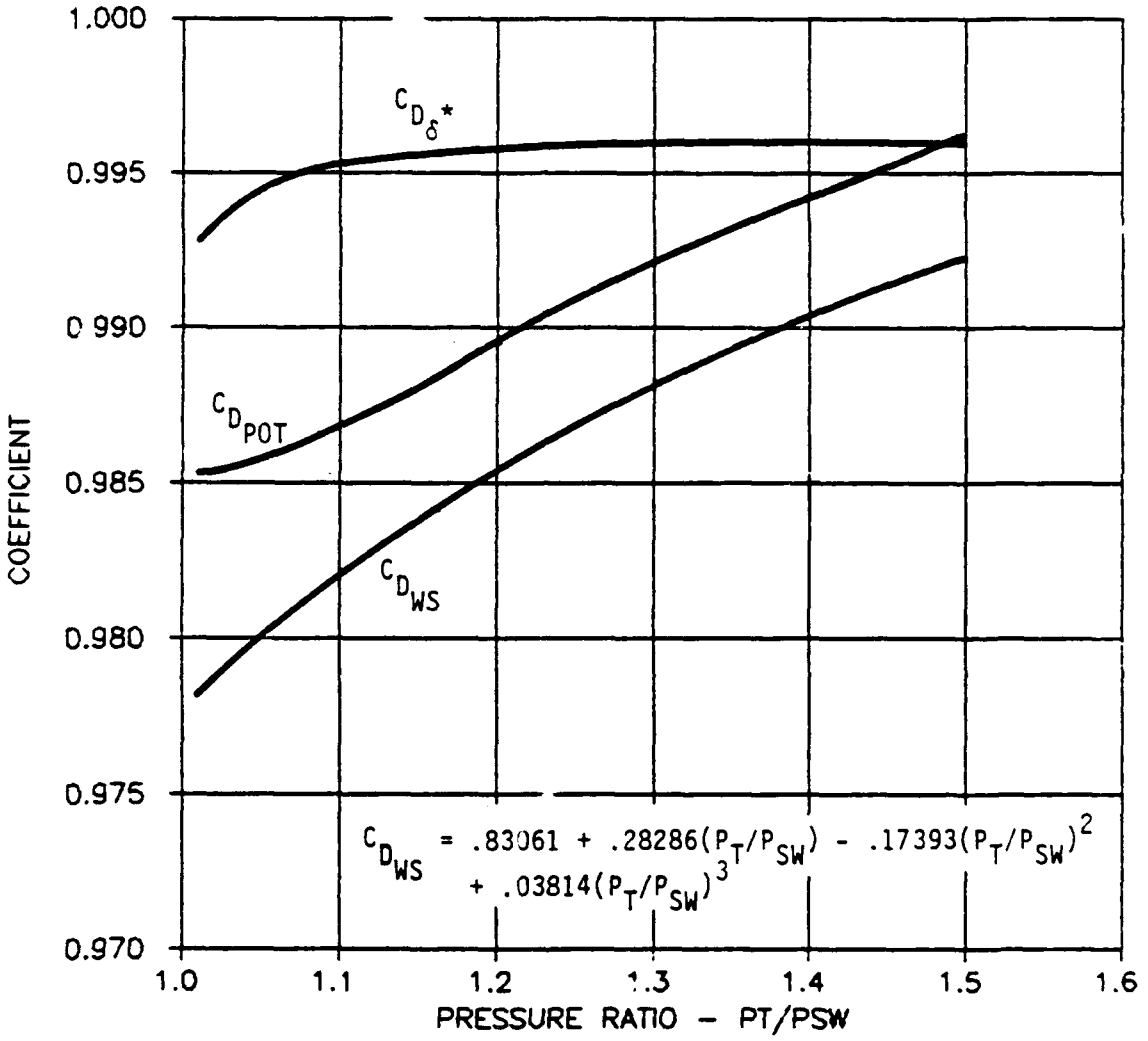

FIGURE 16. DISCHARGE COEFFICIENT COMPONENTS.

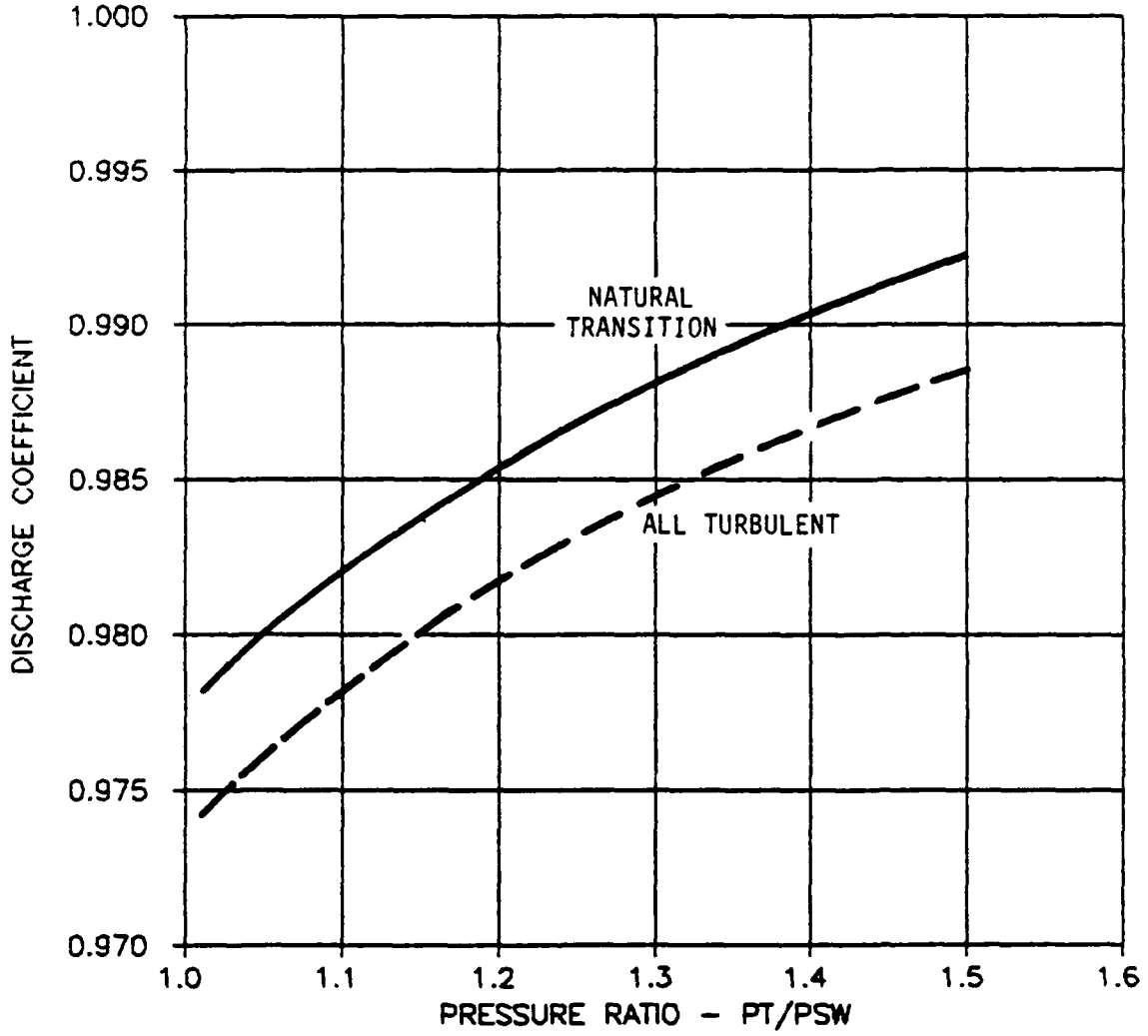

FIGURE 17. PREDICTED DISCHARGE COEFFICIENTS.

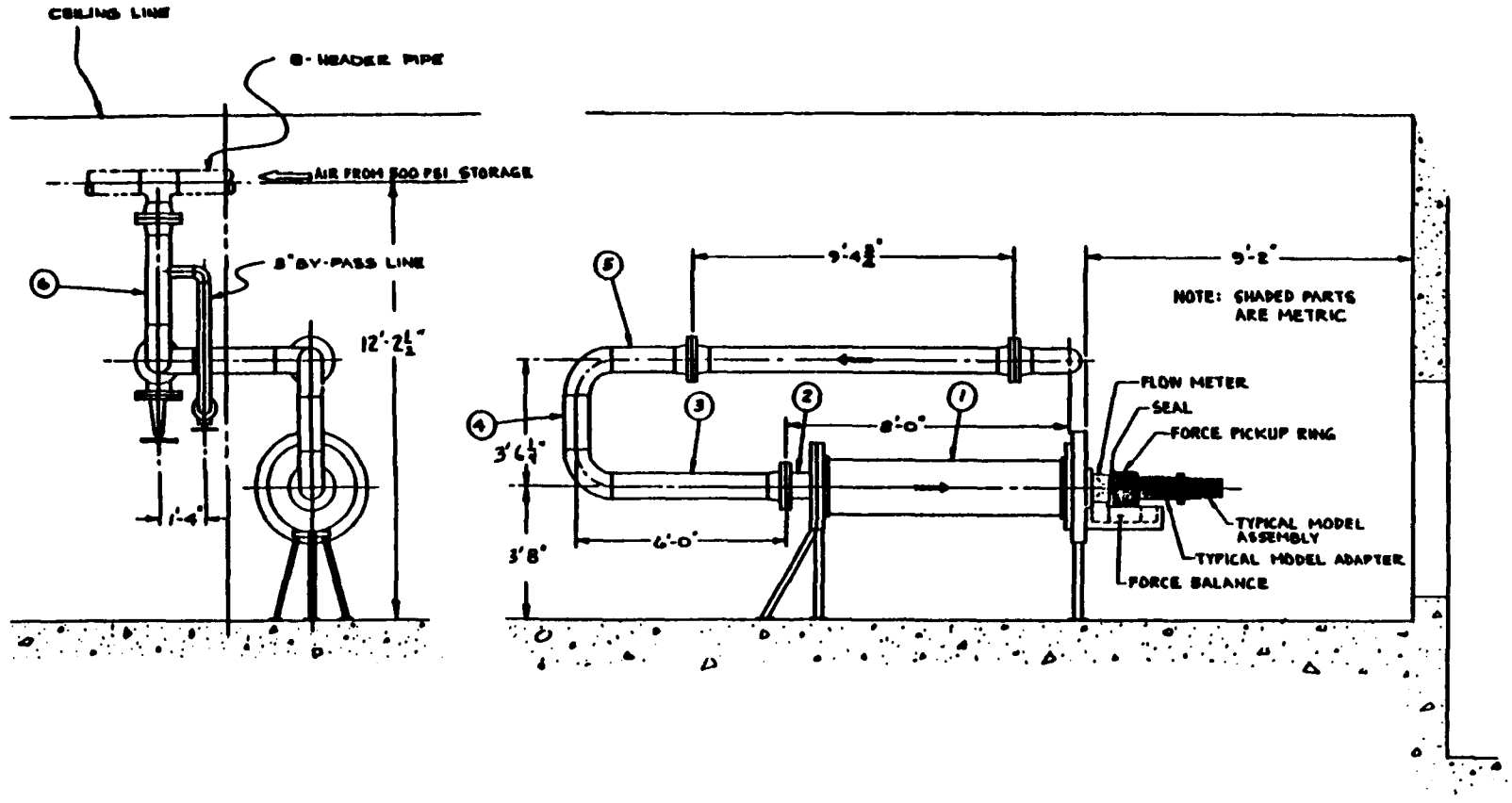

FIGURE 18. FLUIDYNE CHANNEL 12 STATIC TEST STAND.

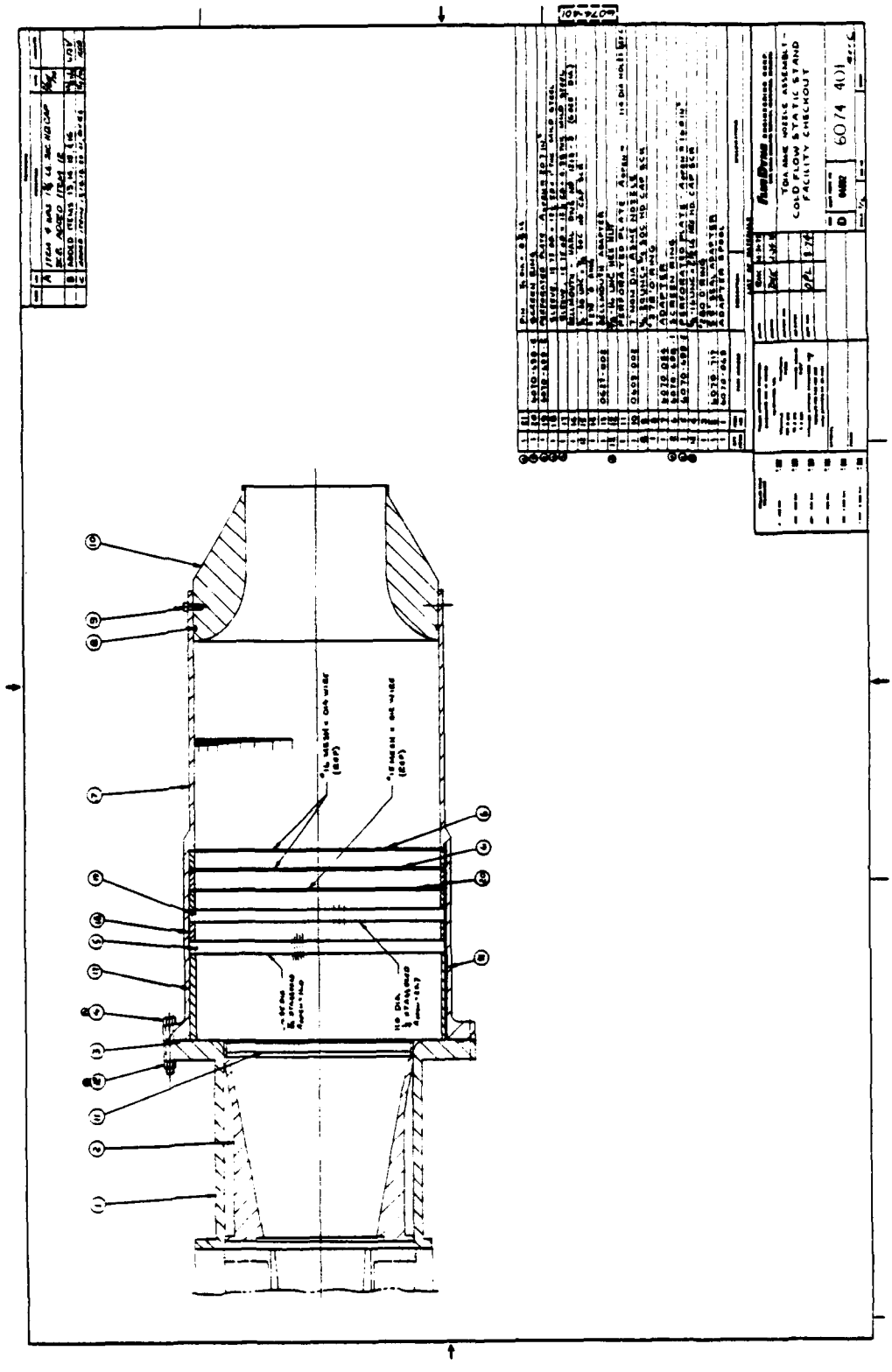

FIGURE 19. ASME NOZZLE.

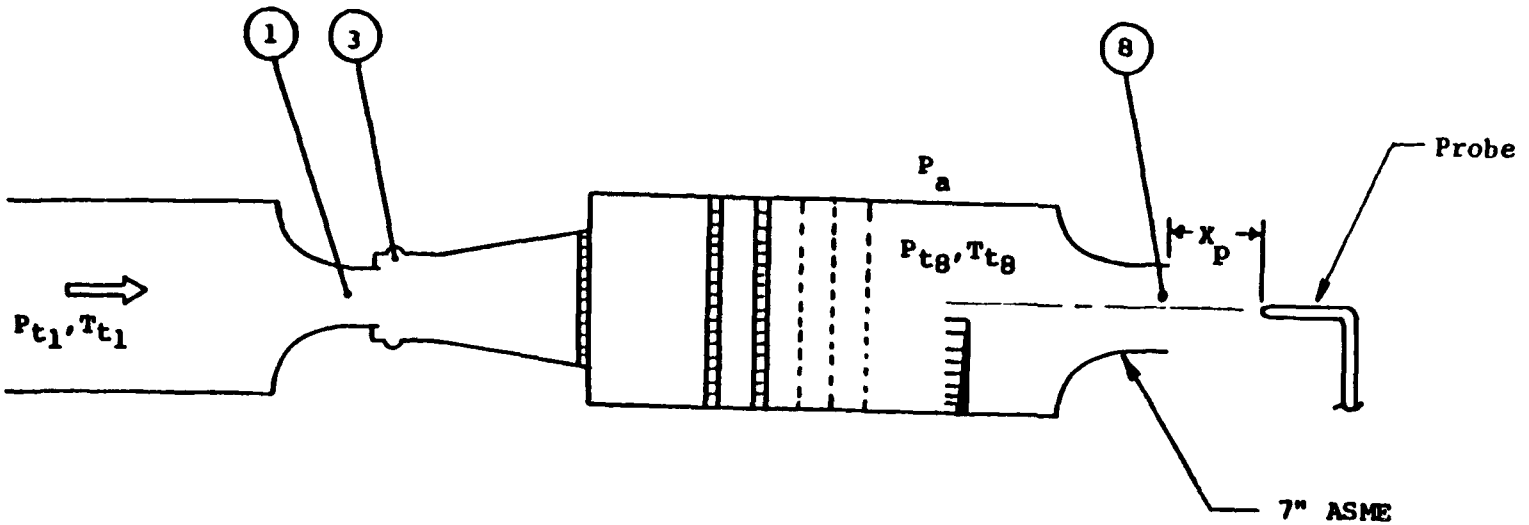

Station	Description
1	ASME meter throat
3	Flexible seal cavity
8	ASME nozzle

FIGURE 20. ASME NOZZLE STATION DESIGNATIONS.

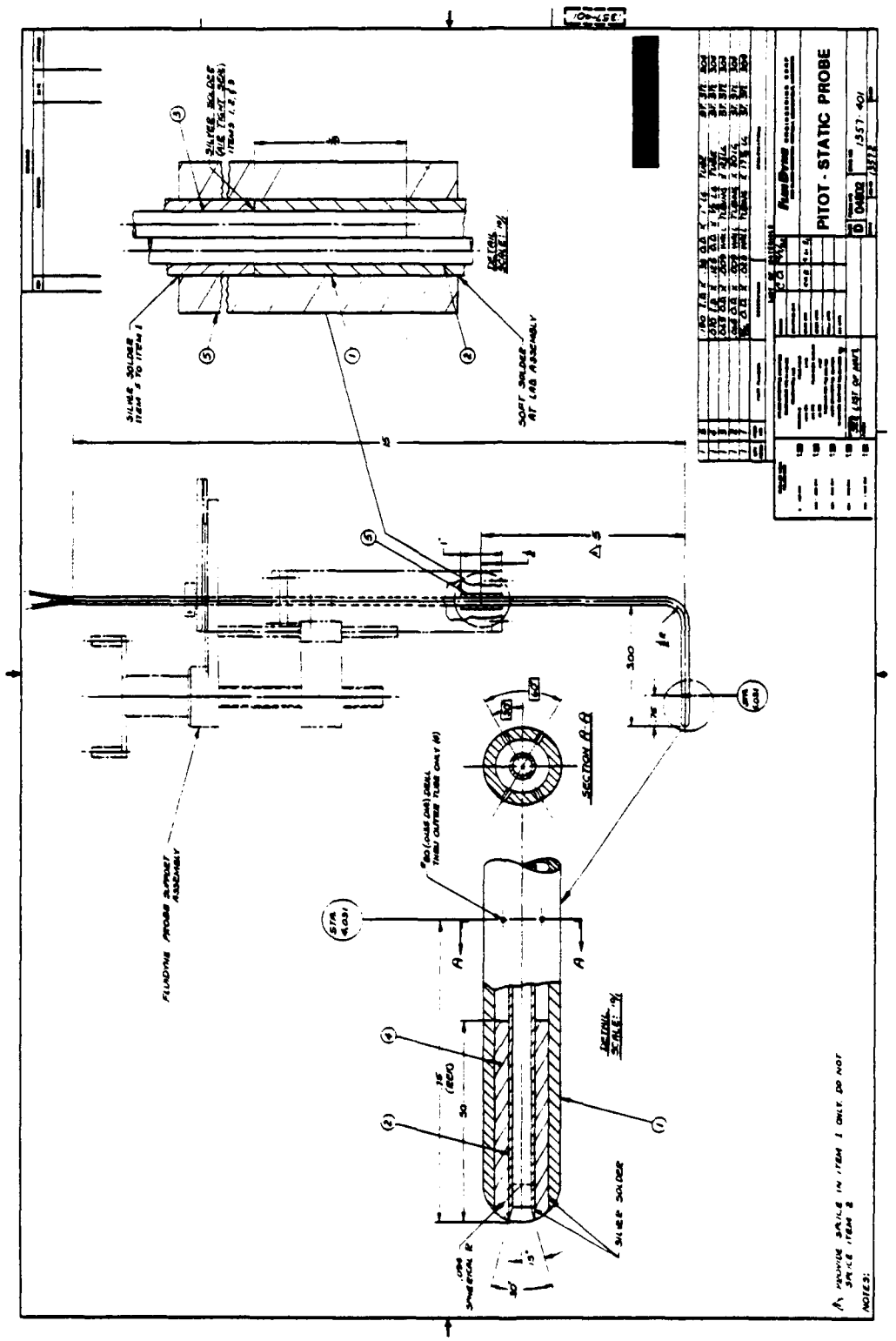

FIGURE 21. PITOT STATIC PROBE.

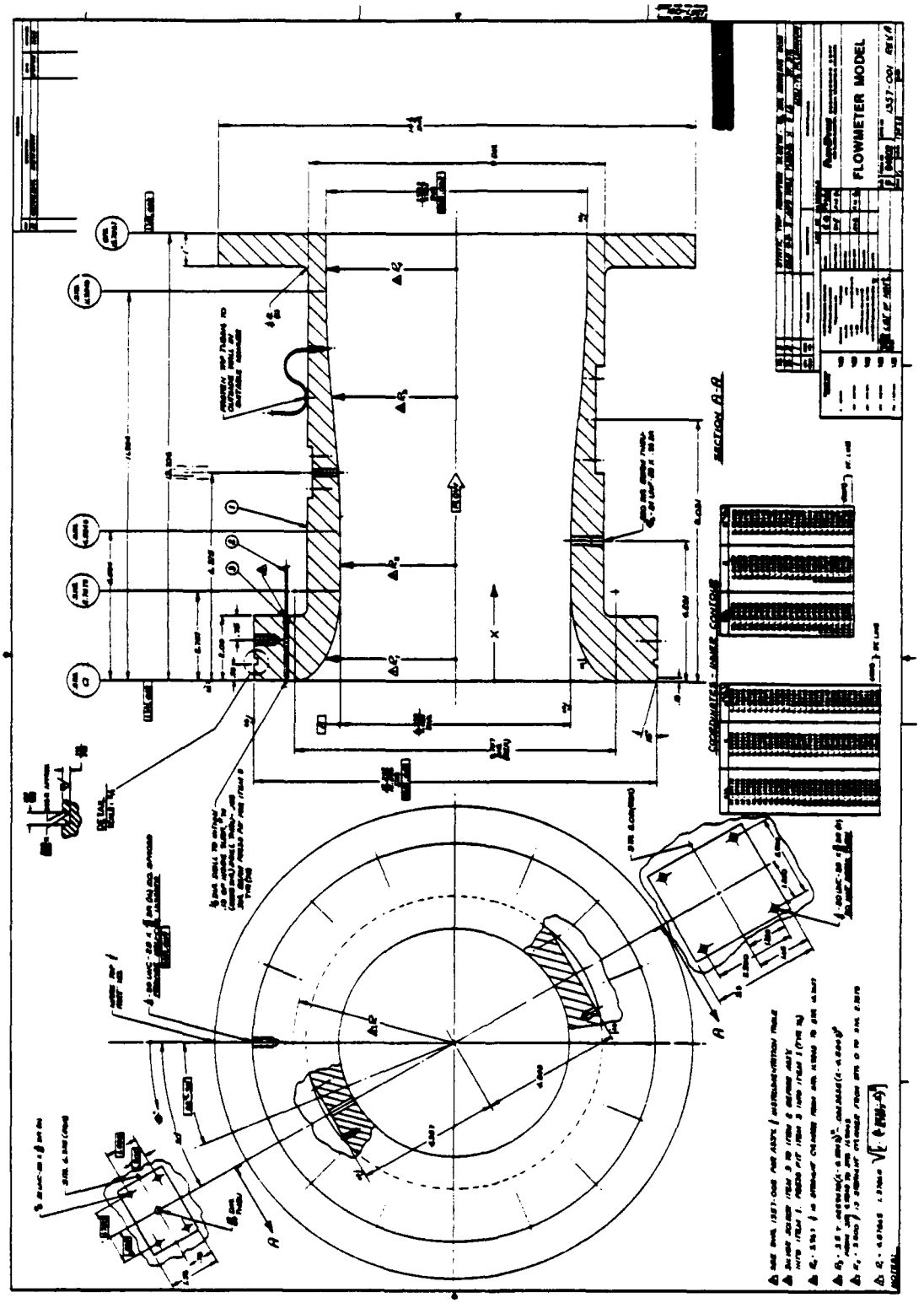

FIGURE 22. FLOWMETER.

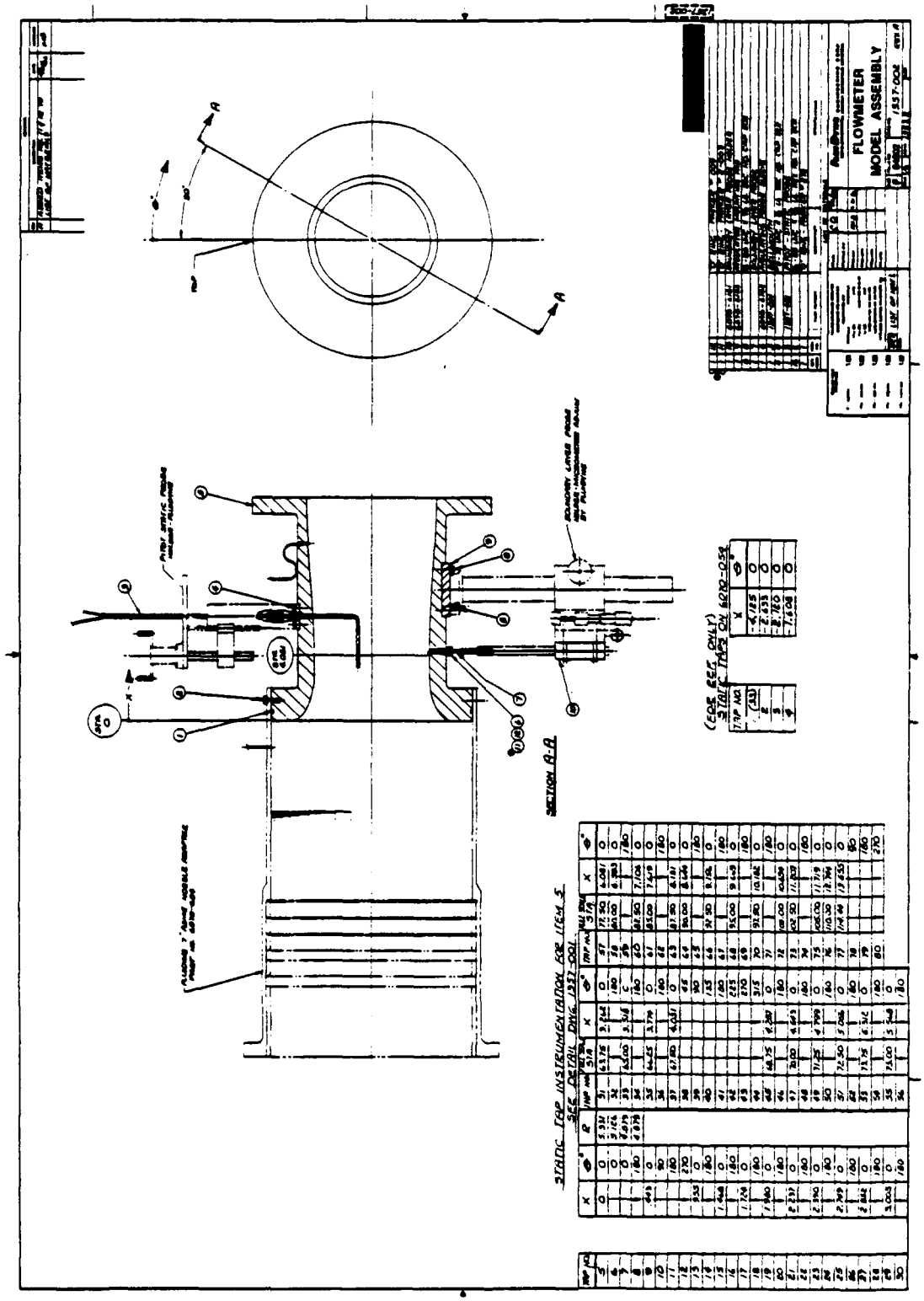

FIGURE 23. FLOWMETER TEST ASSEMBLY.

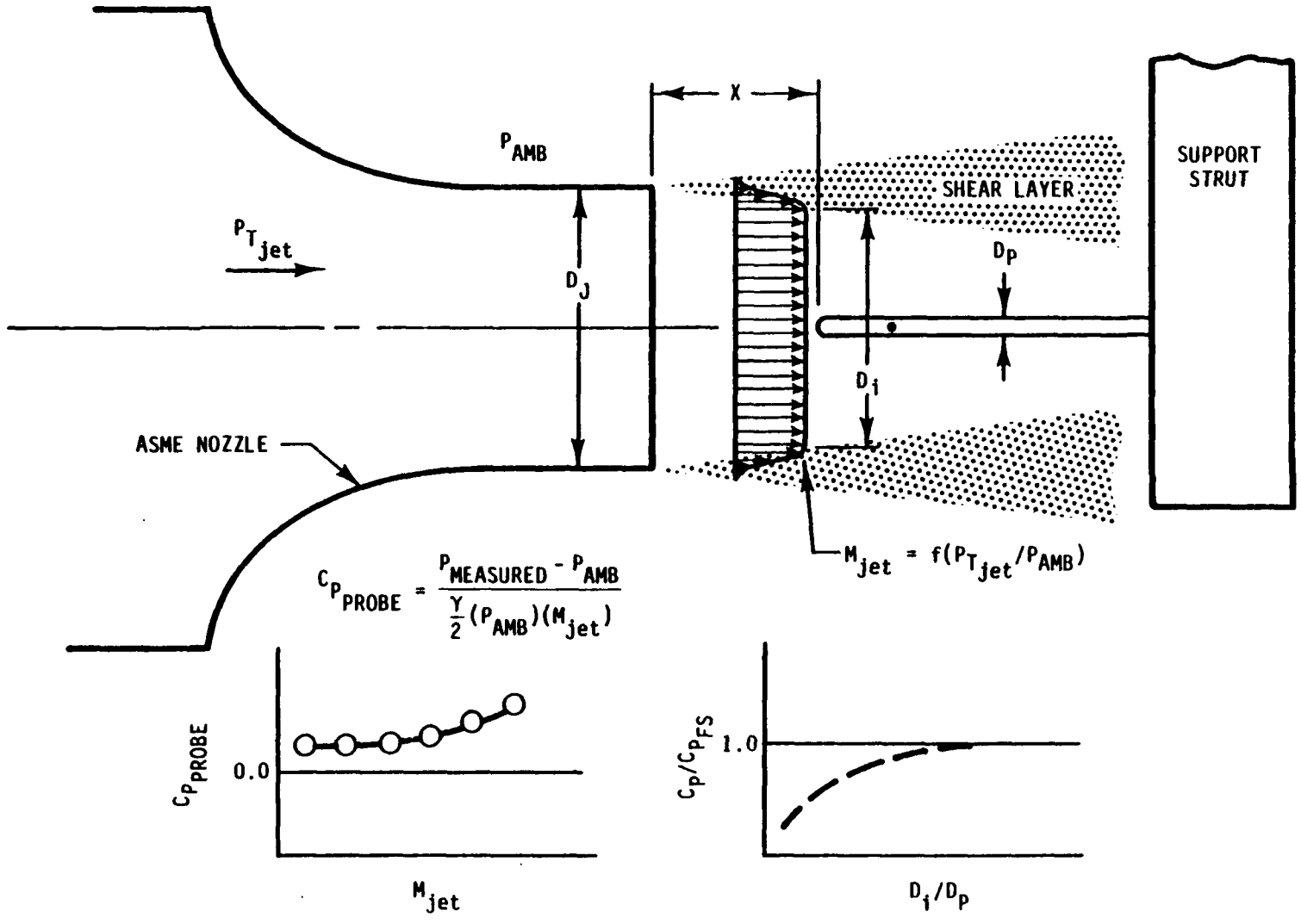

FIGURE 24. PITOT - STATIC PROBE CALIBRATION PROCEDURE.

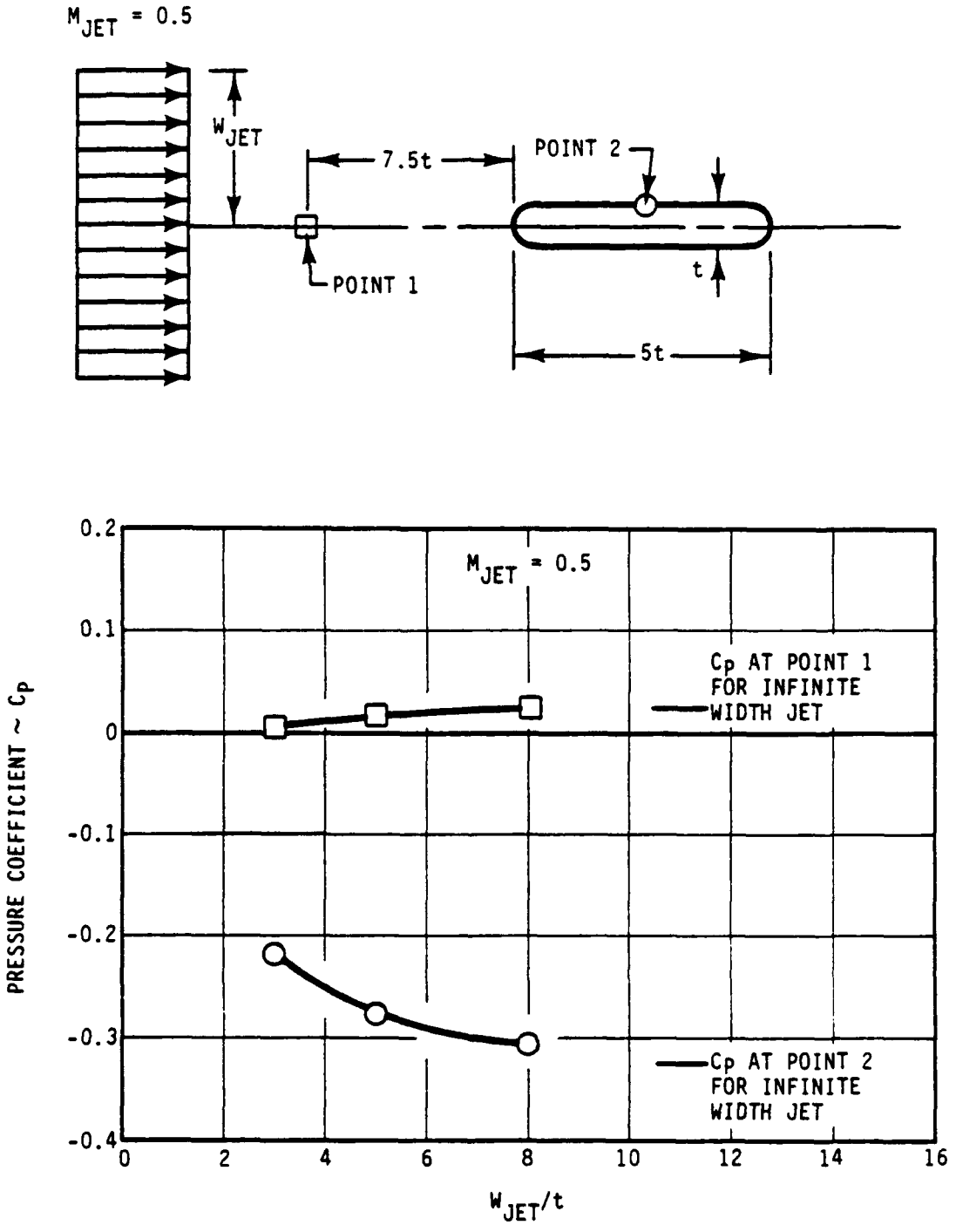

FIGURE 25. INFLUENCE OF CALIBRATION NOZZLE JET WIDTH ON CALIBRATION ACCURACY.

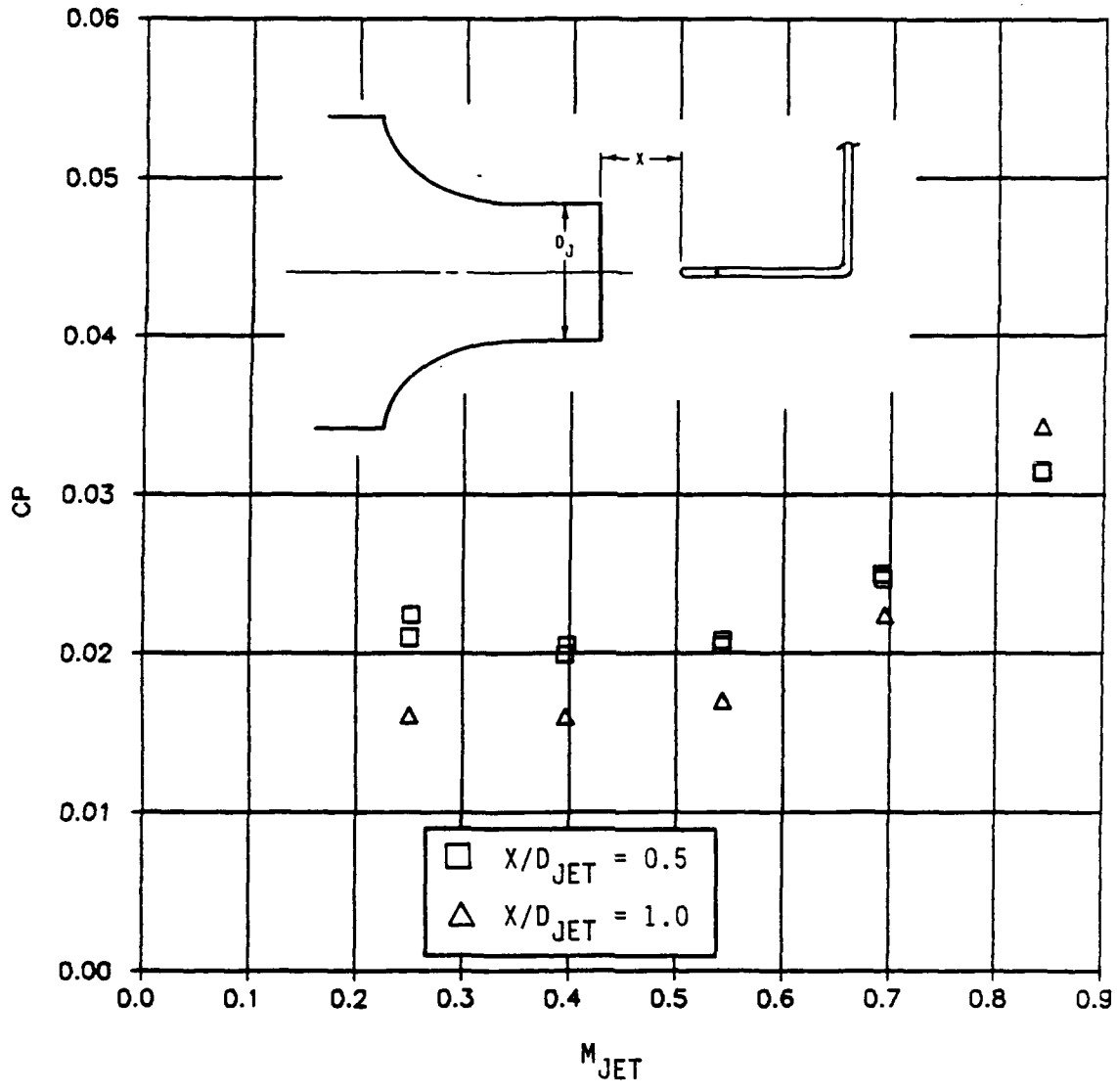

FIGURE 26. PRESSURE SURVEY PROBE FREE JET CALIBRATION TEST RESULTS.

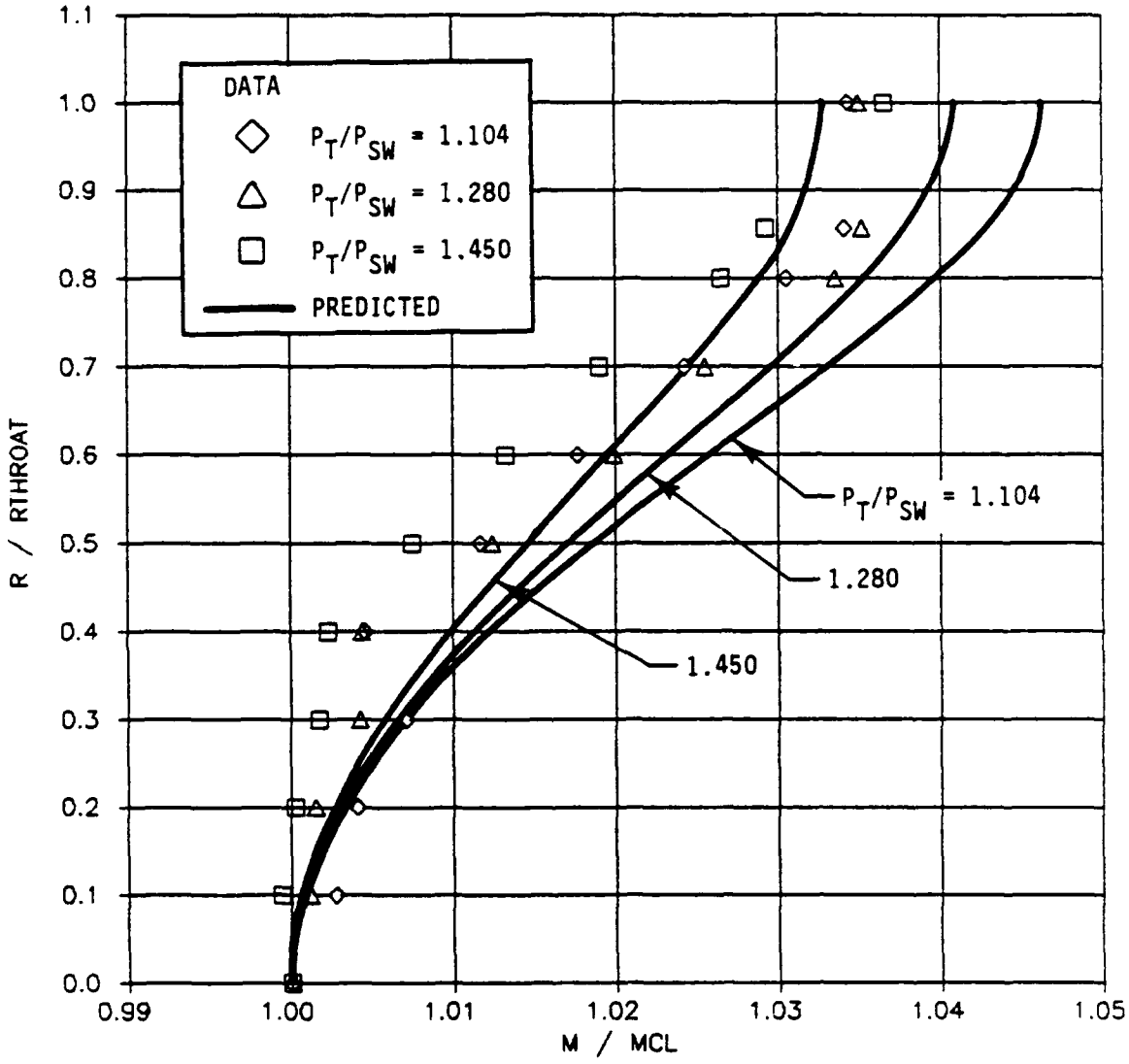

FIGURE 27. PREDICTED AND MEASURED THROAT MACH PROFILES.

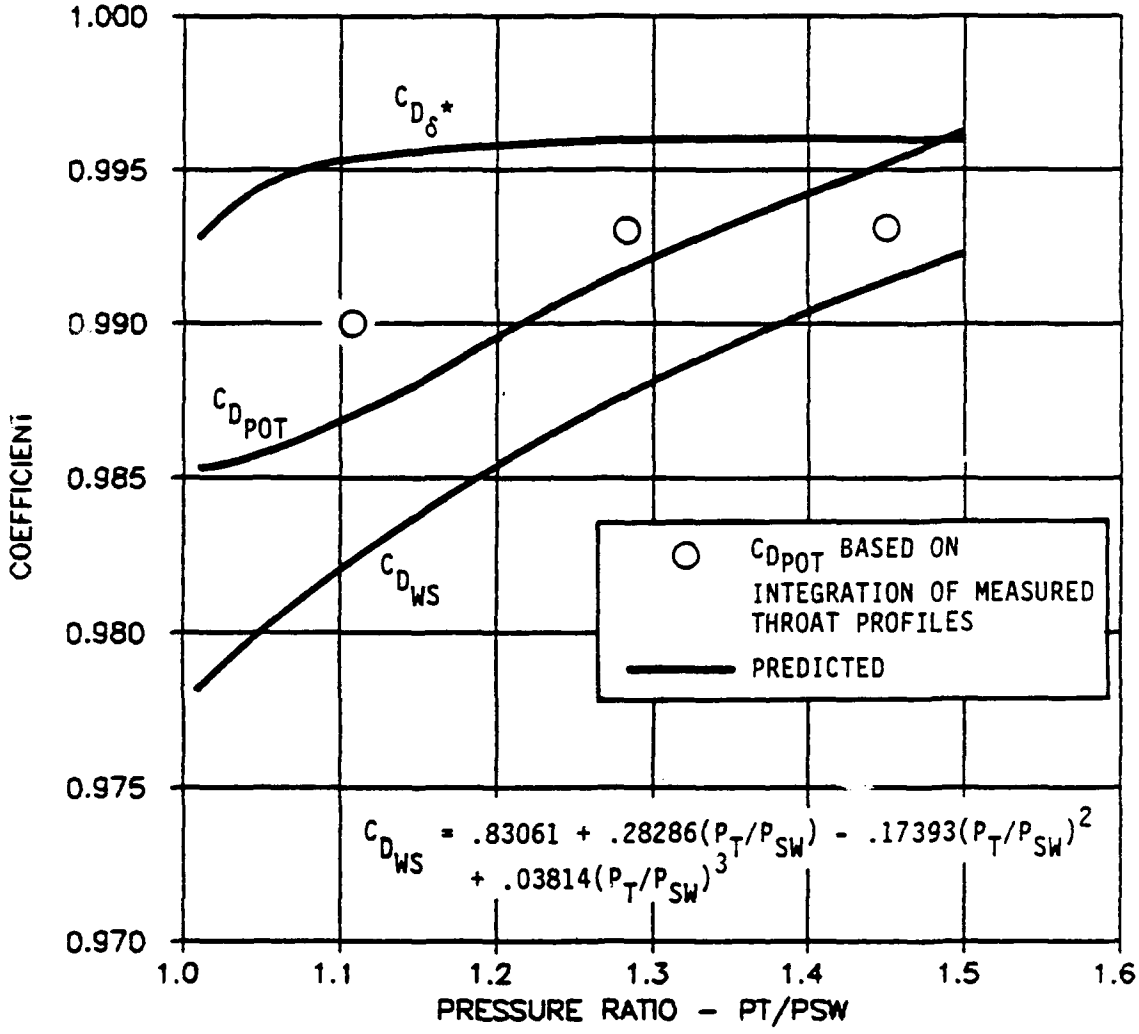

FIGURE 28. DISCHARGE COEFFICIENT COMPONENTS.

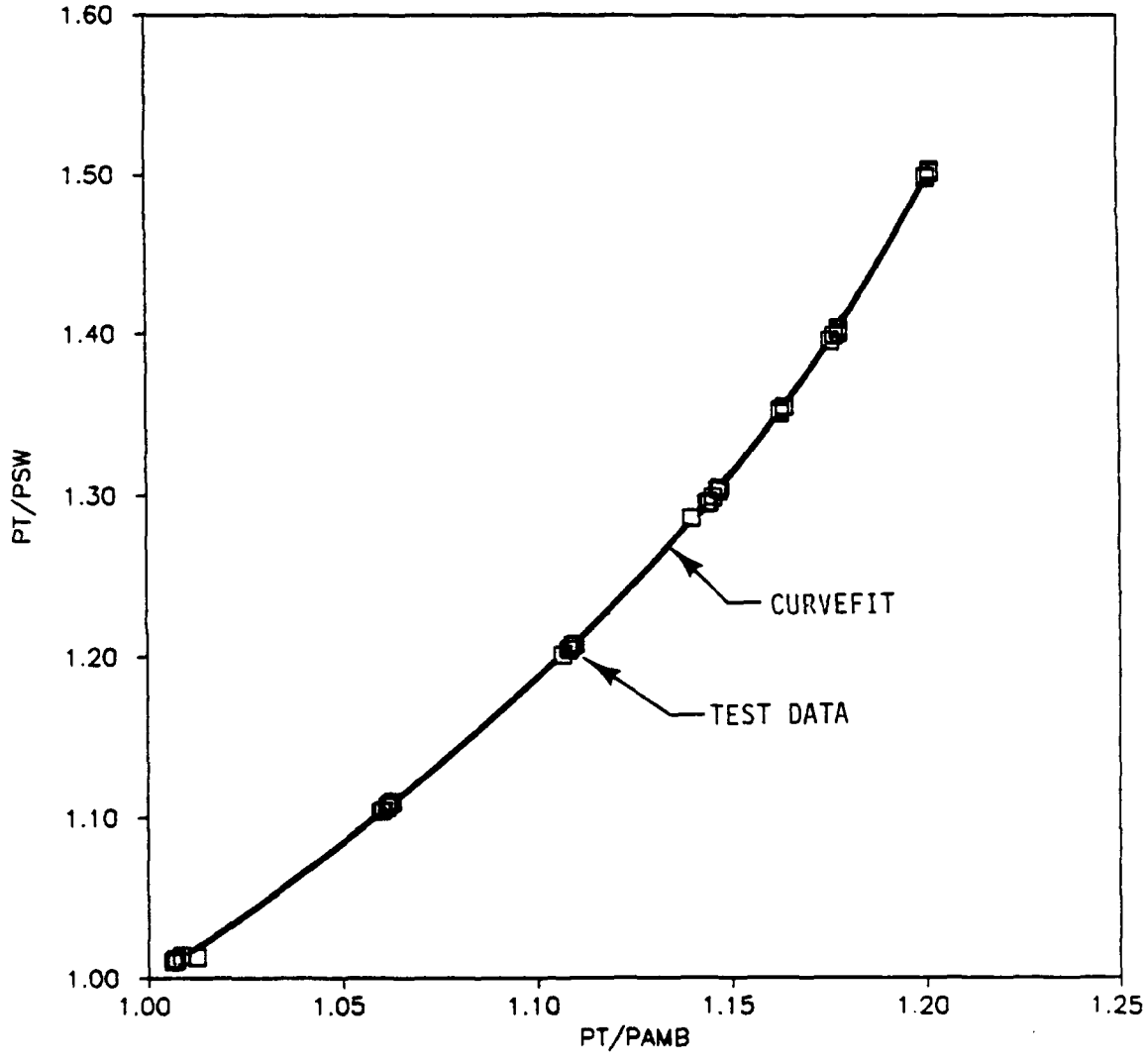

FIGURE 29. THROAT WALL AVERAGE STATIC PRESSURE RATIO VERSUS OVERALL PRESSURE RATIO.

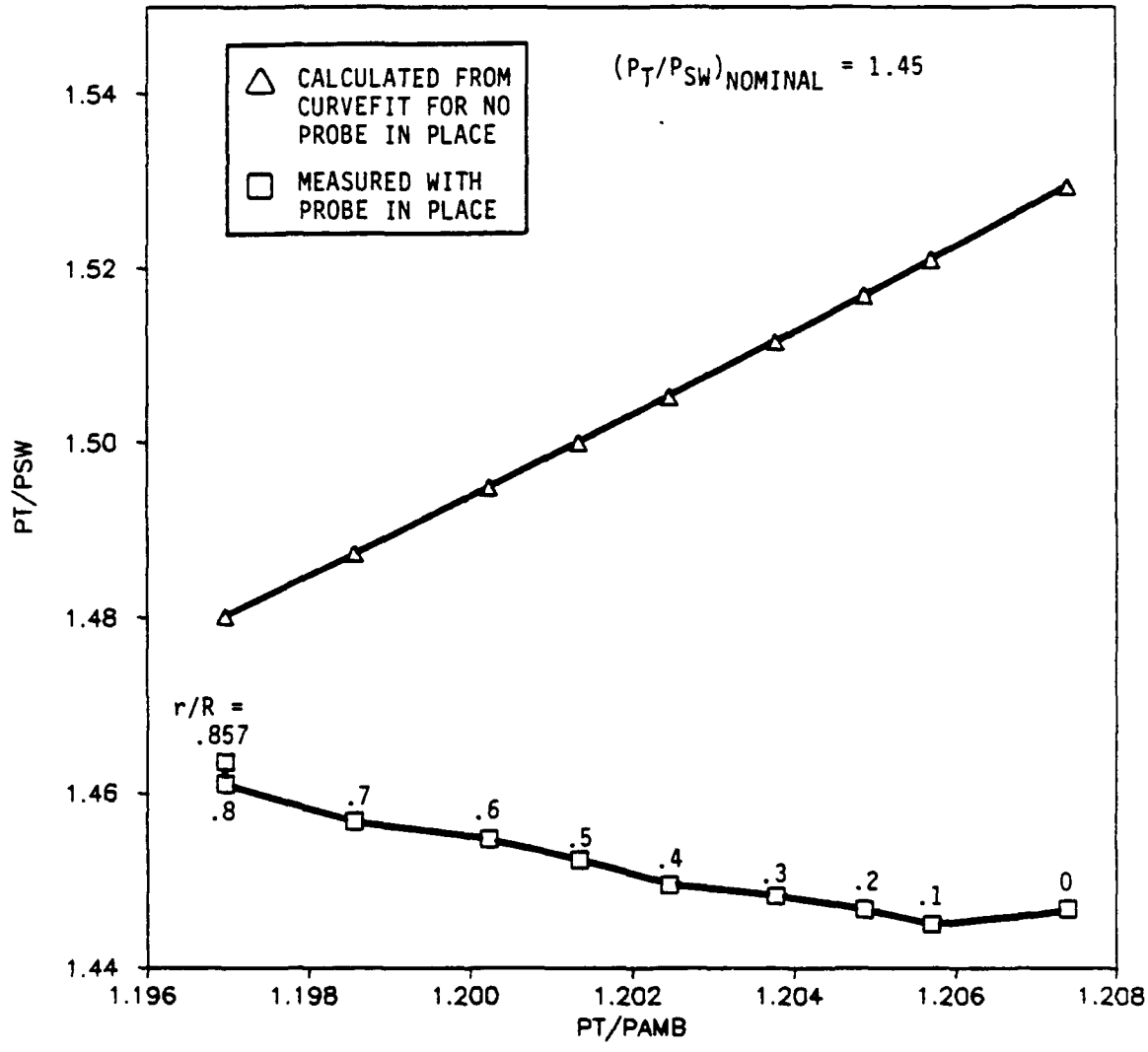

FIGURE 30. SURVEY PROBE EFFECT ON THROAT WALL AVERAGE STATIC PRESSURE RATIO.

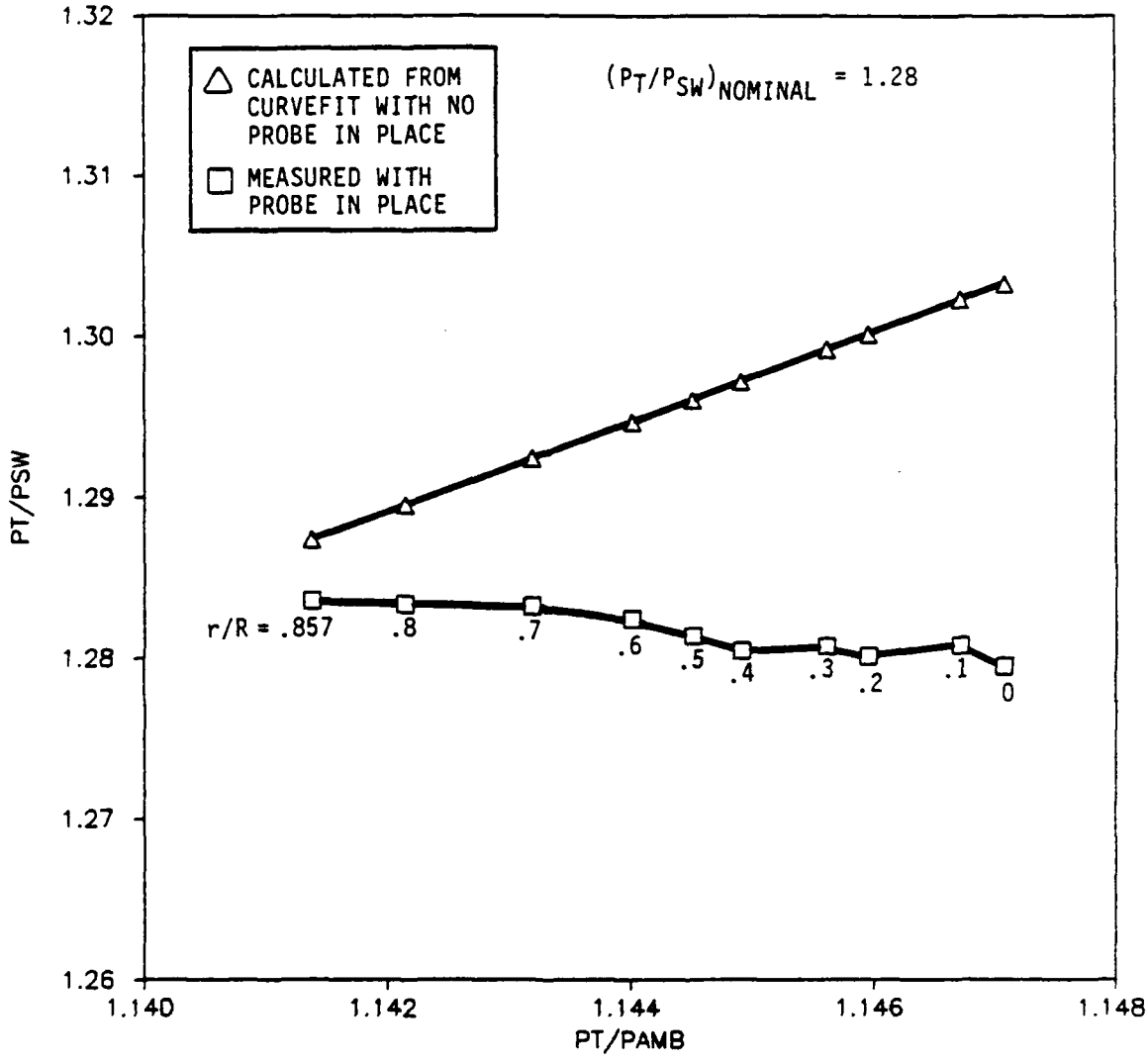

FIGURE 31. SURVEY PROVE EFFECT ON THROAT WALL AVERAGE STATIC PRESSURE RATIO.

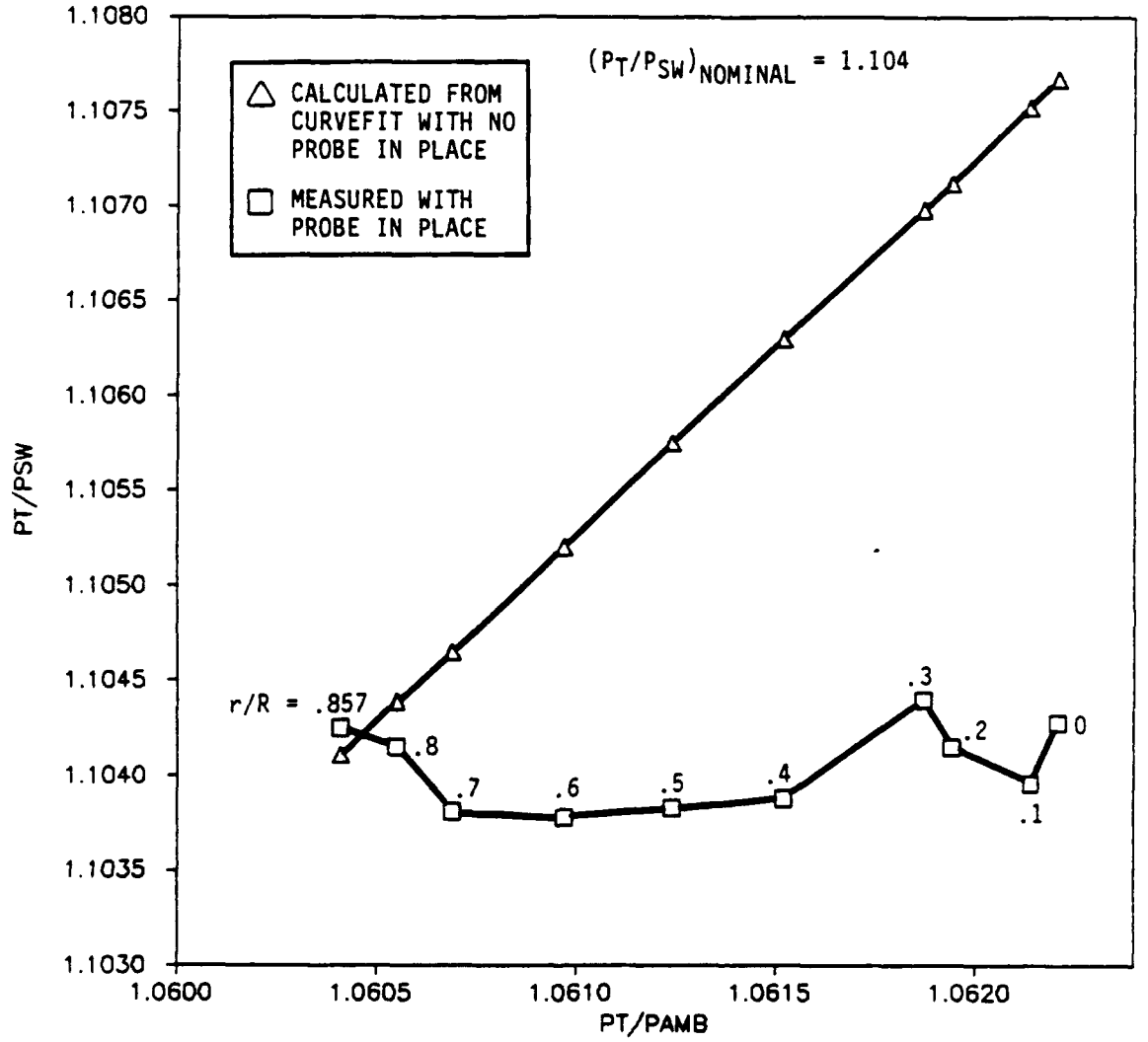

FIGURE 32. SURVEY PROBE EFFECT ON THROAT WALL AVERAGE STATIC PRESSURE RATIO.

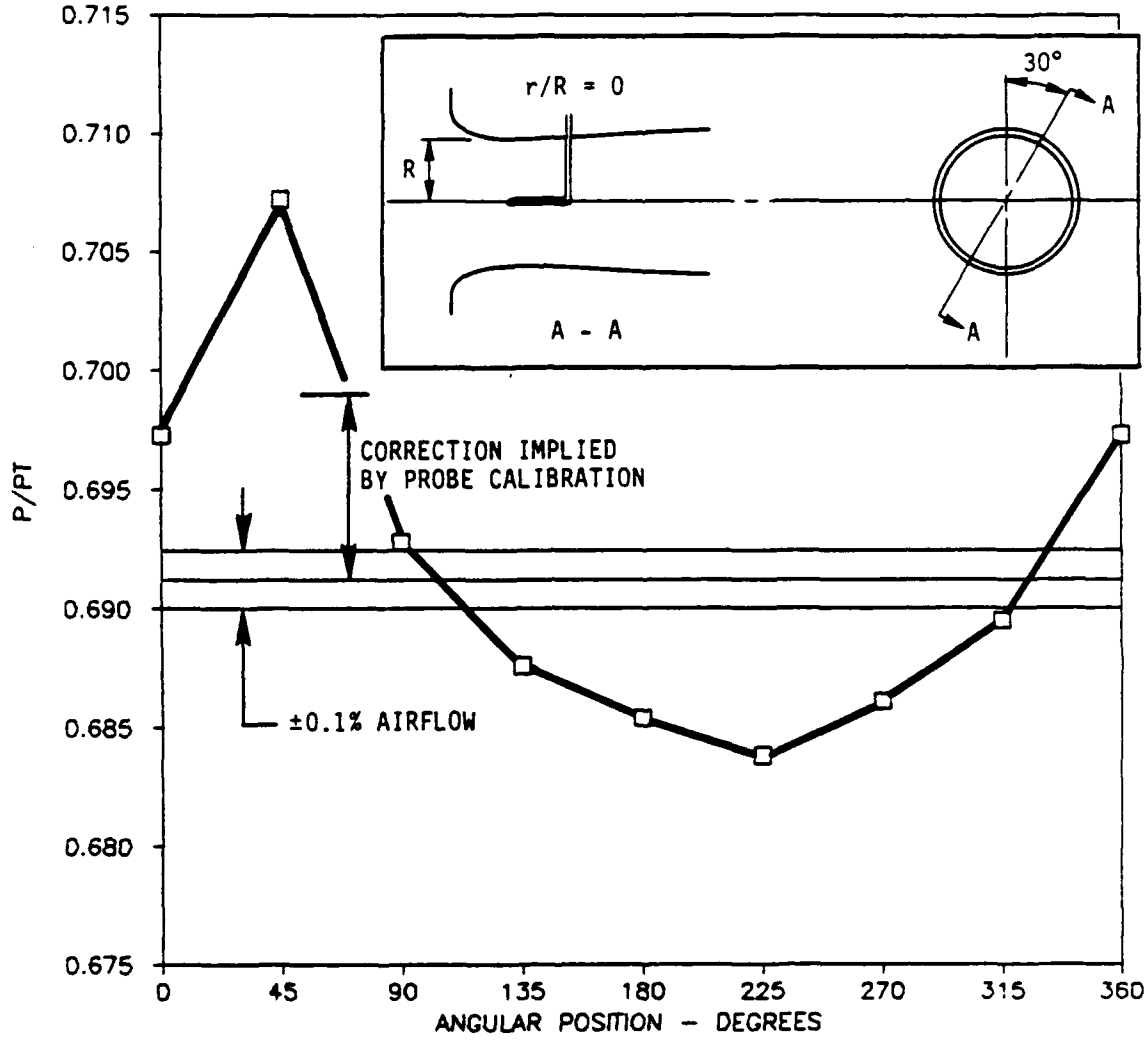

FIGURE 33. EFFECT OF SURVEY PROBE ON MEASURED THROAT STATIC PRESSURES.

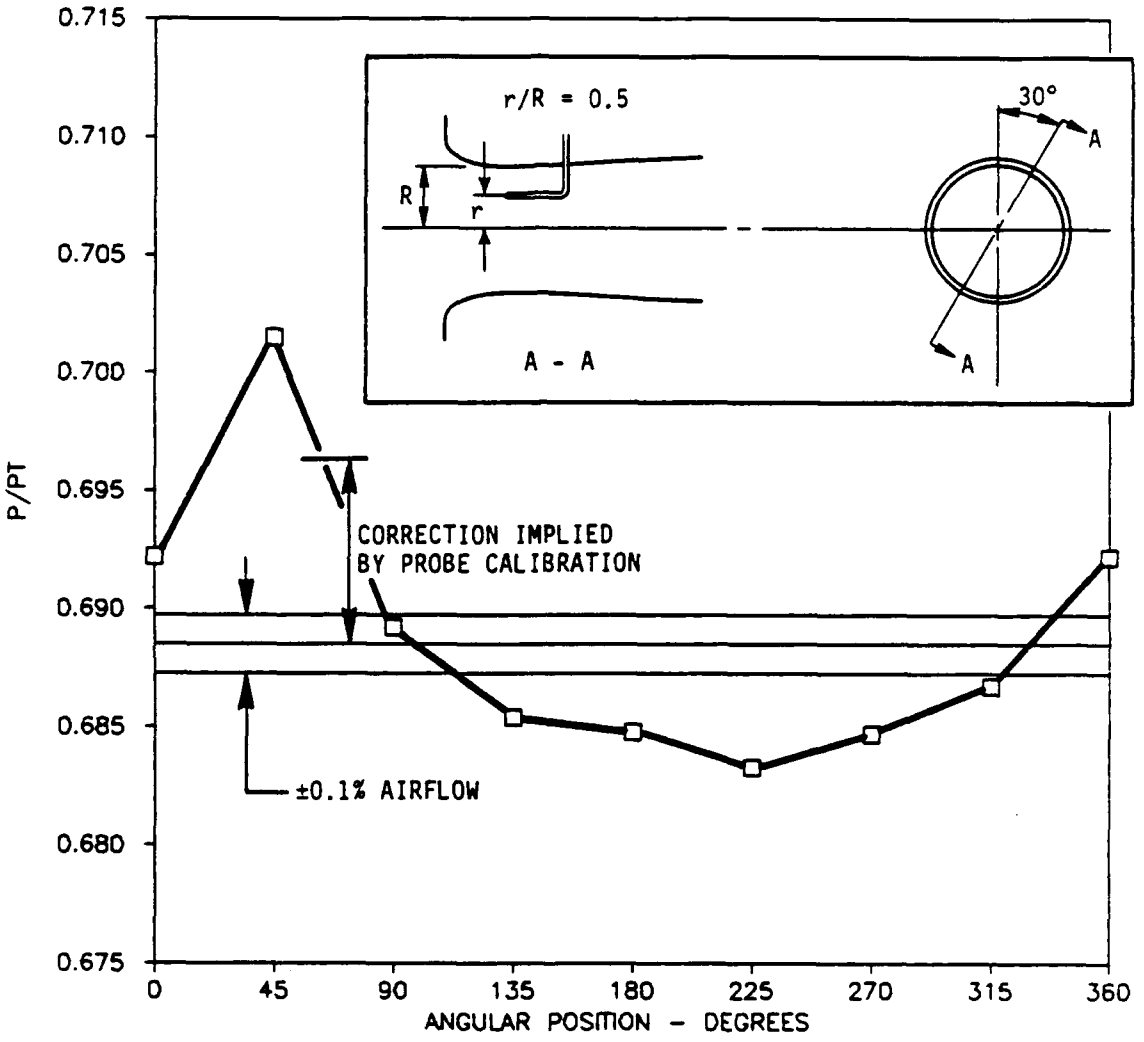

FIGURE 34. EFFECT OF SURVEY PROBE ON MEASURED THROAT STATIC PRESSURES.

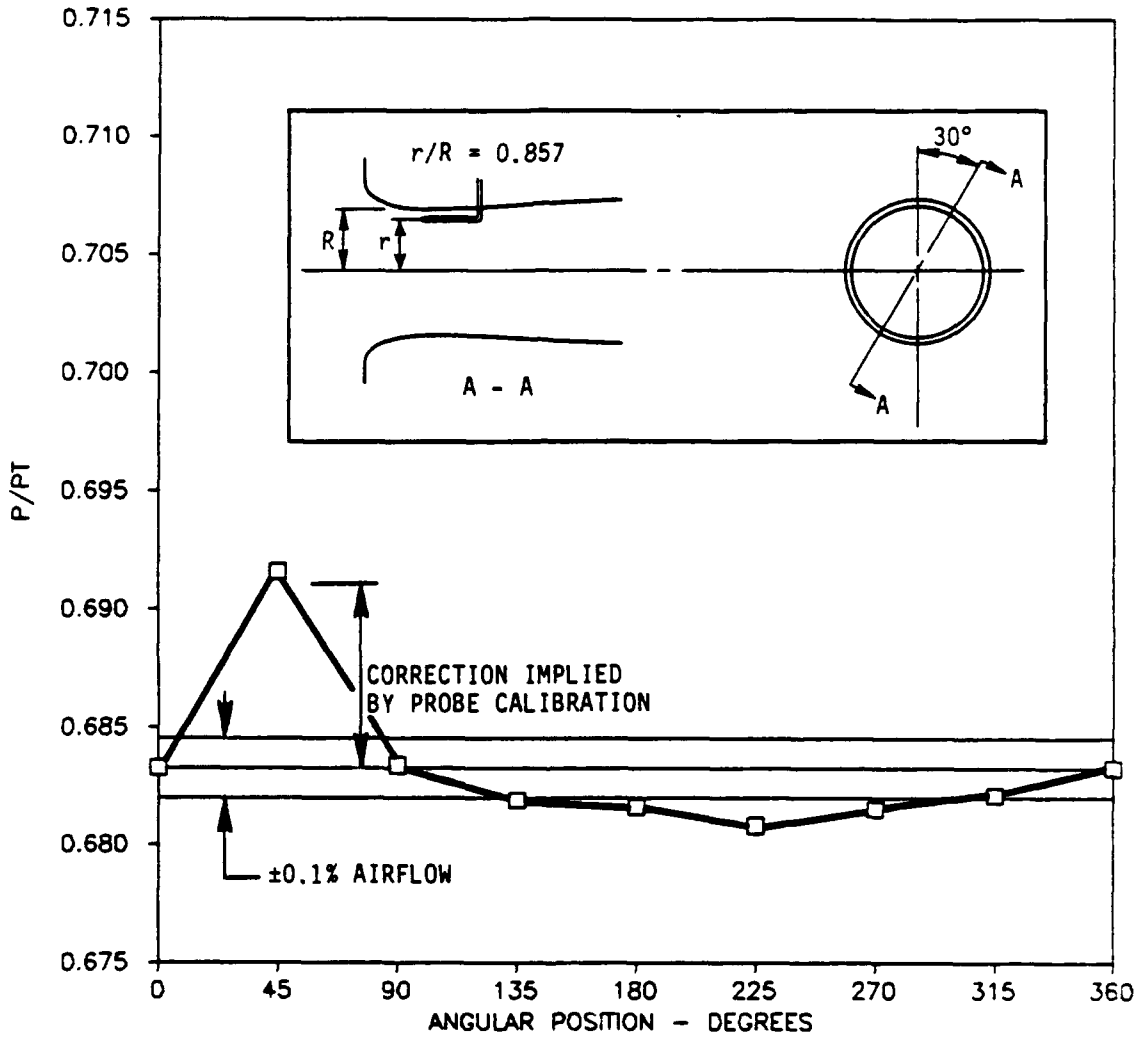

FIGURE 35. EFFECT OF SURVEY PROBE ON MEASURED THROAT STATIC PRESSURES.

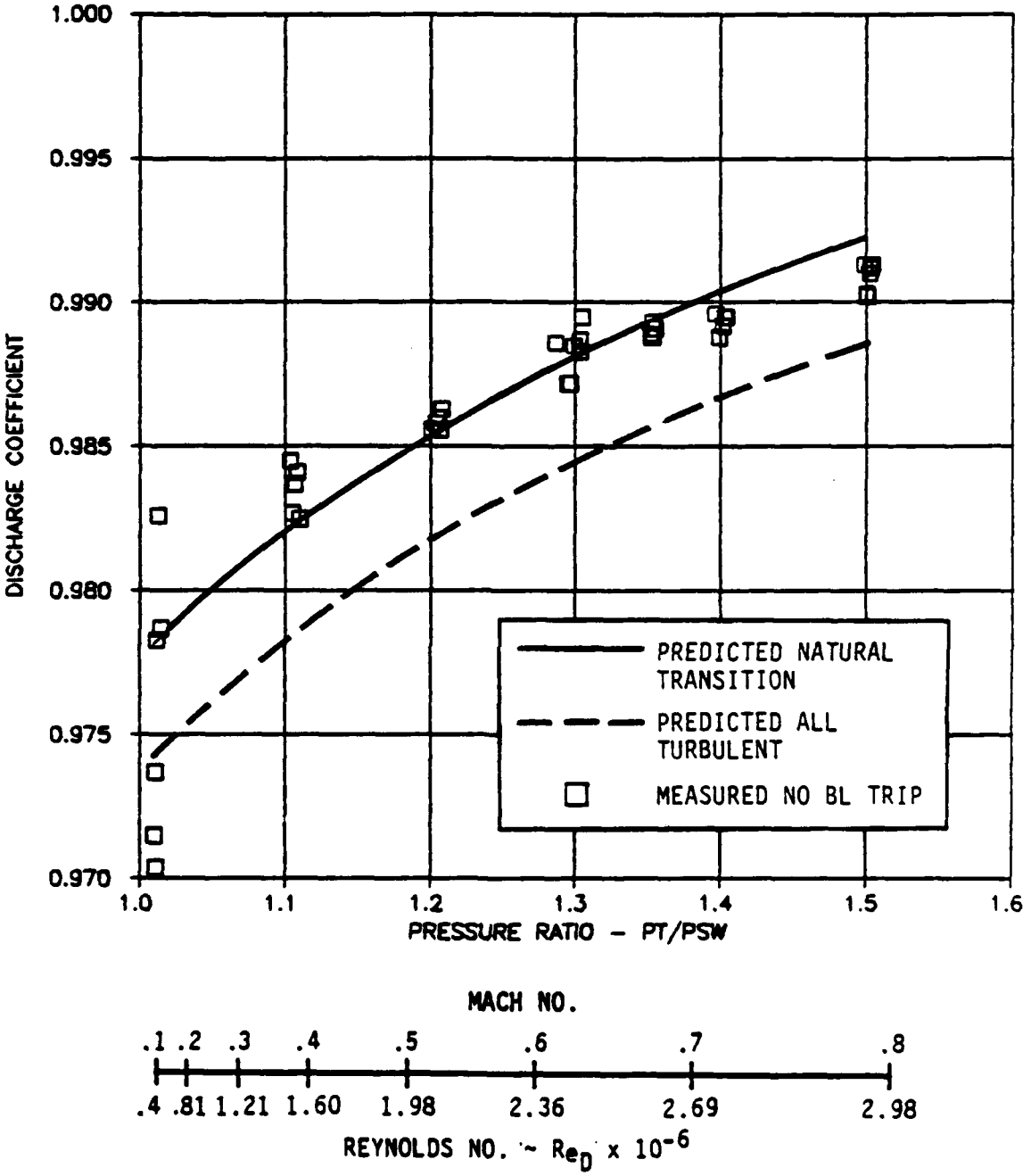

FIGURE 36. DISCHARGE COEFFICIENT VERSUS WALL STATIC PRESSURE RATIO.

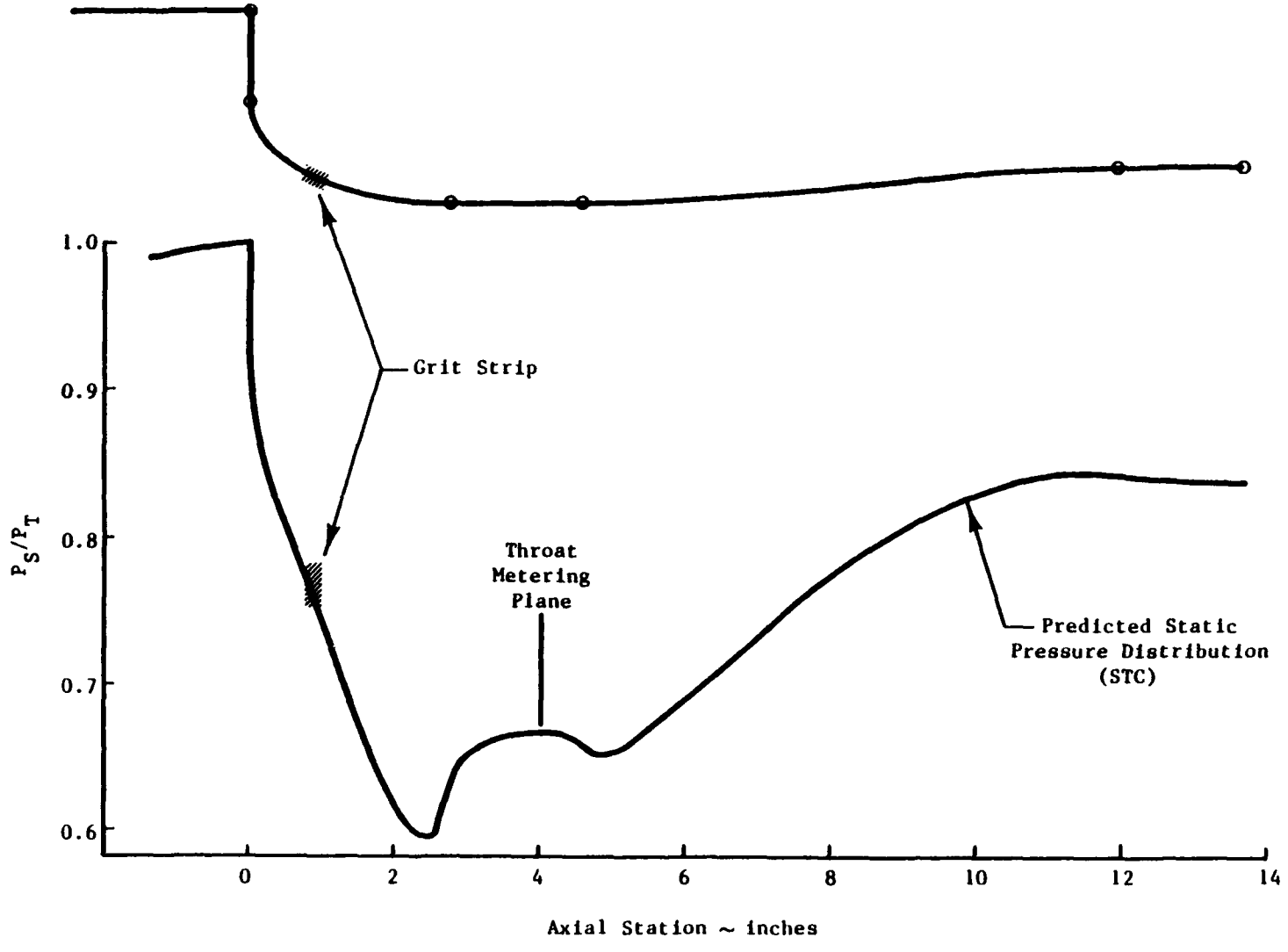

FIGURE 37. BOUNDARY LAYER TRIP LOCATION.

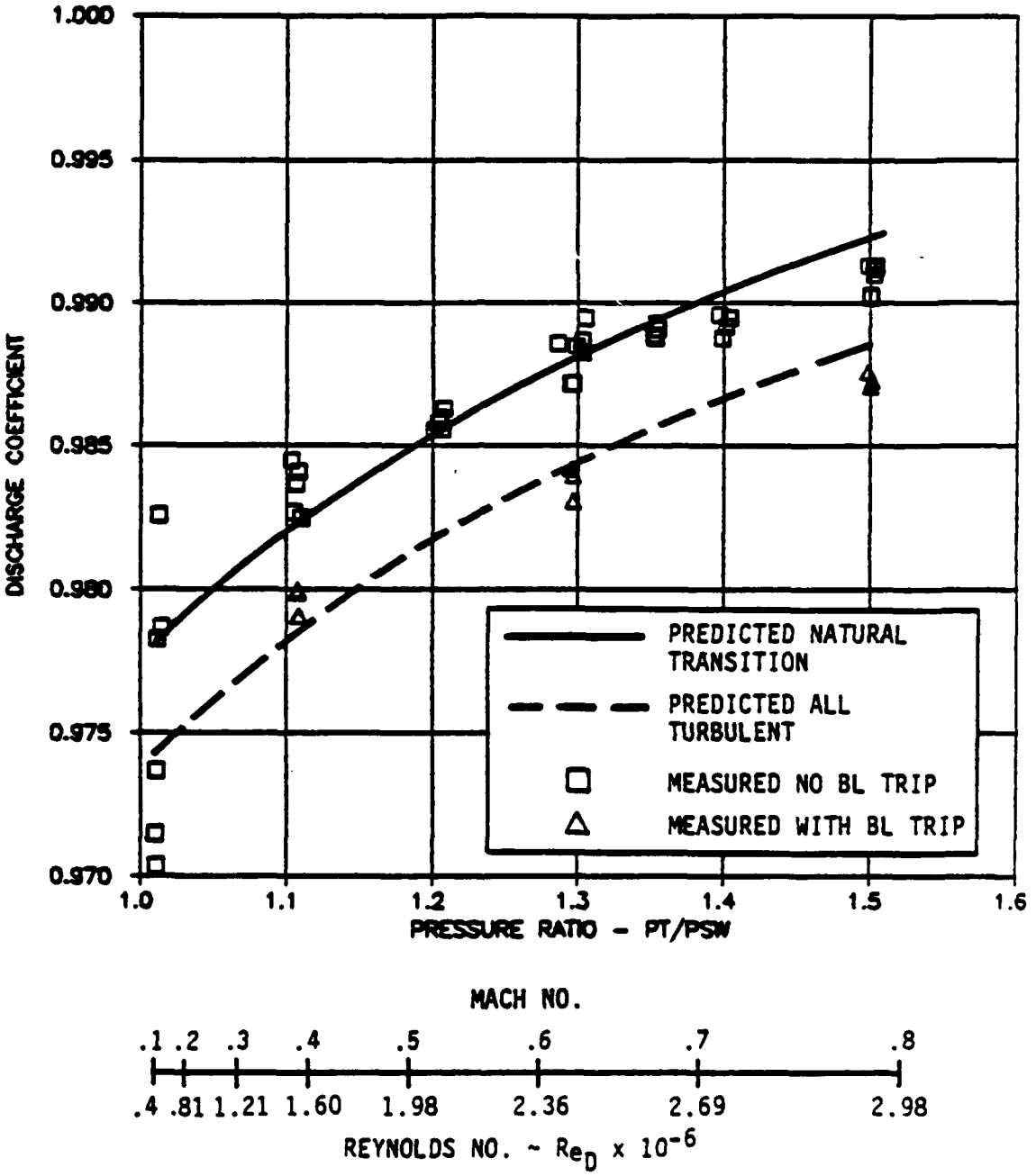

FIGURE 38. DISCHARGE COEFFICIENT VERSUS WALL STATIC PRESSURE RATIO.

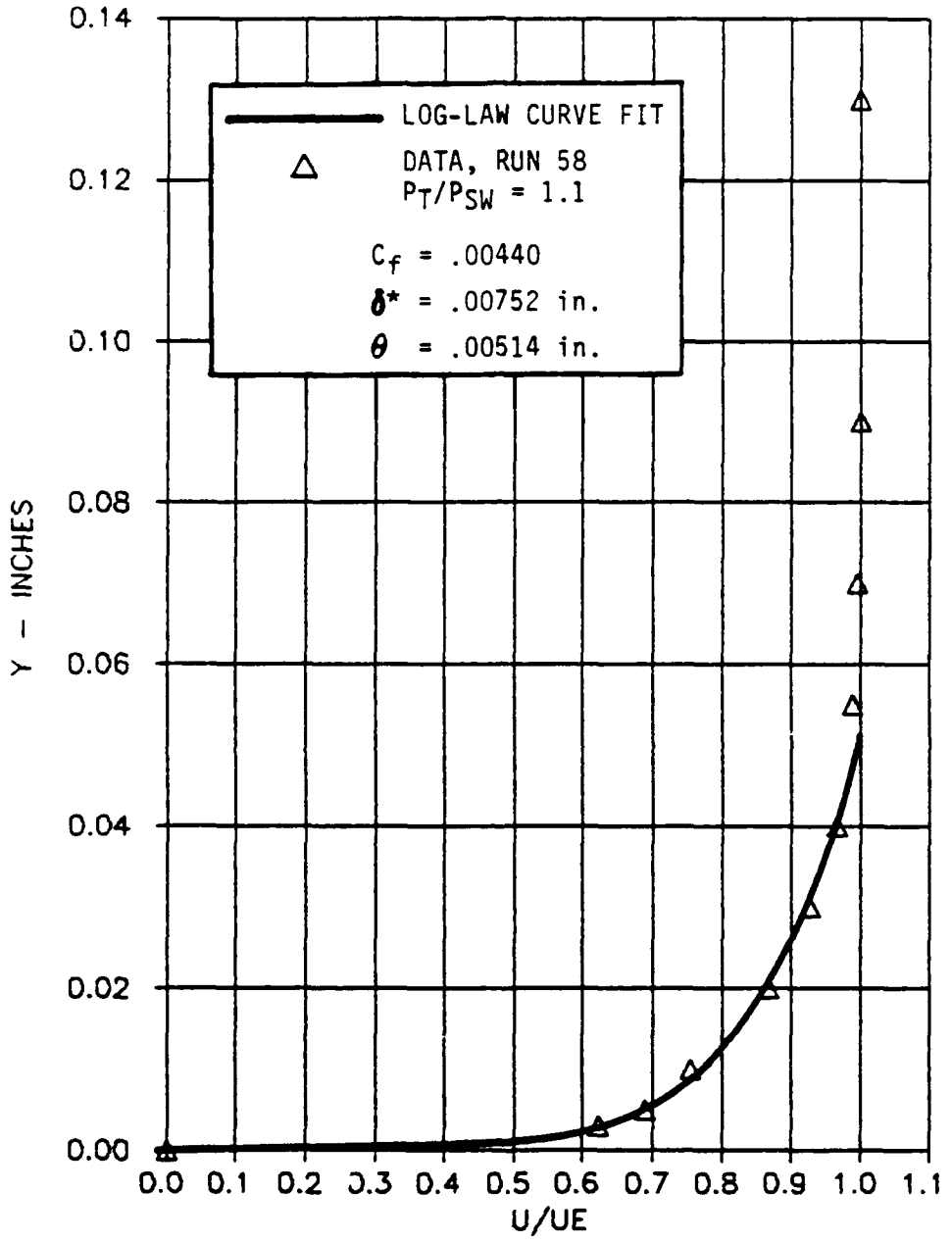

FIGURE 39. MEASURED BOUNDARY LAYER AT THROAT.

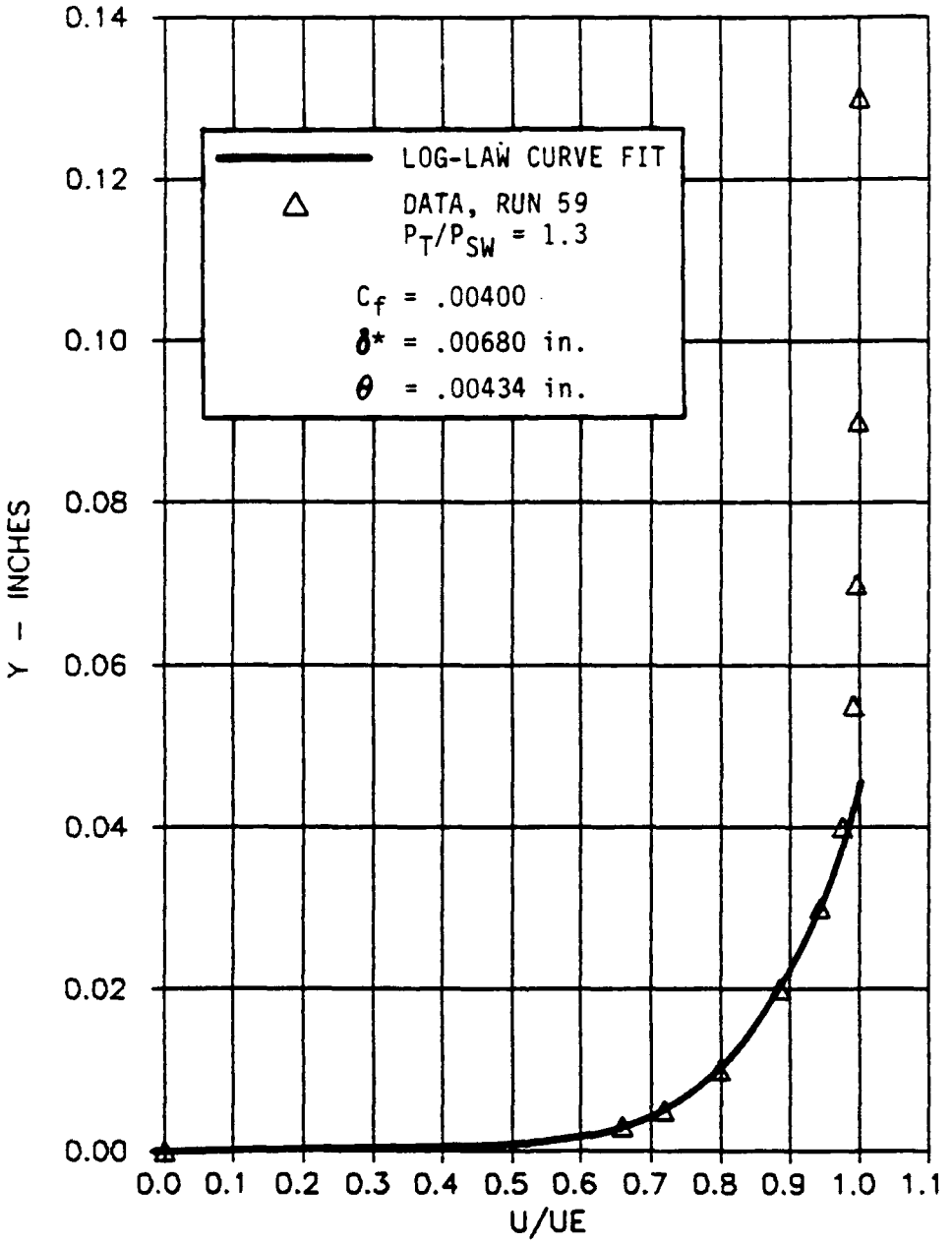

FIGURE 40. MEASURED BOUNDARY LAYER AT THROAT.

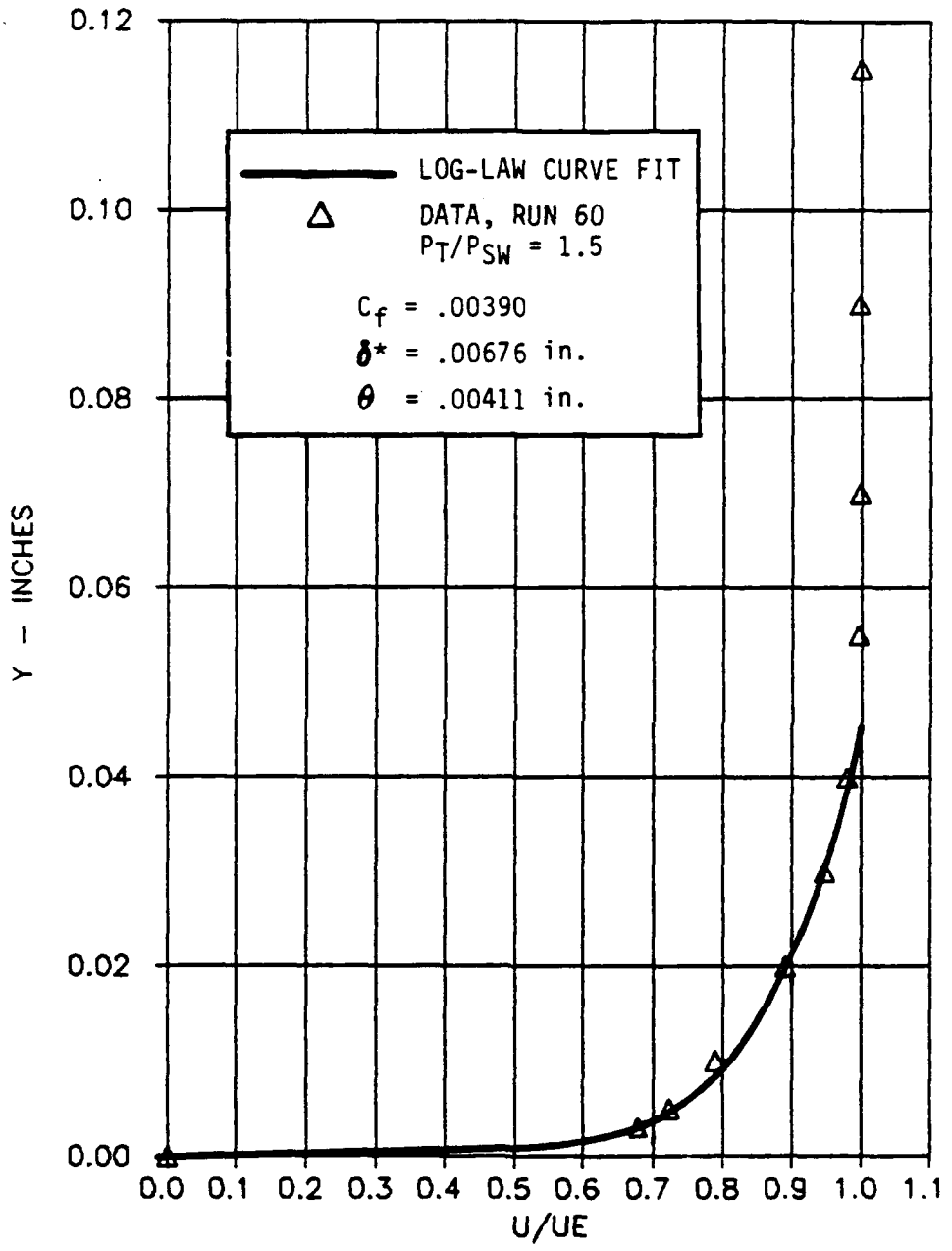

FIGURE 41. MEASURED BOUNDARY LAYER AT THROAT.

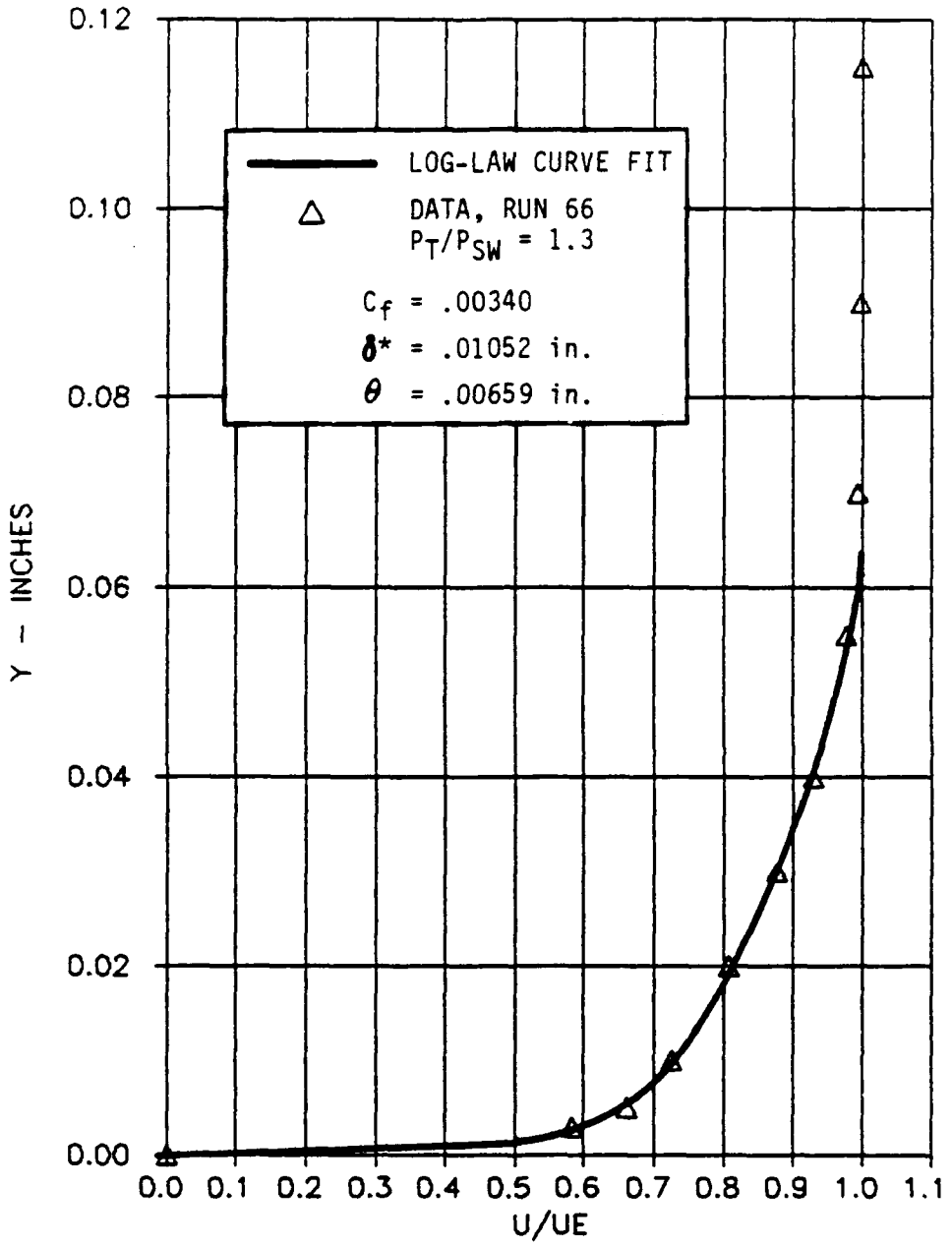

FIGURE 42. MEASURED BOUNDARY LAYER AT THROAT. (EFFECT OF TRIP)

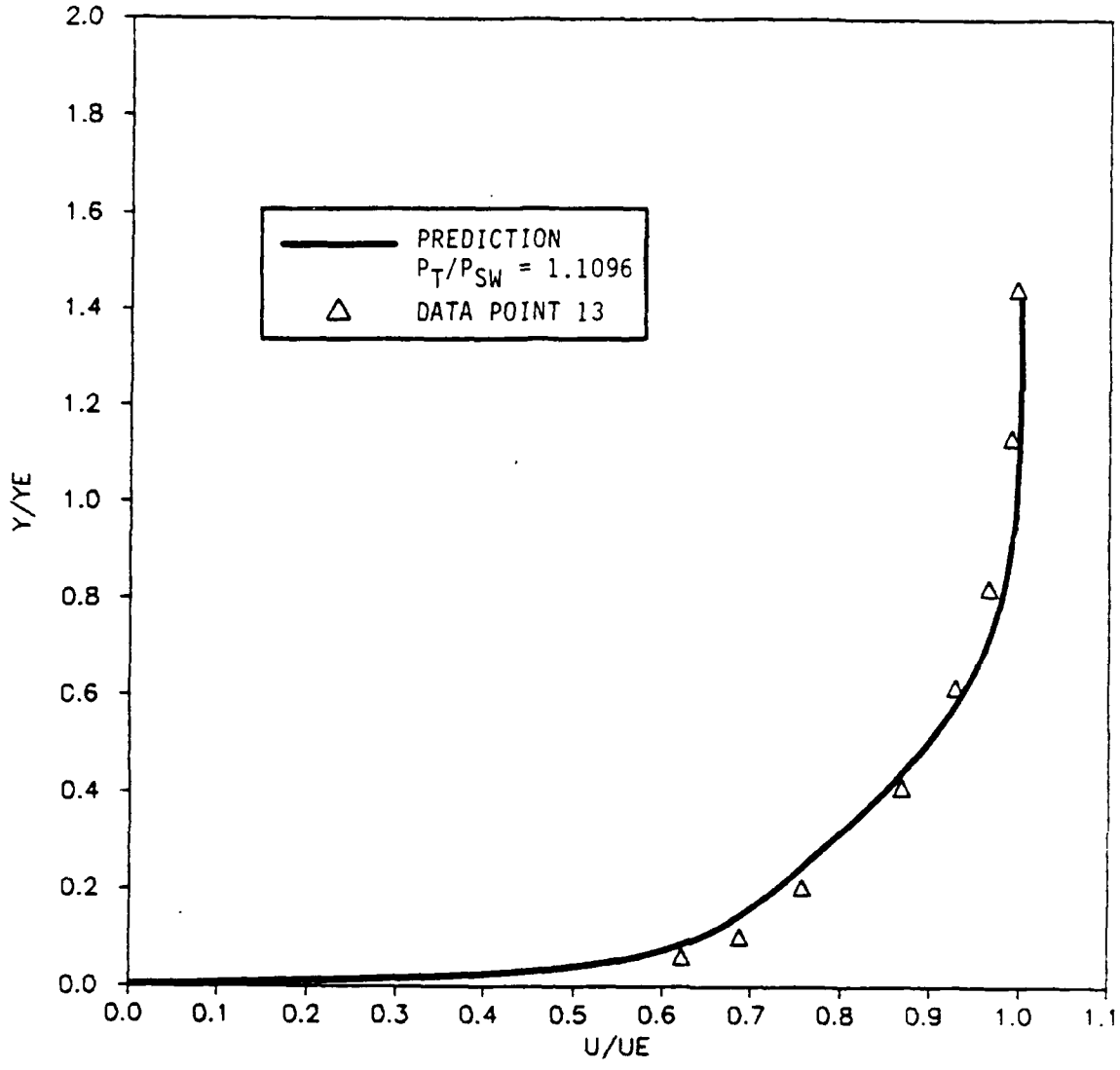

FIGURE 43. PREDICTED VS MEASURED BOUNDARY LAYER PROFILE.

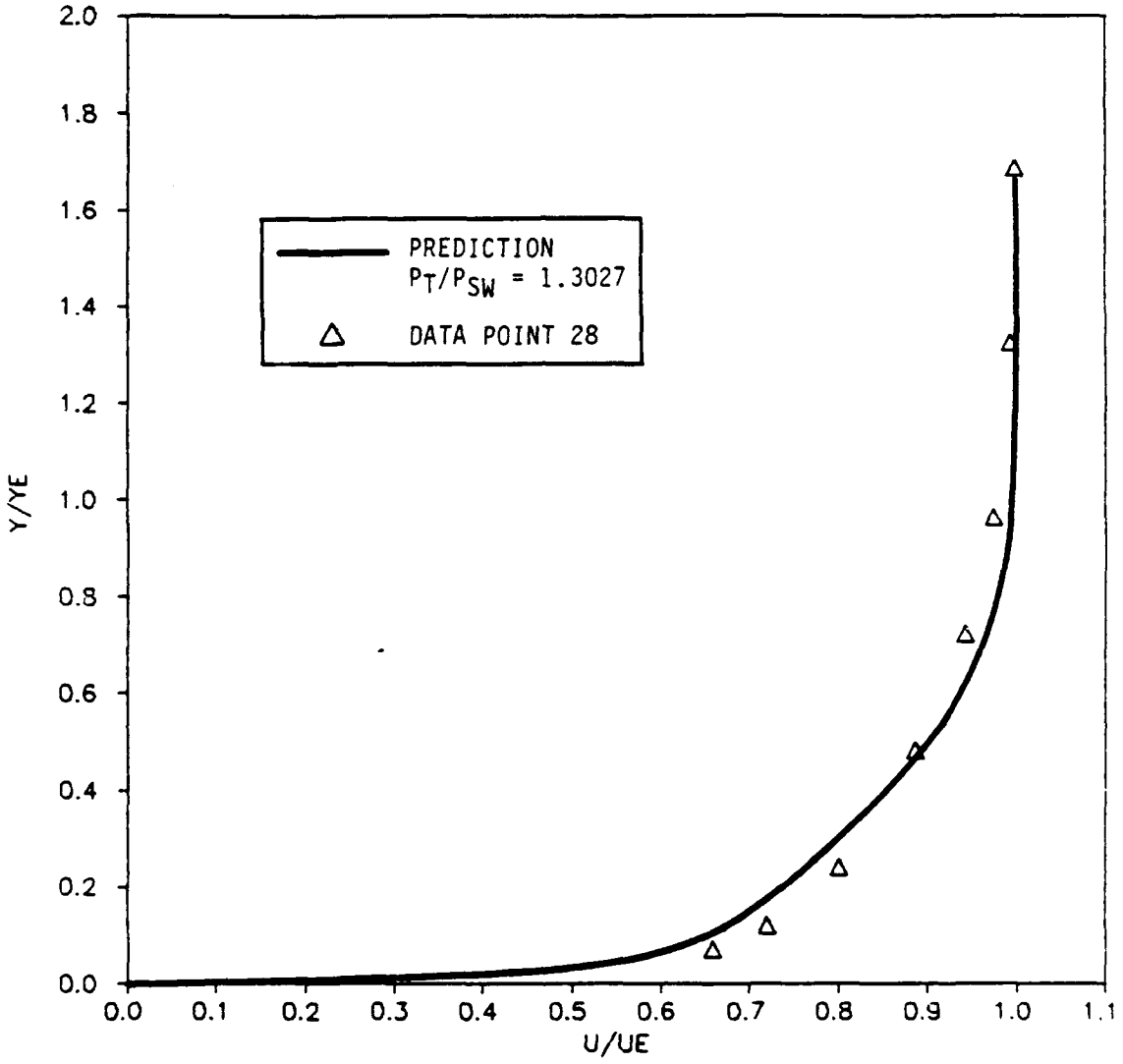

FIGURE 44. PREDICTED VS MEASURED BOUNDARY LAYER PROFILE.

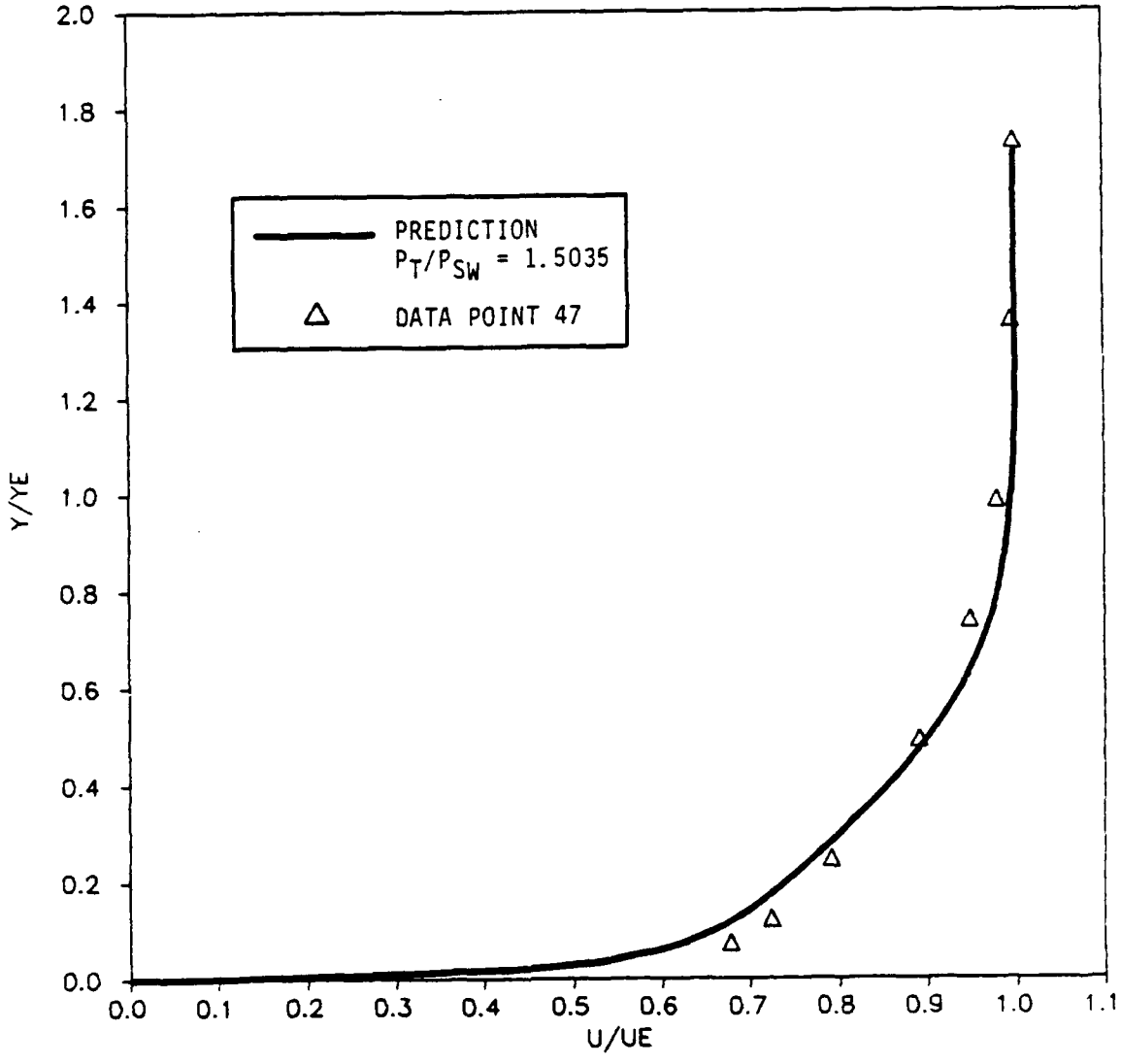

FIGURE 45. PREDICTED VS MEASURED BOUNDARY LAYER PROFILE.

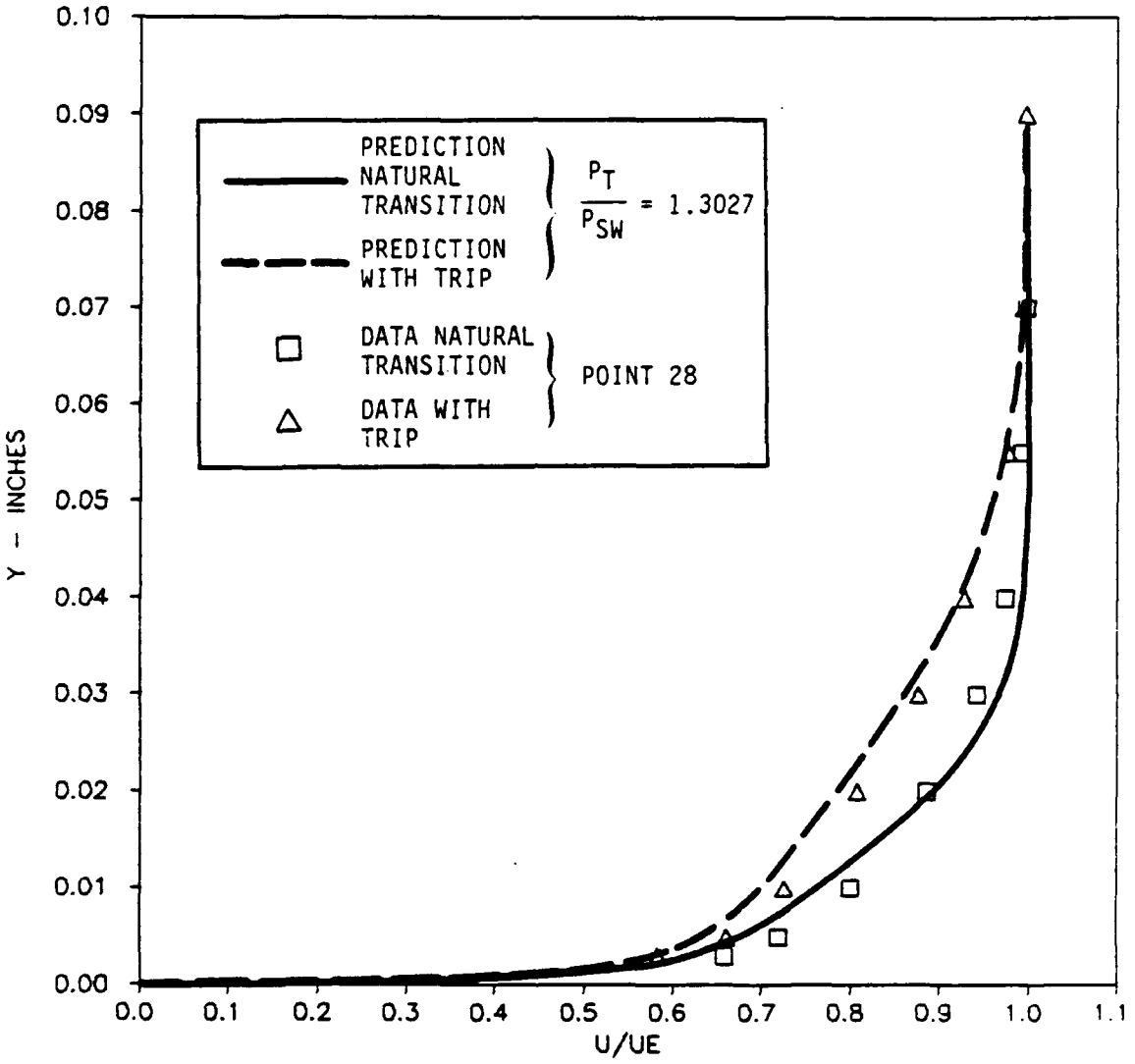

FIGURE 46. PREDICTED VS MEASURED BOUNDARY LAYER PROFILES.

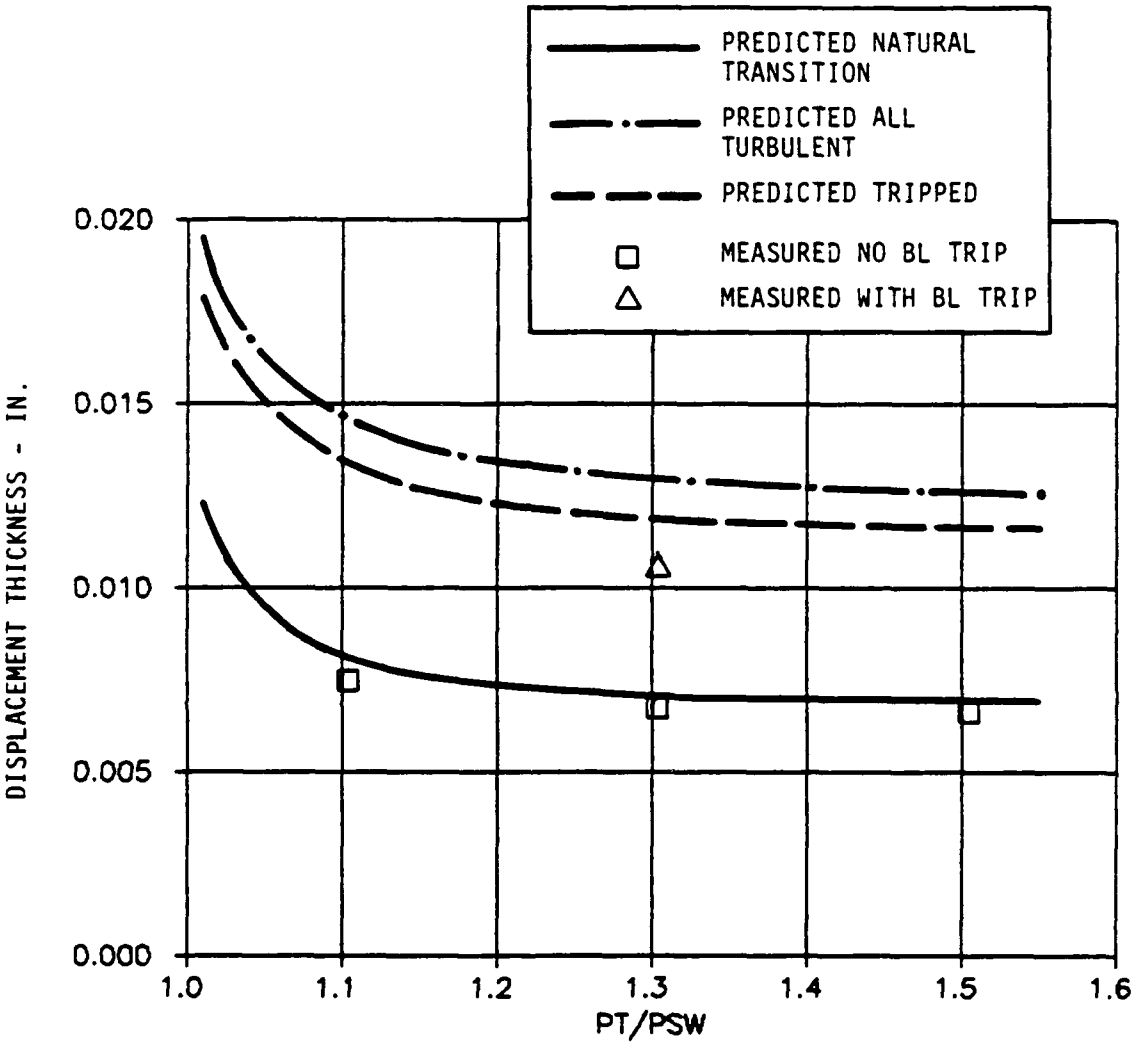

FIGURE 47. THROAT DISPLACEMENT THICKNESS.

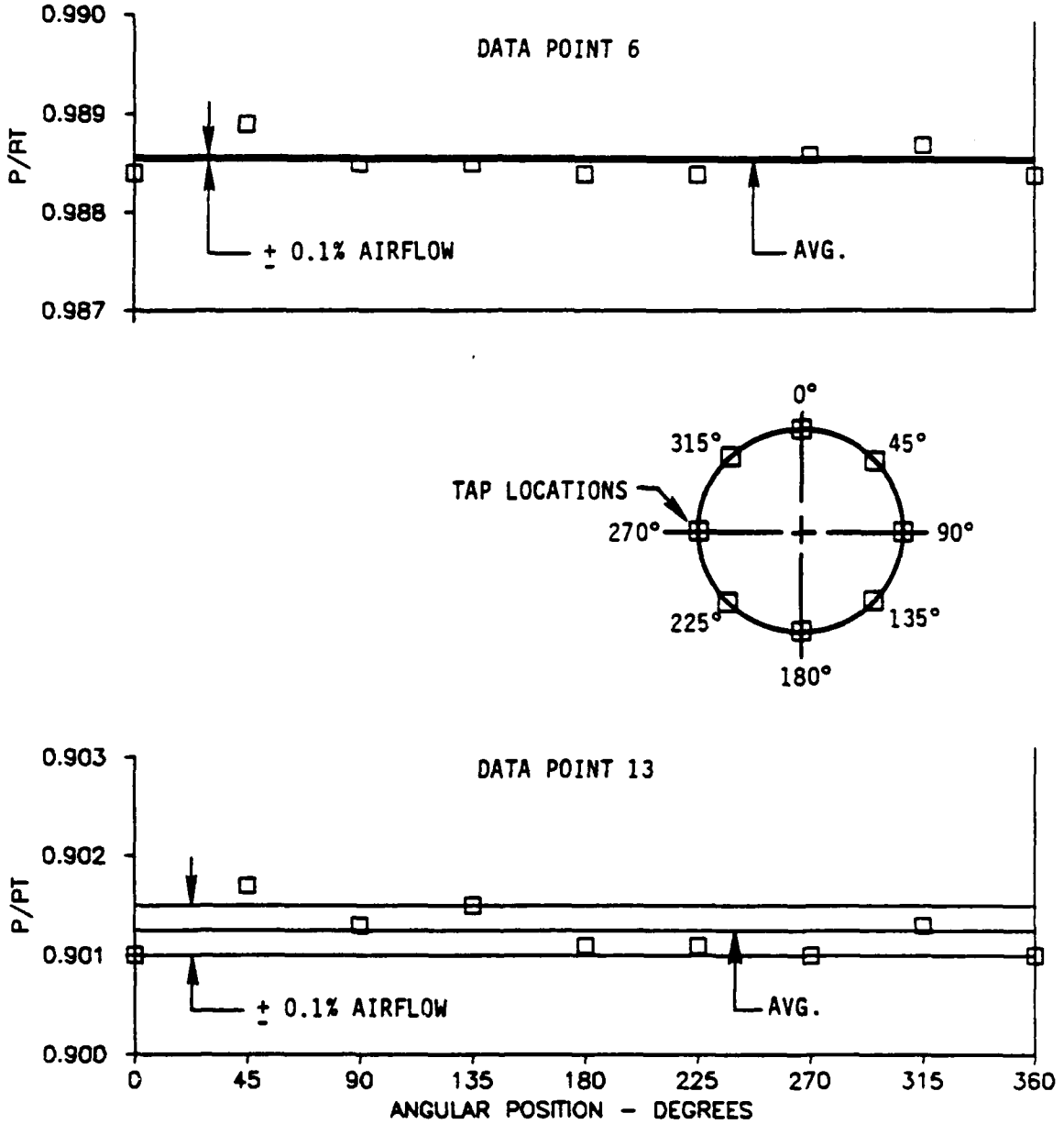

FIGURE 48. MEASURED THROAT STATIC PRESSURES.

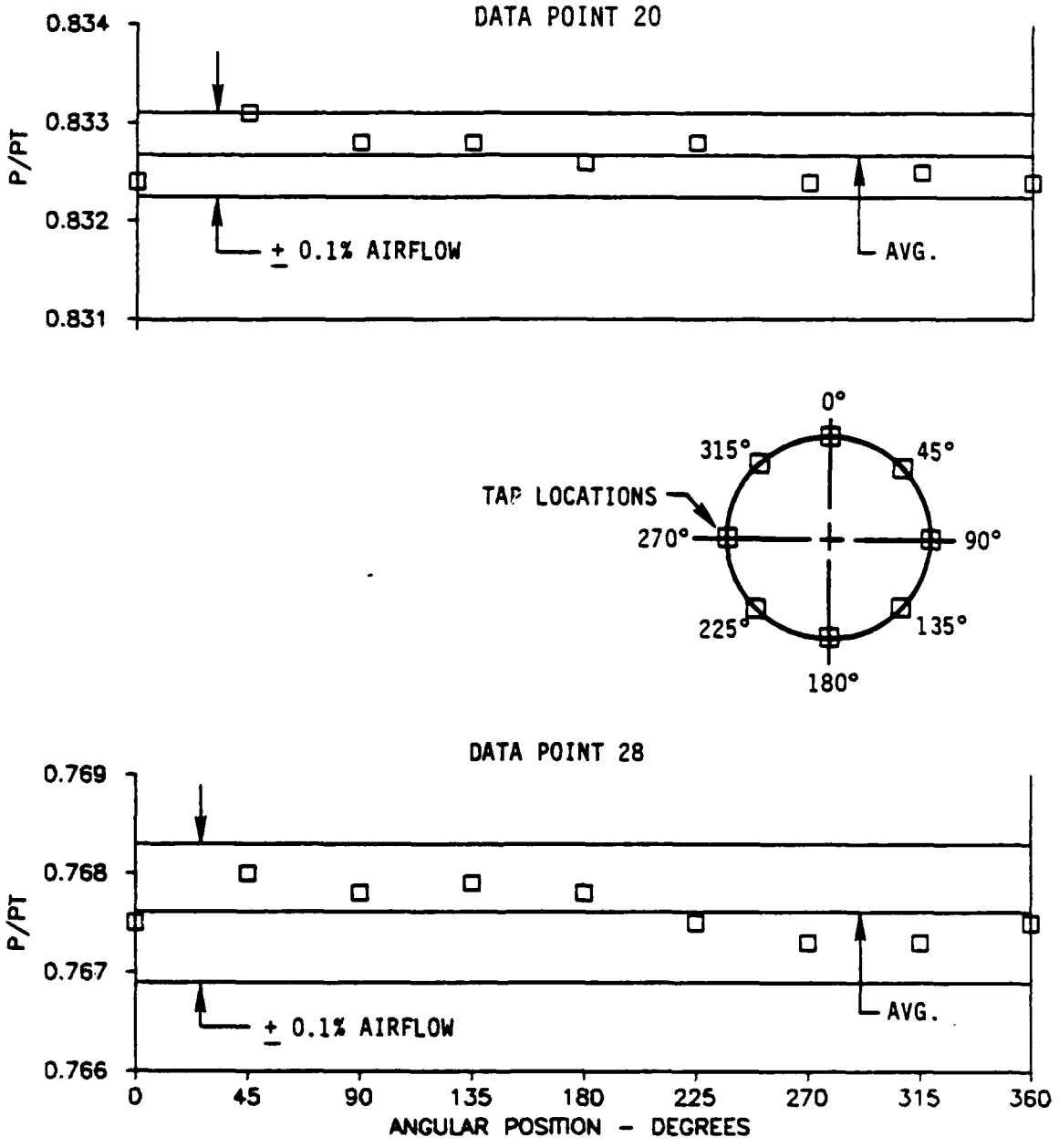

FIGURE 49. MEASURED THROAT STATIC PRESSURES.

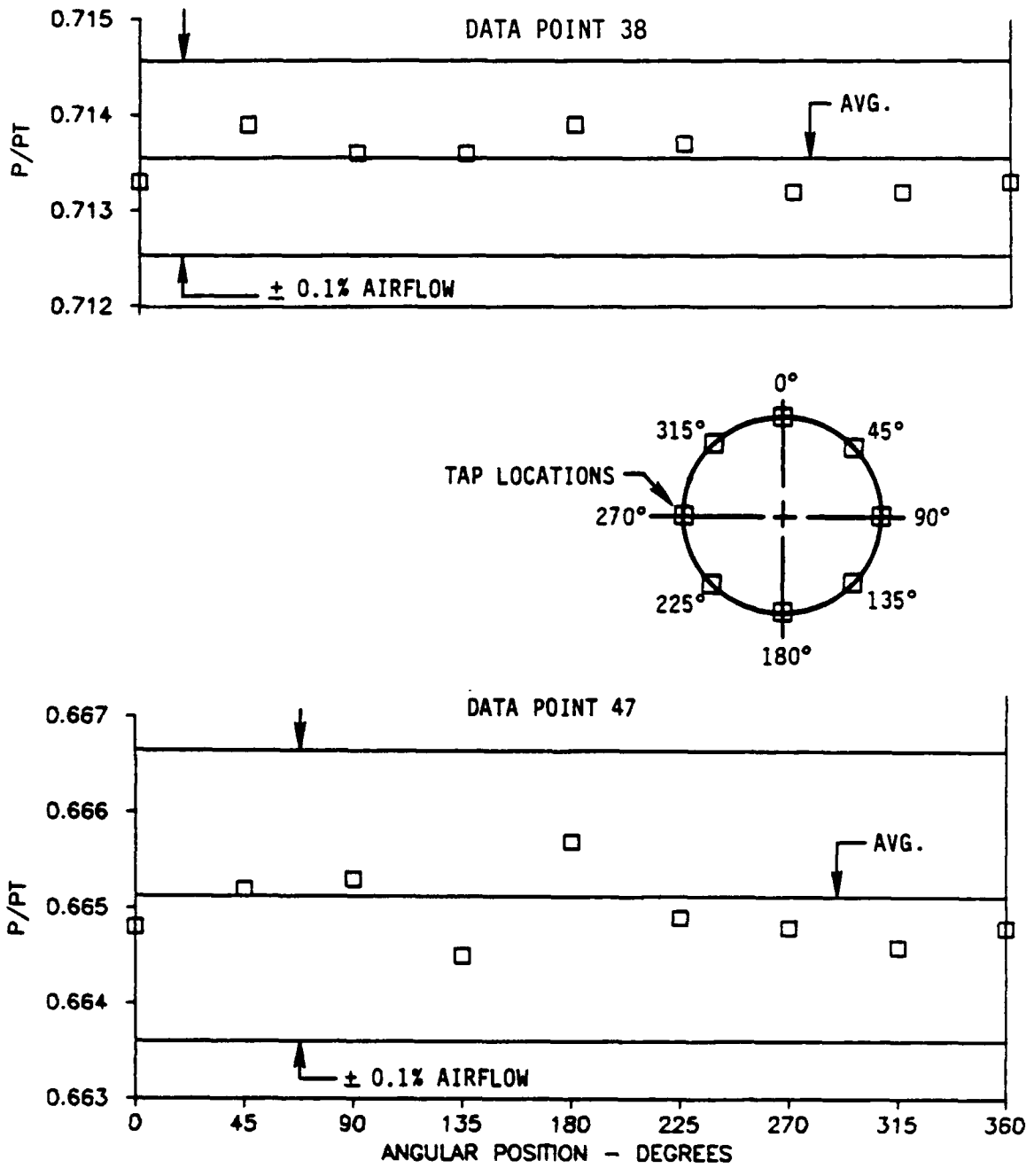

FIGURE 50. MEASURED THROAT STATIC PRESSURES.

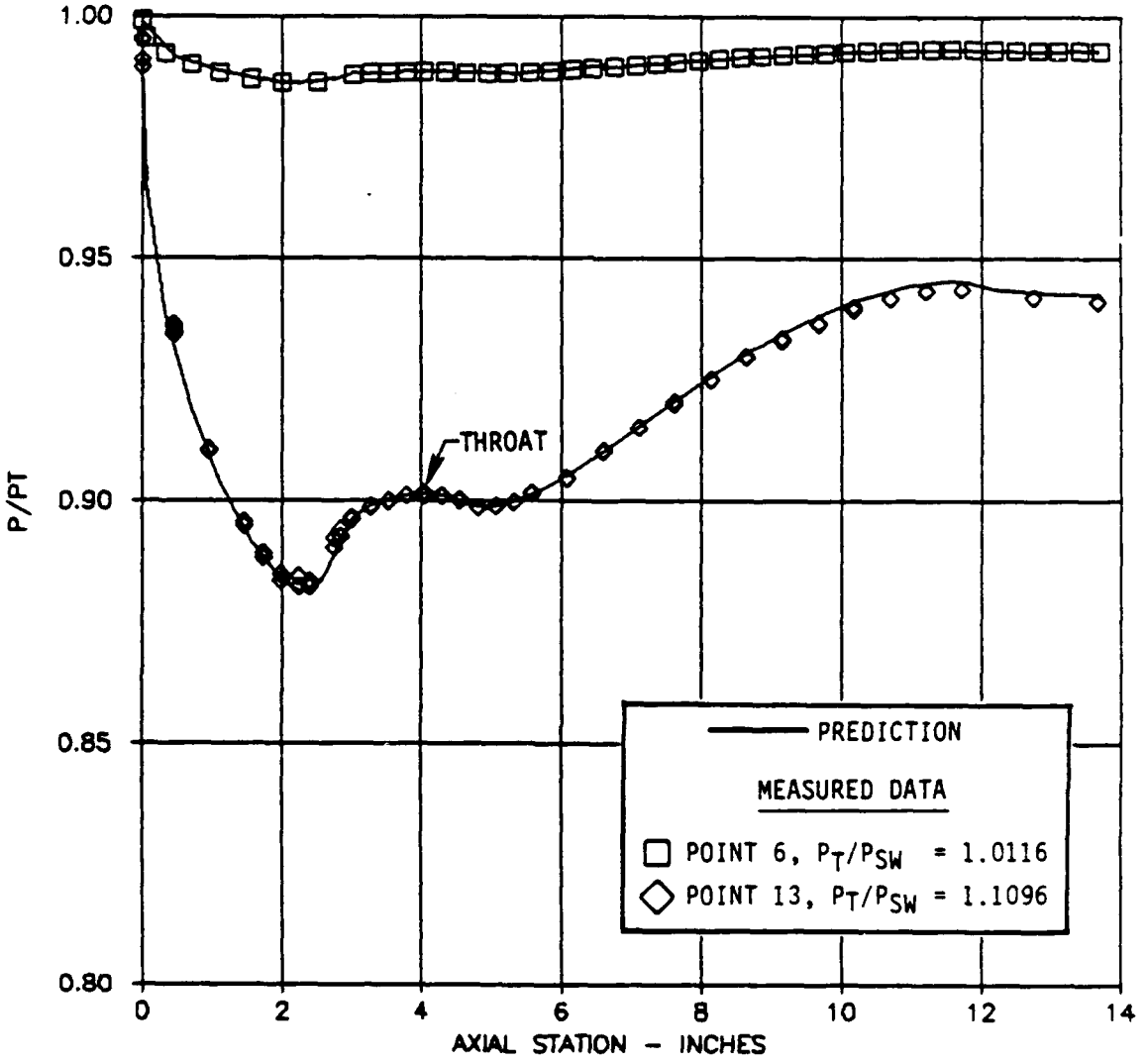

FIGURE 51. PREDICTED VERSUS MEASURED AXIAL WALL STATIC PRESSURE DISTRIBUTIONS.

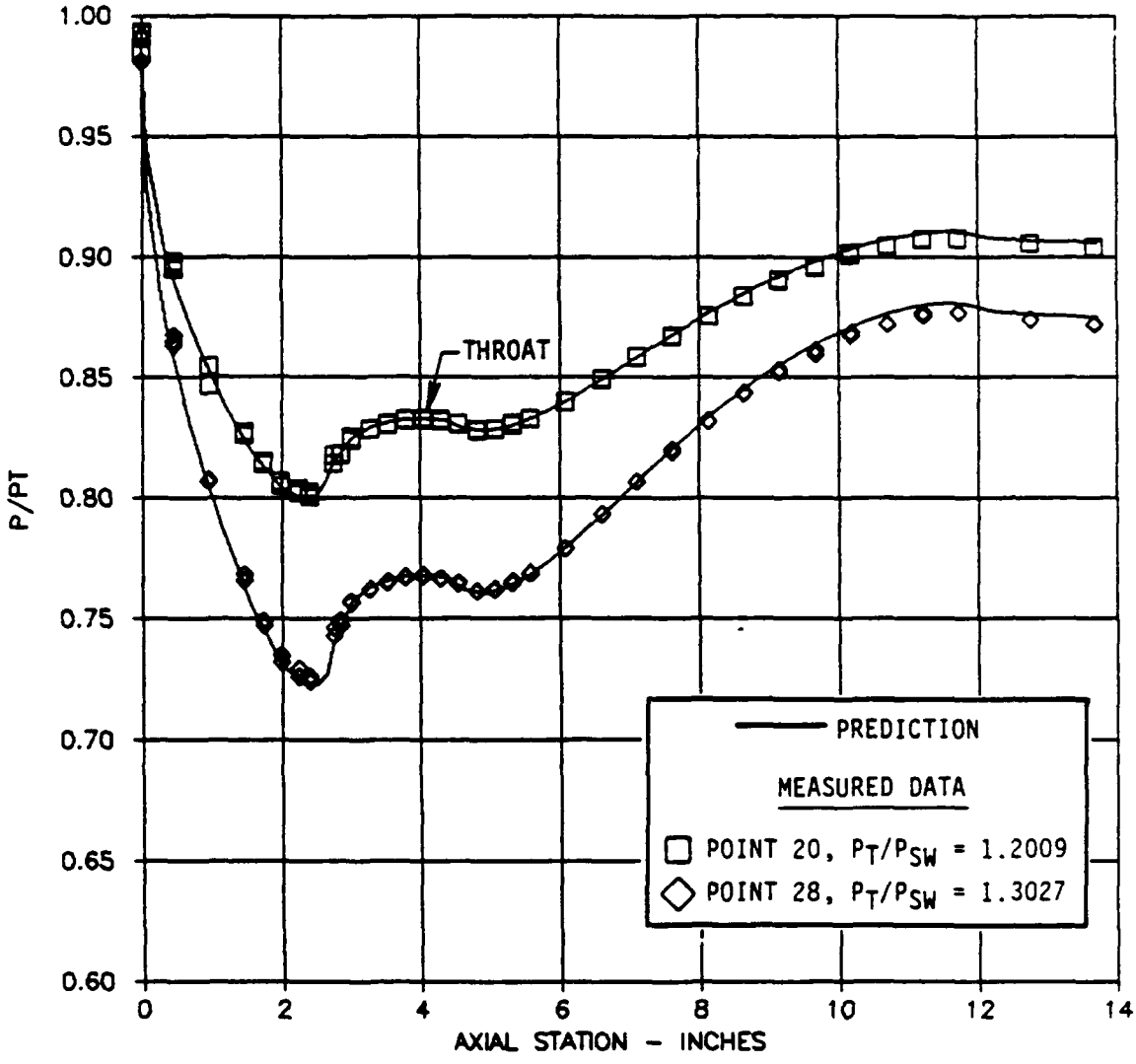

FIGURE 52. PREDICTED VERSUS MEASURED AXIAL WALL STATIC PRESSURE DISTRIBUTIONS.

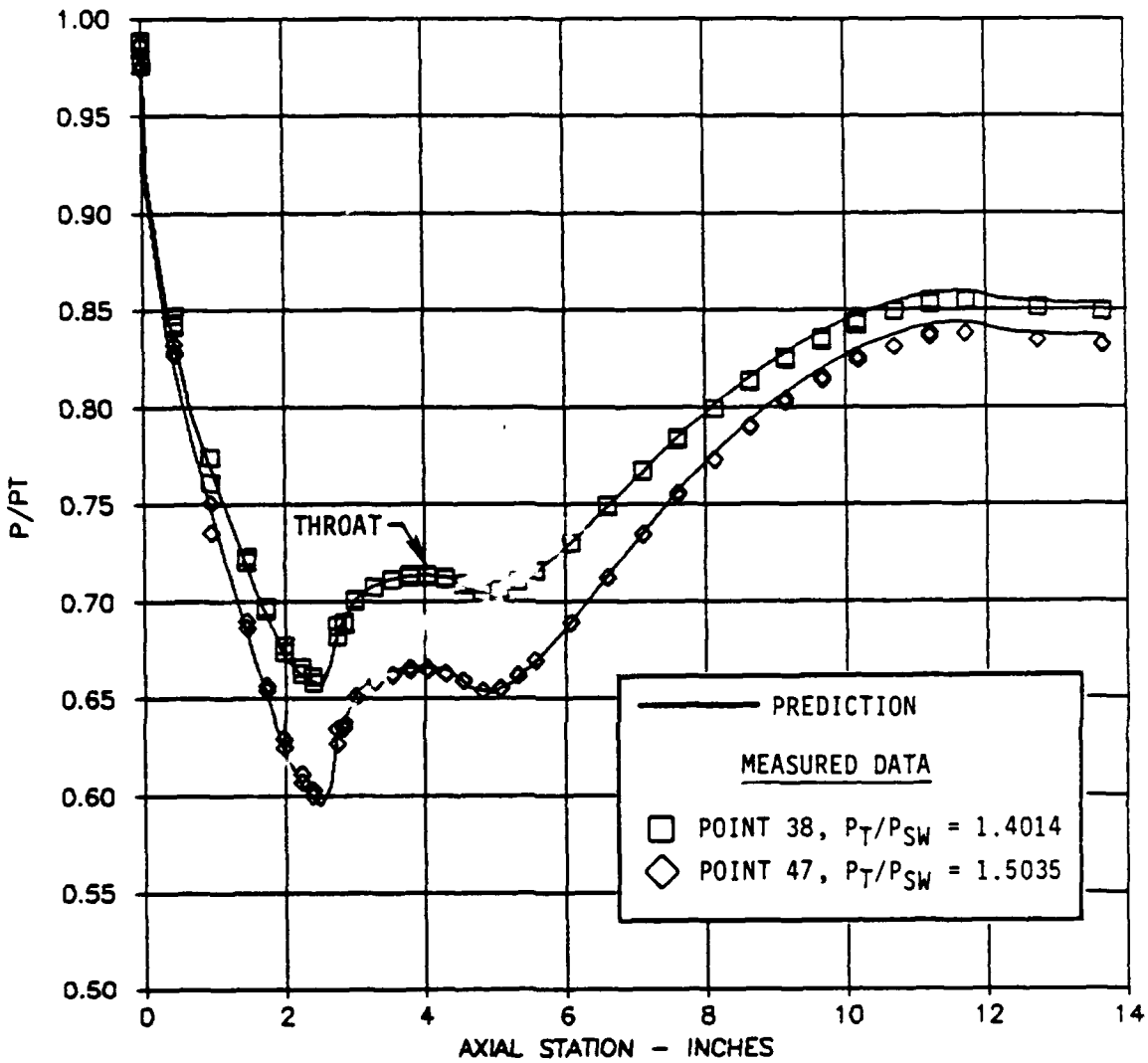

FIGURE 53. PREDICTED VERSUS MEASURED AXIAL WALL STATIC PRESSURE DISTRIBUTIONS.

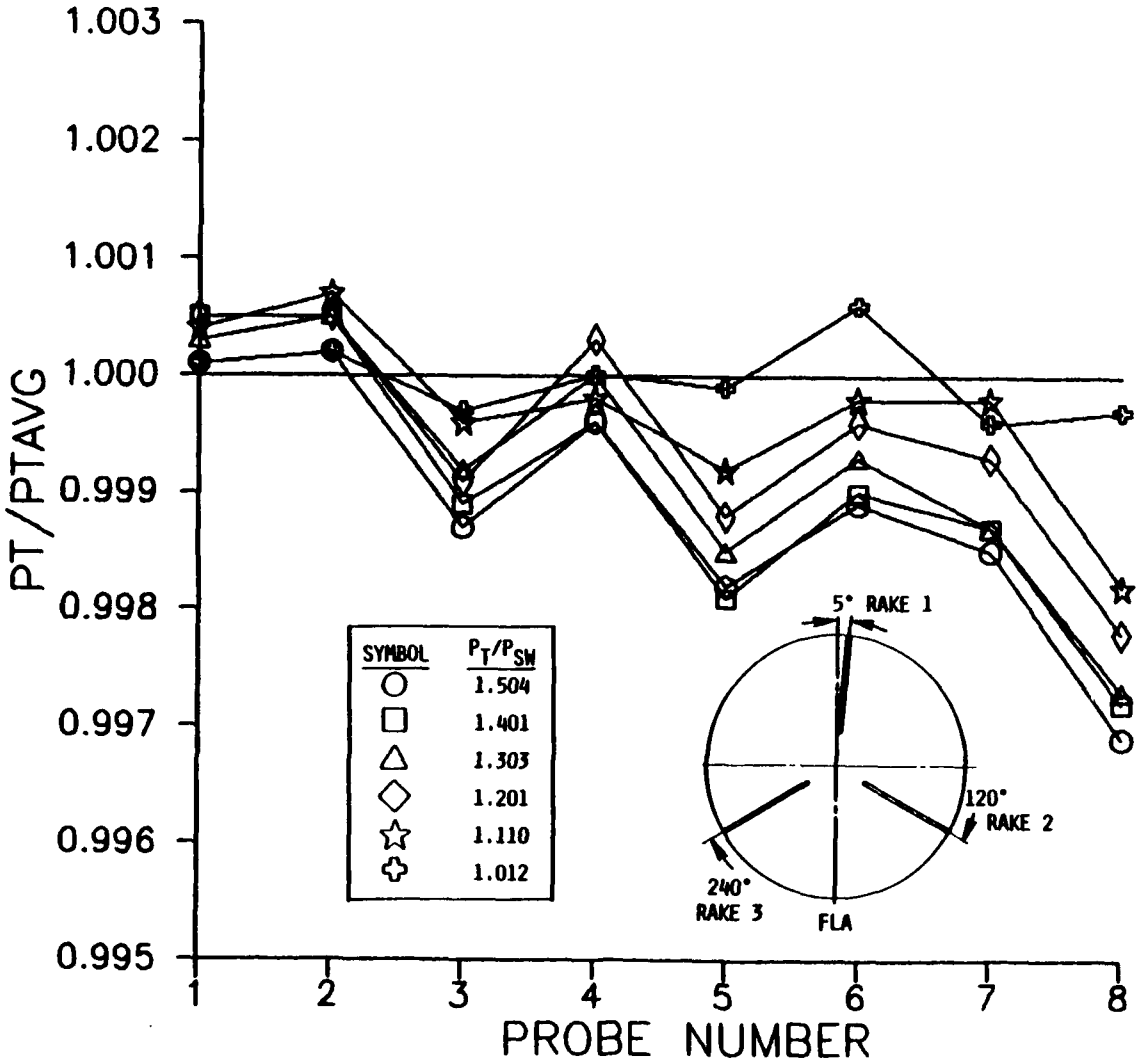

FIGURE 54. CHARGING STATION PRESSURE DISTORTION, RAKE 1.

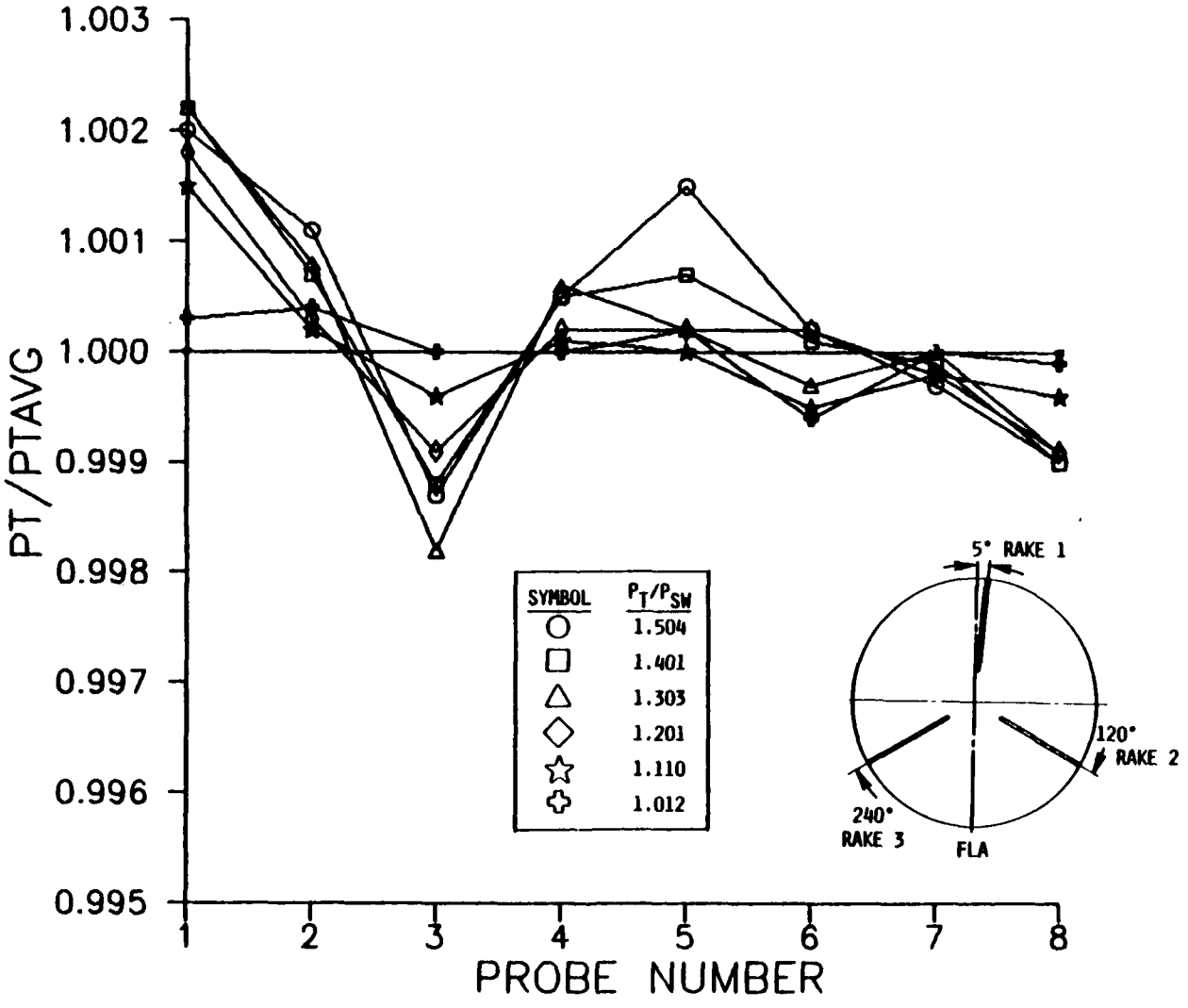

FIGURE 55. CHARGING STATION PRESSURE DISTORTION, RAKE 2.

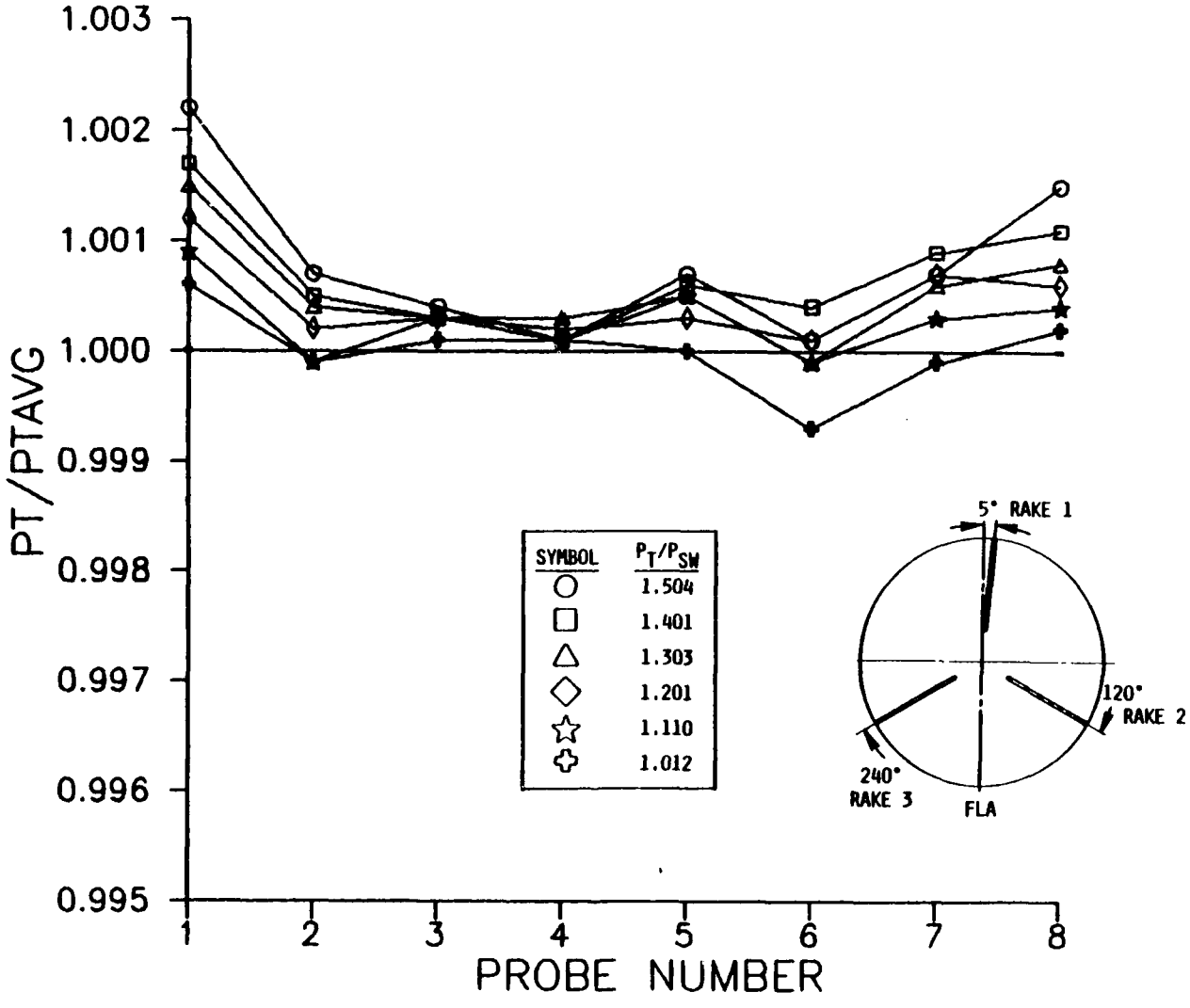

FIGURE 56. CHARGING STATION PRESSURE DISTORTION, RAKE 3.

1. ASSUME A CRUDE GRID.

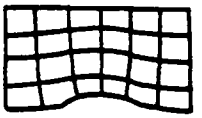

2. EVALUATE CURVATURE.

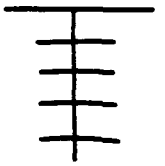

3. INTEGRATE THE CROSS-STREAM MOMENTUM EQUATION AND THE CONTINUITY EQUATION TO DETERMINE THE "CORRECT" STREAMLINE POSITIONS.

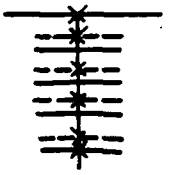

4. SOLVE THE MATRIX EQUATION FOR δn AND MOVE THE GRID POINTS.

FIGURE 57. SOLUTION PROCEDURE.

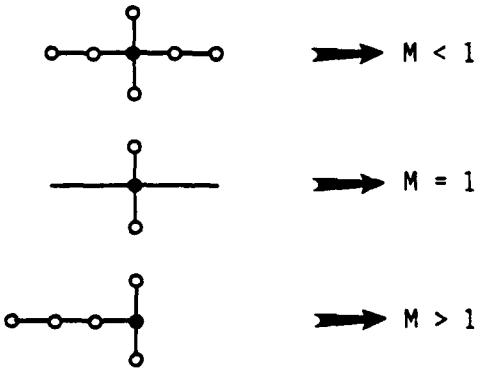

FIGURE 58. FINITE DIFFERENCE STARS FOR SUBSONIC AND SUPERSONIC FLOW.

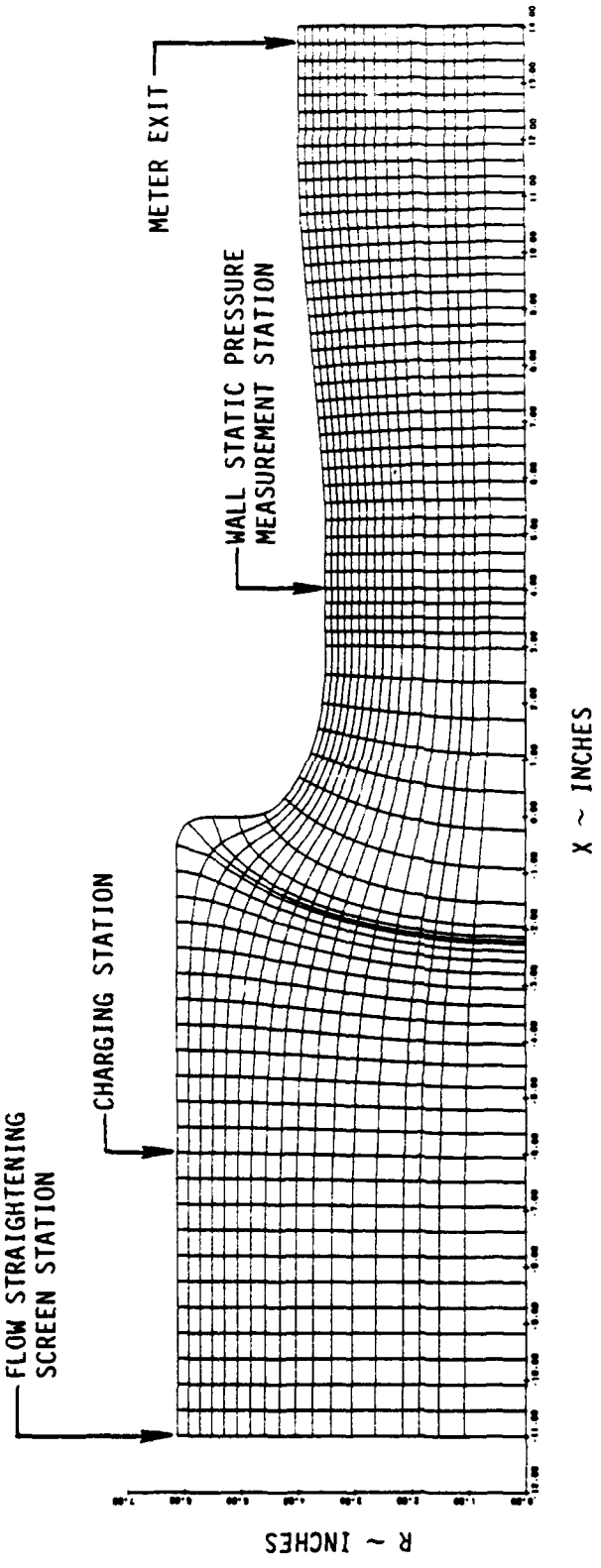

FIGURE 59. STC STREAMLINE/ORTHOGONAL LINE SOLUTION GRID.

APPENDIX A

The Streamtube Curvature (STC) computer program (Reference 14) was developed by General Electric for NASA Langley in the early 1970's for calculating the inviscid transonic flow field about nacelles and inlets. Since that time other methods, particularly time dependent techniques, have proven to be more successful for that purpose. However, over the course of the past 15 years of use on a very wide variety of aerodynamic components and configurations the program has demonstrated a versatility for highly accurate solutions for general subsonic and supersonic planar and axisymmetric flows. The flowfield in unchoked flow meters is a particular example where it is felt that accuracy improvements offered by newer methods are probably not likely. Therefore the STC code was chosen for this program.

The STC method has not been discussed much in the open literature, however the method is a natural one, being similar to the way one would rely on one-dimensional compressible flow relationships for a first order solution to ducted flows. The STC approach however solves for a number of confluent streamtubes, each with slightly different properties to obtain the total flow in the channel. In the limit, as the size of each streamtube

approaches zero, the STC method satisfies the inviscid equations of motion exactly. The following description extracted from Reference 14 presents key features of the method.

The method uses a natural coordinate system. That is the solution grid is composed of streamlines (ψ = constant lines) and lines which are orthogonal to the streamlines (ξ = constant lines).

Across the streamlines, the continuity and momentum equations are:

Continuity:

$$\partial A = \frac{\partial \psi}{\rho V}$$

Momentum:

(a) Normal form:

$$\frac{\partial P}{\partial n} = C\rho V^2$$

(b) Crocco form:

$$\frac{1}{2}\frac{\partial (V^2)}{\partial n} = -CV^2 + \frac{\partial H}{\partial n} - T\frac{\partial S}{\partial n} \qquad (\xi = \text{Const.})$$

Along the streamlines the energy and momentum equations are:

Momentum:

$$\frac{DS}{Ds} \qquad (\psi = \text{Const.})$$

Energy:

$$\frac{DH}{Ds} \qquad (\psi = \text{Const.})$$

where, the independent variables s and n are the distances measured along and across the streamlines, respectively.

The solution method is an extension of the streamline curvature method. It may be briefly described as follows: First, a crude grid of streamlines and orthogonal lines is assumed (Figure 57); second, the curvature of the streamlines at each of the grid points is evaluated, third, the momentum equation is integrated along a line normal to the streamlines to obtain velocity, and the continuity equation is integrated to determine the "correct" streamline positions (for the assumed curvature field). These are indicated by the "x" in Figure 57. Fourth, an adjustment (δn) is computed by considering: (1) the difference between the computed and assumed streamline positions and, (2) the effect of the implied curvature modification in the integrated momentum equation. Finally, the streamlines are repositioned by the δn values.

Because the movement of any one grid point alters the velocity at nearby points through a change in curvature, it is highly desirable to account for these interrelating point adjustments simultaneously. The utilization of a simultaneous solution procedure, employed here, is not part of the classical streamline curvature method (References 20, 21, and 22). In comparison, the classical method yields calculation times which are very slow, especially for a closely spaced calculation grid. In concept, the set of simultaneous equations for the normal streamline adjustments is formulated from the finite difference equivalent of the following equation.

$$\frac{\partial^2(\delta n)}{\partial \psi^2} + \frac{(1 - M^2)}{(\rho V)^2} \frac{\partial^2(\delta n)}{\partial s^2} = F$$

where,

δn = Required streamline adjustment in the normal direction

ψ = Stream function

s = Curvilinear distance along a given streamline

M = Mach number

ρV = Flow per unit area

F = Driving (or error) function derived from the solution to the integral continuity and normal momentum equations

From a mathematical point of view, the above equation is similar to the small perturbation form of the velocity potential equation employed by Murman and Cole (Reference 23).

$$\frac{\partial^2 \phi}{\partial y^2} + (1 - M^2)\frac{\partial^2 \phi}{\partial x^2} = 0$$

$$\frac{v}{a} << 1, \quad M \approx \frac{u}{a}$$

In either case, it is possible to numerically solve the equations for either subsonic flow or supersonic flow by changing the finite difference star from a subsonic representation to a supersonic representation as illustrated in Figure 58. Notice that the supersonic representation includes no points downstream of the cross-stream line, reflecting the physical reality that disturbances downstream will not be felt upstream. The star-switching process is directly related to the coefficient $(1-M^2)$; and, because this coefficient is zero at unity Mach number, the switch from one star to the other is performed smoothly.

Considerable complexity is introduced when this equation is expanded to allow the vertical component of velocity, v, to be the order of magnitude of the axial component u. In this

case when the grid system is not aligned with the flow direction, a cross-derivative term:

$$\frac{uv}{a^2} \frac{\partial^2 \phi}{\partial x \partial y}$$

appears in the differential equation, and the star-switching concept (as explained above) cannot be applied. On the other hand, with the intrinsic coordinate system utilized in the STC procedure, the arms of the star are always oriented in the streamwise and cross-stream directions, and the star-switching algorithm is always appropriate.

Figure 59 shows a typical streamline/orthogonal line grid for the flowmeter designed for this program. It is representative of all the solutions obtained. Note that the intersection between the downstream end of the facility adapter pipe and the start of the contraction into the meter has been modified slightly by the addition of a small fillet. Although the STC program can accommodate such a stagnation point discontinuity, experience has shown such fillets closely duplicate the small separation bubble that forms in this region without affecting the solution elsewhere in the meter. This is indicated by the comparisons of the measured and calculated pressure distributions at X = 0 in Figures 51 - 53.